DEPARTMENT OF MATHEMATICS AND STATISTICS

UNIVERSITY OF OTAGO

A THESIS SUBMITTED FOR THE DEGREE OF DOCTOR OF PHILOSOPHY

The Numerical Initial Boundary Value Problem for the Generalised Conformal Field Equations in General Relativity

---

Author:

Chris Stevens

Supervisor:

Prof. Jörg Frauendiener

October 18, 2016

Abstract

The purpose of this work is to develop for the first time a general framework for the Initial Boundary Value Problem (IBVP) of the Generalised Conformal Field Equations (GCFE). At present the only investigation toward obtaining such a framework was given in the mid 90's by Friedrich [48] at an analytical level and is only valid for Anti-de Sitter space-time. There have so far been no numerical explorations into the validity of building such a framework.

The GCFE system is derived in the space-spinor formalism and Newman and Penrose's $\eth$-calculus is imposed to obtain proper spin-weighted equations. These are then rigorously tested both analytically and numerically to confirm their correctness. The global structure of the Schwarzschild, Schwarzschild-de Sitter and Schwarzschild-Anti-de Sitter space-times are numerically reproduced from an IVP and for the first time, numerical simulations that incorporate *both* the singularity and the conformal boundary are presented.

A framework for the IBVP is then given, where the boundaries are chosen as *arbitrary* conformal geodesics and where the constraints propagate on (at least) the numerical level. The full generality of the framework is verified numerically for gravitational perturbations of Minkowski and Schwarzschild space-times. A spin-frame adapted to the geometry of future null infinity $\mathscr{I}^+$ is developed and the expressions for the Bondi-mass and the Bondi-time given by Penrose and Rindler [100] are generalised. The Bondi-mass is found to equate to the Schwarzschild-mass for the standard Schwarzschild space-time and the famous Bondi-Sachs mass loss is reproduced for the gravitationally perturbed case.

Acknowledgements

The last three years have been a roller coaster ride of emotions; fun, sad, happy, amazed, puzzled to name a few and I would not have gotten through it without the help of some great people.

Firstly I would like to thank my supervisor Prof. Jörg Frauendiener. He has given me outstanding guidance and showed great patience not just during my time as a postgraduate student, but since the day I walked into his office in my second year as an undergraduate asking for help reading my first relativity textbook. Without his friendliness and open door policy I surely would not be where I am today.

I want to thank my beautiful wife Jessica, for supporting me unequivocally and being understanding during the long days spent away from her. She has been a big part of my life ever since I met her during high school. There is no doubt that I would not be the person I am today, without her. I must also mention her efforts in memorising a sentence explaining what I do to other people. Good effort.

I would also like to thank Dr Jörg Hennig and Dr Florian Beyer for their help during the years, especially when Prof. Frauendiener was overseas. Thanks go to Dr Ben Whale for numerous discussions about the inner workings of COFFEE and relativity in general. To Leon Escobar for many insightful and sometimes random discussions. To Chris Laing for his help on differential geometry in my early postgraduate years and to Boris Daszuta for his numerical expertise.

Contents

Introduction

As far back as the caveman and probably beyond, the human inhabitants of this planet have understood some vague notion of gravity. We know that if we hold up a stone and let it go, it will not float up toward the sky nor travel across the ground and out of sight. No, we know with all certainty that it will fall toward the ground. For most of our time here on earth, we did not question the why or the how of this, but simply understood that this is the way of things and that is that.

It was not until Issac Newton published a theory of gravity in his work Philosophiæ Naturalis Principia Mathematica [89] in 1687, showcasing his new mathematical techniques, that there existed a plausible theory of gravity. The foundation of this theory was that there exists a gravitational force between masses, with larger masses "pulling" smaller ones toward them via their gravitational field. Although later this notion of a pulling force proved to be incorrect, the theory worked very well for studying the gravitational interaction of slow-moving and not too dense bodies. Contrary to this success, it did not agree with all observations such as the perihelion shift of Mercury. Newton thought that the theory was incomplete but did not find a correction to resolve these anomalies.

Introducing Albert Einstein. Born 14th March 1879 in Germany, Einstein was to found an entirely different view of gravity which became known as the General Theory of Relativity. Graduating in 1900 with a degree in Physics, Einstein struggled to find work. After two years of searching he finally acquired the job of assistant examiner at the Federal Office for Intellectual Property; the patent office. He worked there while completing his PhD, which was eventually finished in April 1905. That same year, Einstein published four ground-

breaking papers that have become known as the Annus Mirabilis papers (Annus Mirabilis translating from Latin as "extraordinary year"). They were papers on the photo electric effect [34], Brownian motion [31], mass-energy equivalence [30] and of course special relativity and the notion of space-time [32]. Although not known to him yet, Einstein had just formulated ideas that would be used to transform the theory of gravity forever.

His paper introducing special relativity reconciles Maxwell's equations with the laws of mechanics by modifying the theory at velocities close to the speed of light. In 1907 he would have what he would later refer to as his "happiest thought". Namely realising the principle of relativity, which says that the equations describing the laws of physics should have the same form in all admissible reference frames, can be applied to the gravitational field. Following this he conducted thought experiments to test his ideas. In the same year he founded the equivalence principle, a foundation of his theory, which identifies inertial motion with free fall. He also predicted time dilation that year and in 1911 he predicted the deflection of light around massive bodies. But perhaps most crucially, was his turntable thought experiment. He noticed that an observer sitting on the turntable as it rotated would measure a different value for π than if the turntable was at rest, due to the length contraction of the circumference but not the radius. He concluded that space-time must be curved and this led him to pursue the mathematics of differential geometry, the language in which his theory of gravity will subsequently be formulated.

With the help of Italian geometer Tullio Levi-Civita he formulated the first form of the field equations as $R_{\mu\nu} = T_{\mu\nu}$ in October 1915. This equation successfully fixed the anomaly in the perihelion shift of Mercury, which was of great excitement for Einstein. However it was quickly discovered that these fields equations were inconsistent with the local conservation of energy and momentum. However this was quickly remedied and the field equations $R_{\mu\nu} - \frac{1}{2}Rg_{\mu\nu} = T_{\mu\nu}$ were produced a month later.

These equations comprise of a system of non-linear Partial Differential Equations (PDEs), which Einstein speculated would be near impossible to solve. However barely a month

after they were published Karl Schwarzschild who was serving in the war on the Russian front, found the first exact solution, which described the space-time around a static spherically symmetric body [117]. This was shortly after generalised by Reissner to include charge [109]. Willem de Sitter followed in 1917 and published a constant curvature solution now known as de Sitter space-time [25]. Then in the early 1920's Alexander Friedmann found cosmological solutions where the universe expands or contracts [43, 44]. The notion of an expanding or contracting universe was against Einstein's notion of a static universe. It turned out that the general theory of relativity did not support the notion of a static universe and so Einstein added the famous cosmological constant λ to his equations. This allowed him to formulate the solution known as the Einstein static universe or the Einstein cylinder. However in 1929 Edwin Hubble found evidence that the universe was in fact expanding. This prompted Einstein to drop the cosmological constant from the fields equations and for him to proclaim that it was "the biggest blunder in my career". However modern cosmology still heavily uses the cosmological constant and it is a potential candidate for the so-called "dark energy".

The notion of a gravitational wave was first put forward by Einstein in 1918 [33] as a solution of the linearised vacuum equations. He reported that they would be very hard to detect due to being so weak and in fact in 1936 in a paper published with Rosen [35] he argued against their existence. In the 1950's, Pirani [103] looked into an invariant formulation of gravitational radiation to clear up issues with the notion of singularities that had influenced peoples understandings of the topic (for example Rosen [110]). He proposed that assuming the gravitational radiation is found in the curvature of space-times, space-times with Petrov-type {211} or {31} are found to be the ones with gravitational radiation. This was also the first time the Bianchi equation $\nabla_d R_{abc}{}^d$ was discussed in relation to the propagation of gravitational radiation (Lichnerowicz also discussed this in [76]).

In order to help in the study of gravitational waves, the notion of an isolated system was introduced. This is the idealisation of a system that is alone in an otherwise empty universe. If one chooses the cosmological constant to vanish, the curvature dies off going toward

infinity and hence the space-time becomes Minkowskian. Further progress was made using this idealisation in the investigation of gravitational waves between 1955 and 1967 by the group centred around Bondi and Pirani in London. They published a series of papers ([17, 18, 79, 79, 80, 104, 111, 113]) in which of particular importance was their notion of Bondi-coordinates used to investigate the asymptotic properties of gravitational radiation and the notion of Bondi-mass for space-times that became catagorised as asymptotically flat by Penrose [94]. By using these special coordinates and defining certain asymptotic fall off conditions they were able to show that outgoing gravitational radiation takes away energy from the system. This property later became known as the Bondi-Sachs mass-loss. They also looked into the group of coordinate transformations that left the metric and their boundary conditions invariant and founded the Bondi-Metzner-Sachs (BMS) symmetry group, which has been studied extensively (see [82, 83, 84, 84, 85, 87, 98, 112]).

During this period Newman and Penrose [86] formulated the Newman-Penrose formalism, bringing together ideas from Penrose's spinors [92] and Newman's null tetrad approach. They found that the Bianchi equation $\nabla_d R_{abc}{}^d$ can be thought of as a field equation for the Weyl tensor, and hence describes the propagation of gravitational radiation. This was a huge revelation and is used heavily in modern day numerical relativity.

By this time the conformal structure of space-times was seen to play a larger and larger role in discussions of gravitational radiation and the notion of mass. This accumulated in a groundbreaking paper by Penrose [93] where he first formulated the idea to look at Minkowski space-time with metric $\widetilde{g}$ only up to arbitrary conformal rescalings $g = \Omega^2 \widetilde{g}$. The set of end points of null geodesics in the physical space-time (which are not in the physical space-time themselves) can then be represented by a "light-cone at infinity" in the conformal space-time with an appropriate choice of conformal factor. These are regular points in the conformal space-time and hence local differential geometrical methods can be used there. From this point of view the investigation of infinity and the asymptotics of space-times simplifies dramatically as one does not need any sort of limiting process. This geometric procedure of attaching points at infinity can be done for many interesting space-

times and hence it is not so restrictive that it eliminates the gravitational systems one wants to study. Penrose furthered this description a few years later in another seminal paper [95] which gives us the description of conformal infinity we use today.

The idea of asymptotic simplicity originated from Penrose [94] in 1963, who was trying to develop a mathematical framework for studying the asymptotic behaviour of isolated systems. He formulated the notion of asymptotic simplicity as a description of space-times that were still general enough to be interesting while maintaining nice properties at conformal infinity. The idea in relation to the detection of gravitational radiation was to put a detector at the "infinity" of the gravitational radiation so that the only information it detects comes from gravitational radiation emanating from the system.

Definition 1. *A smooth (time- and space-orientable) space-time $(\widetilde{M}, \widetilde{g}_{ab})$ is called* asymptotically simple *[41], if there exists another smooth Lorentzian manifold (M, g_{ab}) such that*

- *$\widetilde{M}$ is an open submanifold of M with smooth boundary $\partial\widetilde{M} = \mathscr{I}$;*
- *there exists a smooth scalar field Ω on M, such that $g_{ab} = \Omega^2\widetilde{g}_{ab}$ on $\widetilde{M}$, and so that $\Omega = 0$, $d\Omega \neq 0$ on $\mathscr{I}$;*
- *every null geodesic in $\widetilde{M}$ acquires a future and a past endpoint on $\mathscr{I}$.*

An asymptotically simple space-time is called asymptotically flat, *if in addition $\widetilde{R}_{ab} = 0$ in a neighbourhood of $\mathscr{I}$.*

An informal description of this idea is that one can take an asymptotically simple space-time, which is usually identified as being the physical space-time, perform a compactification by rescaling the metric with an appropriate conformal factor, and embed the entire space-time including the limiting points that represent infinity into another space-time. The benefit of doing this mathematical procedure is that one can then investigate conformal infinity of the physical space-time with local mathematical methods in the conformal space-time.

An important property of $\mathscr{I}$ is whether it is time-like, space-like, or null. Using some equations we derive in part I (namely (1.4.10) and (1.1.1)) we find that $\mathscr{I}$ is space-like, time-like,

or null if the cosmological constant is positive, negative, or zero respectively. Hence the cosmological constant plays an important role in the structure of $\mathscr{I}$.

In the years following this, there were many attempts to understand conformal infinity by Penrose himself [96], Schmidt [114, 115], Sommers [119], Persides [101, 102, 102], Ko, Newman and Tod [67], Ashtekar [4, 5], Geroch [61, 62], and later Friedrich [45, 46, 48, 50] to name a few. Of particular note was the early work by Geroch [61, 62] which studied null infinity and an early view of space-like infinity. Later Friedrich ([45, 46, 48, 50]) also looked at null infinity but gave a completely different picture of space-like infinity, namely the idea of "blowing up" the point i^0 to a 2-sphere which then lead to the idea of a cylinder that connects future and past null infinity.

The field of numerical relativity emerged in later years in attempts to solve Einstein's equations on the computer in the form of a Cauchy problem, mainly with an Initial Value Problem (IVP). The initial space-time is given on some hypersurface and the equations split into evolution equations that describe how to get from this hypersurface to another and constraint equations that have to be satisfied on each surface. The property that the constraints, if satisfied initially, are satisfied on the subsequent hypersurfaces is one of the main issues in numerical relativity. The ADM formalism, founded by Arnowitt, Deser and Misner [3] in 1962, was the first method used to numerically solve Einsteins equations. However the systems of equations derived using this method were found to not be strongly hyperbolic and hence generally not well posed. The lack of this important property led to instabilities within the codes of many groups. Modifications to the ADM formalism came in the form of the Baumgarte-Shapiro-Shibata-Nakamura (BSSN) formalism in the late 1990's [7, 118] which addressed some of these issues. The generalised harmonic formalism introduced by Friedrich [47] and its numerically-adapted version by Garfinkle [59] was another method that has been successfully used in numerical relativity. In particular, Pretorius used this formalism to solve the binary black hole problem in the mid 2000's [105, 106, 107, 108]. Whereas the methods aforementioned are usually written in terms of an IVP on a space-like hypersurface, there have also been characteristic IVP formulations of the standard Einstein

equations and a mixture of both that have been used to great success. It was only in the late 1990's that a well-posed formulation of an Initial Boundary Value Problem (IBVP) for the standard Einstein equations was derived by Friedrich and Nagy [58], which utilised the Newman-Penrose formalism. The main issue with having boundaries was the propagation of constraints. This was a very difficult problem to overcome as in general the boundary data causes constraint violating modes to propagate in from the boundary and stop the constraints being satisfied in the entire computational domain. However this formulation was deemed too complicated to be of immediate use in the numerical relativity community and it was not until 2014 that this was successfully implemented for the first time by Frauendiener, Stevens and Whale [42] for the case of colliding plane gravitational waves.

All of the aforementioned methods have been shown to be successful for simulations in the physical space-time. However, for investigations at infinity, one would want to somehow formulate the Einstein equations in terms of quantities from the conformal space-time where the conformal boundary of the physical space-time are just regular points. This was first accomplished by Friedrich in [45, 46], where the resulting equations were dubbed the Metric Conformal Field Equations (MCFE), wherein the variables evolved were quantities from the conformal space-time. The downside of this formulation was that the conformal factor between the physical and conformal space-times is also a variable in the system. Hence one does not know where the conformal boundary is *a-priori*. This formalism however was successfully used in numerical codes by Frauendiener [36, 37, 38, 39, 40] to study radiation at infinity. The MCFE was generalised later also by Friedrich [48] by the introduction of a conformal Weyl connection. This gave rise to an extra gauge freedom which was then fixed in such a way that all of the fields in the system became Ordinary Differential Equations (ODEs) except for the rescaled Weyl curvature components[1]. A surprising result of this gauge choice was that the conformal factor could be computed *a-priori* and hence one knows the location of conformal infinity using only initial data. These equations became known as the Generalised Conformal Field Equations (GCFE). Although seeming to have superior properties for studying conformal infinity to the previously mentioned approaches, they

[1]What is meant by "rescaled" is defined in section 1.5 by equation (1.5.4).

have only been implemented once numerically in a PhD thesis by Beyer [9], a student of Friedrich's, in the form of an IVP for the global study of de Sitter space-time.

One issue that has not been dealt with to a great extent is the IBVP for the GCFE, which is the main theme of this document. A way to start exploring this issue is to write the GCFE equations as a system of evolution and constraint equations as usual. As aforementioned, it is only the equations for the components of the rescaled Weyl spinor that are PDEs. These are known to be symmetric hyperbolic which is a crucial property for a stable numerical evolution, and checking this is straightforward. The first problem is to investigate how to impose boundary conditions for these equations, and what surfaces should be chosen for the boundaries. The boundary conditions need to be numerically stable and the characteristic quantities of the system, i.e. the ingoing and outgoing modes and the modes that propagate along the boundaries, need to be classified in order to know which modes to specify and which to leave alone. This problem deals with the evolution system side of the equations, but a major issue is the constraint system. In order to investigate how the constraints propagate, the so-called subsidiary system (sometimes called the constraint propagation system), which is essentially the time derivative of the constraint equations, needs to be studied. An important property of the GCFE is that each constraint propagation equation is a combination of the constraints themselves, and all are ODEs except for the rescaled Weyl spinor constraints, which are PDEs. So for an IVP, if the constraints are satisfied initially, they are satisfied for all time *from an analytic perspective*. However as they can only be numerically approximated to some finite precision on the computer, *constraint propagation on the numerical level is unclear*. Moreover, the chosen boundary data for the IBVP may violate the constraints, and hence the constraint propagation equations that are PDEs may propagate this violation into the interior of the domain and destroy the accuracy there as well. This is the major problem to address in the formulation of the IBVP.

An investigation into the IBVP for the GCFE has been done before. Friedrich presented a particular way of writing the equations for Anti-de Sitter space-time [48] so that one obtains a well posed IBVP where the subsidiary system is made up entirely of ODEs. This forgoes

the problem of constraint violating modes propagating in from the boundary. He chooses the boundary to be the time-like conformal boundary and utilises properties of this special surface to derive his system. This means that this formulation can not be generalised to other space-times, in particular to asymptotically flat space-times. This specific case has not been investigated numerically and no investigations into a more general IBVP, whether it be analytical or numerical, have been done.

The fact that the GCFE seems to be the "cleanest", if not the best way to study global properties of space-times and has not been numerically investigated in any great detail is surprising. There is even more need to investigate the numerical implementation now that LIGO have directly detected gravitational waves on two separate occasions [1, 2]. Hence this thesis is primarily concerned with the numerical implementation of the GCFE and in particular its IBVP formulation.

Chapter 1 gives an overview of the relevant mathematics and the MCFE and GCFE are derived in the tensor formalism. Chapter 2 gives a derivation of the GCFE written in the space-spinor formalism and the $\eth$-calculus is introduced and imposed on the system. Chapter 3 discusses the equation describing the rescaled Weyl spinor and a boundary treatment is formulated which implies the propagation of the constraints. Chapter 4 discusses necessary checks of correctness of our system from an analytical perspective. Chapter 5 presents the numerical implementation of the system derived in chapter 2 and chapter 6 shows results of tests against an exact solution and the boundary treatment detailed in chapter 3 is verified for a simple case. Chapter 7 summarises the global structure of space-times with constant curvature and black holes embedded in them and chapter 8 reproduces the global structure of these black hole space-times numerically. Finally, chapter 9 presents numerical results from the application of gravitational perturbations of the Schwarzschild space-time as a 2+1 axially-symmetric system. The setup of the IBVP for gravitational perturbations of Schwarzschild is discussed and our boundary treatment is numerically shown to propagate constraints. An approach to compute the Bondi-mass on null-infinity is presented and applied to the perturbed Schwarzschild space-time and the Bondi-Sachs mass-loss is

reproduced.

Part I

The conformal representation of Einstein's field equations

Chapter 1

The derivation

1.1 Motivation

In order to study the global properties of isolated systems, we must solve the vacuum field equation

$$\tilde{R}_{ab}[\tilde{g}] = \lambda \tilde{g}, \tag{1.1.1}$$

where we will use a $\tilde{}$ to denote the quantities coming from the "physical" Lorentzian space-time $(\tilde{M}, \tilde{g})$ and λ the cosmological constant. However one cannot solve (1.1.1) directly at points an infinite distance from an observer as these points are "at infinity" and hence undefined. A resolution to this problem is to change how distance is measured. Rescaling the physical metric by a conformal factor Θ,

$$g = \Theta^2 \tilde{g}, \tag{1.1.2}$$

allows us to see conformal infinity, i.e. the points $\{\Theta = 0\}$ of the physical space-time, as regular points in the "conformal/unphysical space-time" (M, g). We can think about this as follows: If we were to measure the distance from a point to infinity with respect to metre-sticks from the physical metric, this would, by definition, take forever. However, if we were to increase the length of these metre-sticks each time we used one by a large enough amount, we may in fact get to infinity within a finite time with respect to these rescaled metre-sticks. We can then think of the conformal metric as measuring distance using these ever larger metre-sticks. This conformal rescaling obviously alters distance but preserves angles. The

consideration of the metric structure up to scaling by a conformal factor is called the conformal structure.

In order to study points at infinity, we must rewrite (1.1.1) in terms of quantities from the conformal space-time. First, we consider some properties of the conformal structure.

1.2 Weyl connections

The most common type of connection used in the field of general relativity is the unique Levi-Civita connection (also called the metric connection) for a given space-time. Given we have a Levi-Civita connection $\widetilde{\nabla}$ for a space-time $(\widetilde{M}, \widetilde{g})$, the connection satisfies the torsion-free property

$$[\widetilde{\nabla}_a, \widetilde{\nabla}_b] f = 0,$$

for all functions f and the metric-compatibility property

$$\widetilde{\nabla}_a \widetilde{g}_{bc} = 0.$$

We want to study a generalisation of this type of connection, namely a *conformal Weyl connection* (also just called a Weyl connection) which is still torsion-free but does not have the metric-compatibility property. Dropping metric-compatibility means that were are not interested in distances, only the conformal structure. This type of connection is exploited by Friedrich in his derivation of the generalised conformal field equations, derived in section 1.6.

Let $\widetilde{\nabla}$ be a Levi-Civita connection for a space-time $(\widetilde{M}, \widetilde{g})$. Then using $g_{ab} = \Theta^2 \widetilde{g}_{ab}$ for some conformal factor Θ, the connection $\widetilde{\nabla}$ acts on the conformally rescaled metric g like

$$\widetilde{\nabla}_a g_{bc} = 2\Theta^{-1} \nabla_a \Theta g_{bc}.$$

We want to generalise from a Levi-Civita connection by dropping metric-compatibility but keeping the torsion-free property. Then a Weyl connection $\widehat{\nabla}$ of the conformal structure is defined by

$$\widehat{\nabla}_a g_{bc} = -2 f_a g_{bc}, \tag{1.2.1}$$

with some 1-form f_a. The logical question is how these connections act on arbitrary vectors and co-vectors. There exists a tensor $f_{ab}{}^c$ that transforms one covariant derivative to another and so we define the action on co-vectors as

$$(\widehat{\nabla}_b - \nabla_b)\omega_a = -f_{ab}{}^c\omega_c, \tag{1.2.2}$$

from which it can be shown that

$$(\widehat{\nabla}_b - \nabla_b)v^a = f_{bc}{}^a v^c, \tag{1.2.3}$$

for some $f_{ab}{}^c$ which is symmetric in its first two indices. It follows that the relationship between connection coefficients defined by $\widehat{\Gamma}_{\mathbf{ab}}{}^{\mathbf{c}} := \delta^{\mathbf{c}}{}_b\delta_{\mathbf{a}}{}^a\widehat{\nabla}_a\delta_{\mathbf{b}}{}^b$ and $\Gamma_{\mathbf{ab}}{}^{\mathbf{c}} := \delta^{\mathbf{c}}{}_b\delta_{\mathbf{a}}{}^a\nabla_a\delta_{\mathbf{b}}{}^b$ is given by

$$\widehat{\Gamma}_{\mathbf{ab}}{}^{\mathbf{c}} = \Gamma_{\mathbf{ab}}{}^{\mathbf{c}} - f_{\mathbf{ab}}{}^{\mathbf{c}}. \tag{1.2.4}$$

In order to compute an expression for this, we write

$$\begin{aligned}
&\widehat{\nabla}_a g_{bc} = \nabla_a g_{bc} - f_{ab}{}^d g_{dc} - f_{ac}{}^d g_{bd} \\
&\Rightarrow f_{ab}{}^d g_{dc} + f_{ac}{}^d g_{bd} = 2f_a g_{bc} \\
&\Rightarrow f_{abc} + f_{acb} = 2f_a g_{bc}.
\end{aligned}$$

Using the same trick that is used to derive the expression for a metric equipped with a Levi-Civita connection in terms of Christoffel symbols, we permute the indices of the above equation to obtain

$$\begin{aligned}
f_{abc} + f_{acb} &= 2f_a g_{bc}, \\
f_{bac} + f_{bca} &= 2f_b g_{ac}, \\
f_{cab} + f_{cba} &= 2f_c g_{ab}.
\end{aligned}$$

Adding the last two and subtracting the first we find

$$f_{ab}{}^c = \delta^c{}_a f_b + \delta^c{}_b f_a - g_{ab}g^{cd}f_d. \tag{1.2.5}$$

The conformally invariant combination $g_{ab}g^{cd}$ guarantees that this formula holds for any metric in the conformal class.

Thus, we have shown that, given two Weyl connections in the same conformal class, we are able to express the action of one on a tensor with the action of the other on the tensor plus additional terms involving the 1-form between them. We will make extensive use of this in the following chapters.

1.3 Conformal geodesics

In this section we derive the conformal geodesic equations and specify a transport equation for a frame along them.

Just as a metric geodesic is related to the metric structure, a conformal geodesic is related to the conformal structure. We know that geodesics are auto-parallel curves, and in order to formulate this we need to introduce a connection defined along the curve in question. However, for the notion of conformal geodesics we have an entire equivalence class to choose from, so we require that the geodesic γ is geodetic with respect to a conformal Weyl connection defined along it. In order to write this down mathematically, fix a connection ∇ from the conformal class and define u^a to be the tangent vector to the geodesic. The geodetic property then implies the existence of a 1-form h_a along γ such that

$$u^b \nabla_b u^a = 2\langle h, u\rangle u^a - (u \cdot u) h^a, \tag{1.3.1}$$

where the scalar products $(\ \cdot\ )$ and $\langle \cdot, \cdot \rangle$ do and do not need the associated metric, respectively. By virtue of (1.2.3), the above says that γ is geodetic with respect to another connection $\bar{\nabla}$ in the conformal class. This is equivalent to saying that u is geodetic with respect to a connection $\bar{\nabla}$ defined on γ by

$$u^a \bar{\nabla}_a v^b - u^a \nabla_a v^b = -(h_a \delta^b_c + h_c \delta^b_a - g_{ac} h^b) u^a v^c.$$

Let $\widehat{\nabla}$ be another conformal Weyl connection, related to ∇ by (1.2.2) with 1-form f. If γ

satisfies (1.3.1), then

$$\begin{aligned} u^a \widehat{\nabla}_a u^b &= u^a f_{ac}{}^b u^c - 2\langle h, u\rangle u^b + (u\cdot u)h^b \\ &= (\delta^b_a f_c + \delta^b_c f_a - g_{ac}g^{bd}f_d) - 2\langle h, u\rangle u^b + (u\cdot u)h^b \\ &= 2\langle f, u\rangle u^b - (u\cdot u)f^b - 2\langle h, u\rangle u^b + (u\cdot u)h^b \\ &= -2\langle h - f, u\rangle u^b + (u\cdot u)(h^b - f^b). \end{aligned}$$

Thus we have that u is geodetic with respect to (∇, h) iff it is geodetic with respect to $(\widehat{\nabla}, h - f)$.

We now want to see the relationship between two connections along γ for which u is geodetic. Let $\bar{\nabla}$ and ∇ be two such connections, then there exists a 1-form f along γ such that

$$u^b \bar{\nabla}_b u^a - u^b \nabla_b u^a = -2\langle f, u\rangle u^a + (u\cdot u)f^a = 0.$$

Thus f^a and u^a are proportional along γ, and writing $f_a = f u_a$, we find that

$$f(u\cdot u)u^a = 0,$$

from which we conclude that $f = 0$ along γ.

Hence the two connections are the same. This suggests the introduction of an equivalence relation between conformal Weyl connections for which γ is a geodesic by saying they are equivalent iff the 1-form defined by their difference vanishes on γ.

Now we have raised the question of how we should pick a representative from this equivalence class. Consider the Schouten tensor for ∇, defined as

$$P_{ab} := -\frac{1}{4}R_{[ab]} - \frac{1}{2}\Big(R_{(ab)} - \frac{1}{6}R g_{ab}\Big),$$

with indices raised and lowered with the metric g and the Schouten tensor for $\widehat{\nabla}$, whose difference is given by

$$P_{ab} - \widehat{P}_{ab} = \nabla_a f_b - f_a f_b + \frac{1}{2}g_{ab}f_c f^c,$$

which is just $\nabla_a f_b$ on γ. Given a connection ∇ in the equivalence class with Schouten tensor P we can seek the solution to the equation

$$u^a \widehat{P}_{ab} = u^a P_{ab} - u^a \nabla_a f_b.$$

Since h_a should satisfy a conformally invariant equation along γ, we look at the difference (defining $\hat{h}_a := h_a - f_a$)

$$\begin{aligned} u^b \nabla_b h^a - u^b \widehat{\nabla}_b h_a &= u^b \nabla_b h_a - u^b \nabla_b h_a + u^b \nabla_b f_a + f^c_{ab} \hat{h}_c u^b \\ &= u^b (P_{ba} - \widehat{P}_{ba} + h_{(a} h_{b)} - \hat{h}_{(a} \hat{h}_{b)} - \frac{1}{2} g_{ab} (h \cdot h)) + \frac{1}{2} g_{ab} (\hat{h} \cdot \hat{h}). \end{aligned}$$

Hence we have

$$u^b \nabla_b h_a - \langle h, u \rangle h_a + \frac{1}{2}(h \cdot h) u_a - P_{ba} u^b = u^b \widehat{\nabla}_b \hat{h}_a - \langle \hat{h}, u \rangle \hat{h}_a + \frac{1}{2}(\hat{h}, \hat{h}) u_a - \widehat{P}_{ba} u^b.$$

Thus the expression

$$u^b \nabla_b h_a - \langle h, u \rangle h_a + \frac{1}{2}(h \cdot h) u_a + P_{ba} u^b$$

is invariant under change of connection and under conformal rescalings. This expression also turns out to vanish on γ. This can be seen by rescaling the metric appropriately so that the corresponding P_{ab} vanishes and using the connection for which the geodesic is an auto-parallel curve.

Lastly, we should define how a frame $e^a_{\mathbf{i}}$, $i = 0, 1, 2, 3$ is transported along the curve. It is easily seen that

$$\begin{aligned} u^b \nabla_b e^a_i - u^b \widehat{\nabla}_b e^a_i &= -f_{bc}{}^a u^b e^a_i \\ &= -\langle h, e_i \rangle u^a - \langle h, u \rangle e^a_i + (u \cdot e_i) h^a, \end{aligned}$$

and requiring that the frame is parallel transported by $\widehat{\nabla}$, we find our equation.

The **Conformal Geodesic Equations** are then given by

$$u^b \nabla_b u^a = -2 \langle h, u \rangle u^a + (u \cdot u) h^a, \tag{1.3.2a}$$

$$u^b \nabla_b h_a = \langle h, u \rangle h_a - \frac{1}{2} u_a (h \cdot h) - u^b P_{ba}, \tag{1.3.2b}$$

where a frame is transported along them according to

$$u^b \nabla_b e_i^a = -\langle h, u\rangle (e_i)^a - \langle h, e_i\rangle u^a + (u \cdot e_i) h^a. \tag{1.3.3}$$

Alternatively, these equations are sometimes written in terms of the difference tensor $f_{ab}{}^c$;

$$u^b \nabla_b u^a = -f_{bc}{}^a u^b u^c, \tag{1.3.4a}$$

$$u^b \nabla_b h_a = \frac{1}{2} h_c f_{ba}{}^c u^b - u^b P_{ba}, \tag{1.3.4b}$$

$$u^b \nabla_b e_i^a = -f_{bc}{}^a e_i^b u^c. \tag{1.3.4c}$$

Let us suppose that we have a solution $\{u^a, b_a\}$ of the conformal geodesic equations above. Then the 1-form b_a defines a unique connection, say $\widehat{\nabla}$. Written with respect to this connection, the equations simplify to

$$u^b \widehat{\nabla}_b u^a = 0, \tag{1.3.5a}$$

$$\widehat{P}_{ab} u^a = 0, \tag{1.3.5b}$$

$$u^b \widehat{\nabla}_b (e_i)^a = 0. \tag{1.3.5c}$$

This simplification will be made use of in section 1.6.2 when we define the conformal Gauss gauge.

1.4 Conformal transformation laws

We now derive the conformal transformation laws of the curvature quantities that are necessary in the derivation of the conformal field equations in 4-dimensions. A summary of these can be found in appendix A.2.

Let ∇ be a Levi-Civita connection with metric g and $\widehat{\nabla}$ a Weyl connection from the conformal class defined by g, related by the usual equation with 1-form f_a. One can decompose the Riemann tensor into trace and trace-free parts, which for a Weyl connection has the form

$$\widehat{R}_{abc}{}^d = 2\Big(\delta^d{}_{[a}\widehat{P}_{b]c} - \delta^d{}_c \widehat{P}_{[ab]} - g_{c[a}\widehat{P}_{b]}{}^d\Big) + \widehat{C}_{abc}{}^d, \tag{1.4.1}$$

where the trace portions are represented by the Schouten tensor

$$\widehat{P}_{ab} = -\frac{1}{4}\widehat{R}_{[ab]} - \frac{1}{2}\Big(\widehat{R}_{(ab)} - \frac{1}{6}\widehat{R} g_{ab}\Big), \tag{1.4.2}$$

and where the $C_{abc}{}^{d}$ is the Weyl tensor. The Weyl tensor is conformally invariant, i.e.

$$\widehat{C}_{abc}{}^{d} = C_{abc}{}^{d}, \tag{1.4.3}$$

and is considered to be the most important invariant of a conformal structure. Note that although we say the Weyl tensor is conformally invariant, this statement is dependent on the position of the indices as the metric g_{ab} and its inverse are not conformally invariant. In the following we raise and lower indices with metric g.

The difference of the curvature tensors is computed to be

$$\widehat{R}_{abc}{}^{d} - R_{abc}{}^{d} = 2\Big(\nabla_{[a}f_{b]c}{}^{d} - f_{[a|c|}{}^{e}f_{b]e}{}^{d}\Big). \tag{1.4.4}$$

We subsequently find the relationship between the Ricci tensors to be

$$\widehat{R}_{ab} - R_{ab} = 3\nabla_a f_b - \nabla_b f_a - 2f_a f_b + g_{ab}(\nabla^c f_c + 2f_c f^c), \tag{1.4.5}$$

and the Ricci scalars to be

$$\widehat{R} - R = 6(\nabla^a f_a + f_a f^a). \tag{1.4.6}$$

By virtue of (1.4.2) and (1.4.4) we find the transformation law for the Schouten tensor to be

$$\widehat{P}_{ab} - P_{ab} = -\nabla_a f_b + f_a f_b - \frac{1}{2}g_{ab}f_c f^c. \tag{1.4.7}$$

It is of interest to look at the special case where the Weyl connection is the Levi-Civita connection for a physical metric $\widetilde{g}$, which we will now write as $\widetilde{\nabla}$, where the two metrics are conformally related by $g_{ab} = \Theta^2\widetilde{g}_{ab}$. In this case the 1-form f_a is exact and is given by

$$f_a = -\Theta^{-1}\nabla_a\Theta. \tag{1.4.8}$$

Substituting this into (1.4.5) we find

$$\widetilde{R}_{ab} - R_{ab} = -\frac{2}{\Theta}\nabla_a\nabla_b\Theta + g_{ab}\Big(\frac{3}{\Theta^2}\nabla^c\Theta\nabla_c\Theta - \frac{1}{\Theta}\nabla^c\nabla_c\Theta\Big). \tag{1.4.9}$$

Contracting[1] gives

$$\widetilde{R} - \Theta^2 R = 12\nabla^c\Theta\nabla_c\Theta - 6\Theta\nabla^c\nabla_c\Theta. \tag{1.4.10}$$

These transformations are singular on the point set $\{\Theta = 0\}$, which is a crucial problem in formulating a conformal representation of (1.1.1) that we will have to overcome.

[1] Remembering that $\widetilde{R}_{ab}$ is lowered with $\tilde{g}$.

1.5 Derivation of the Metric Conformal Field Equations (MCFE)

As can be seen from the general conformal transformation law of the Ricci tensor (1.4.5), the conformal version of the vacuum field equation (1.1.1) is not appropriate for investigations of conformal infinity. The first remedy for this was a set of equations given the name of the Metric Conformal Field Equations (MCFE), first derived by Friedrich in the early 1980's in [46] and [45]. Below, we follow the derivation given by Friedrich in [51], for the special case $\lambda = 0$. This simpler case incorporates the main issues that we want to discuss. For a derivation with non-zero λ and matter fields, see for example [56].

We begin our exploration with the second Bianchi identity for the conformal (Levi-Civita) connection, which is given by

$$\nabla_{[a}C_{bc]d}{}^{e} = 2\nabla_{[e}\Big(g_{|c|a}P_{b]}{}^{d} - \delta^{d}{}_{a}P_{b]c}\Big).$$

Contracting this once and using the fact that $\nabla_{[d}C_{ab]c}{}^{d} = \frac{1}{3}\nabla_{d}C_{abc}{}^{d}$ and $\delta^{a}{}_{a} = 4$ we obtain

$$\nabla_{d}C_{abc}{}^{d} = \nabla_{a}P_{bc} - \nabla_{b}P_{ab}. \tag{1.5.1}$$

Then since the above formula holds for the physical metric and connection as well, i.e.

$$\widetilde{\nabla}_{d}\widetilde{C}_{abc}{}^{d} = \widetilde{\nabla}_{a}\widetilde{P}_{bc} - \widetilde{\nabla}_{b}\widetilde{P}_{ab},$$

and we are assuming the physical metric satisfies the vacuum field equation, we have

$$\widetilde{\nabla}_{d}\widetilde{C}_{abc}{}^{d} = \widetilde{\nabla}_{d}C_{abc}{}^{d} = 0. \tag{1.5.2}$$

It follows that we should hunt for a similar equation in the conformally rescaled space-time. Let us look at a conformal rescaling of the Weyl tensor with conformal weight k, so that it looks like

$$\Theta^{k}\widetilde{\nabla}_{d}C_{abc}{}^{d}. \tag{1.5.3}$$

Then replacing the physical connection with the conformal one, we find the relationship

$$\nabla_{a}(\Theta^{k}C_{abc}{}^{d}) = \Theta^{k}\Big((k+1)\Theta^{-1}C_{abc}{}^{d}\nabla_{d}\Theta + \widetilde{\nabla}_{d}C_{abc}{}^{d}\Big).$$

By defining

$$K_{abc}{}^{d} = \Theta^{-1} C_{abc}{}^{d}, \tag{1.5.4}$$

we obtain the equation

$$\nabla_{d} K_{abc}{}^{d} = 0. \tag{1.5.5}$$

This is the central equation of the conformal field equations.

The rescaled Weyl tensor is called the gravitational tensor, it is conformally invariant and is used in place of $C_{abc}{}^{d}$ to extract gravitational radiation at infinity. It can be shown through the use of the second vacuum Bianchi identity and the topology of $\mathscr{I}$ being $\mathbb{R} \times \mathbb{S}^2$ that $C_{abc}{}^{d}$ vanishes on $\mathscr{I}$ and hence the Weyl tensor is of no use in extracting information about the gravitational field there. As $\Theta = 0$ on $\mathscr{I}$ also, $K_{abc}{}^{d}$ is potentially, and is in fact found to be well-defined on the conformal boundary and hence provides a way of extracting radiation at infinity.

Now rewriting the decomposition of the Riemann tensor, we immediately have

$$R_{abc}{}^{d} = 2\Big(g^{a}{}_{[c} P_{d]b} - g_{b[c} P_{d]}{}^{a}\Big) + \Theta^{-1} K_{abc}{}^{d},$$

and from (1.5.4) and (1.5.5) we find

$$\nabla_{d} C_{abc}{}^{d} = K_{abc}{}^{d} \nabla_{d} \Theta, \tag{1.5.6}$$

which can then be substituted into 1.5.1 to give an equation for the Schouten tensor. This takes the form

$$\nabla_{a} P_{bc} - \nabla_{b} P_{ab} = \nabla_{d} \Theta K_{abc}{}^{d}. \tag{1.5.7}$$

One can already see that we are making progress in the construction of a set of "conformal field equations" that are regular on the conformal boundary. The problem of the conformal factor being in the denominator of (1.4.9) has been overcome! Assuming that we have the conformal factor, we solve (1.5.5) for the gravitational tensor, and then (1.5.7) for the rescaled Schouten tensor. However as Θ is not necessarily known beforehand, it must somehow be added to the set of conformal field equations and be computed along with the other unknowns.

Now we try to find an equation for the conformal factor. We do this in the following way:

- Write the trace-free part of the field equation as $\widetilde{R}_{ab} = \frac{1}{4}\widetilde{R}\widetilde{g}_{ab}$.
- Insert this into the transformation law (1.4.9) and use (1.4.10) to express $\widetilde{R}$ in terms of R.
- Combine the R_{ab} and R terms into a Schouten tensor term, leaving only an R term.
- Solve for $\nabla_a\nabla_b\Theta$.

The result of the above is the equation

$$\nabla_a\nabla_b\Theta = sg_{ab} - \Theta P_{ab}, \tag{1.5.8}$$

where we have defined

$$s := \frac{1}{4}\nabla^c\nabla_c\Theta - \frac{1}{24}R\Theta. \tag{1.5.9}$$

This equation will describe the evolution of the conformal factor, as desired, however we now need an equation for the unknown s.

Obviously (1.5.8) is over determined, due to having multiple equations for one unknown, so we try to derive an integrability condition. We do this by applying ∇_c to both sides, commute ∇_c with ∇_a, contract b and c, and use the twice contracted second Bianchi identity $\nabla^a P_{ab} = -\frac{1}{6}Rg_{ab}$. This eventually yields the simple equation

$$\nabla_a s = -\nabla^b\Omega P_{ab}, \tag{1.5.10}$$

which we will use as our equation for s.

Finally, we rewrite the transformation law (1.4.10) in terms of the scalar s. This gives a nice cancellation of the R terms to leave us with the equation

$$2\Theta s - \nabla^c\Theta\nabla_c\Theta = 0, \tag{1.5.11}$$

which constrains s and Θ.

It is clear that equations (1.5.8), (1.5.10), and (1.5.11) are regular on the conformal boundary and can be used to determine Θ. Thus, we now have a closed system of equations for the unknowns

$$g_{ab},\ \Theta,\ s,\ P_{ab},\ K_{abc}{}^{d}. \tag{1.5.12}$$

These equations are called the **Metric Conformal Field Equations**:

$$\nabla_d K_{abc}{}^{d} = 0, \tag{1.5.13a}$$

$$R_{abc}{}^{d} = 2\Big(g^{a}{}_{[c}P_{d]b} - g_{b[c}P_{d]}{}^{a}\Big) + \Theta K_{abc}{}^{d}, \tag{1.5.13b}$$

$$\nabla_a P_{bc} - \nabla_b P_{ac} = \nabla_a \Theta K_{abc}{}^{d}, \tag{1.5.13c}$$

$$\nabla_a \nabla_b \Theta = s g_{ab} - \Theta P_{ab}, \tag{1.5.13d}$$

$$\nabla_a s = -\nabla^b \Theta P_{ab}. \tag{1.5.13e}$$

These equations are regular in the limit $\Theta \to 0$ and, by construction, conformally invariant. The MCFE derived above were the first equations to rewrite (1.1.1) in a conformal setting with regularity at the conformal boundary. They have one major drawback, however, namely that the conformal factor Θ is an unknown in the system, and hence one does not know where the conformal boundary is *a-priori*. This begs the question as to whether a set of equations can be obtained where one has Θ *a-priori*. These equations do exist, and are known as the Generalised Conformal Field Equations. We will derive these in the next section using our knowledge of Weyl connections.

1.6 Derivation of the Generalised Conformal Field Equations (GCFE)

The idea of the GCFE is to introduce extra gauge freedom into the equations by generalising to a Weyl connection. A specific choice of Weyl connection is defined which leads to a gauge in which the evolution equations are significantly simpler than those derived from the MCFE, and of particular importance, in which one knows the conformal factor *a-priori*. We will eventually write these in the space-spinor formalism, however in order to get the idea of how they work it is much simpler to consider the tensorial version first.

1.6.1 Generalising to a Weyl connection

Let $\tilde{g}$ be a solution to the vacuum EFE with cosmological constant λ and let $g = \Theta^2\tilde{g}$ be the conformal metric. Furthermore, let f and b be smooth 1-forms. We denote by ∇ and $\widetilde{\nabla}$ the Levi-Civita connections of g and $\tilde{g}$ respectively and by $\widehat{\nabla}$ a Weyl connection in the conformal class. Its action on the metric tensors $\tilde{g}$ and g are given by

$$\widehat{\nabla}_a\tilde{g}_{bc} = -2b_a\tilde{g}_{bc}, \tag{1.6.1}$$

$$\widehat{\nabla}_a g_{bc} = -2f_a g_{bc}. \tag{1.6.2}$$

It follows immediately that the 1-forms are related via

$$f_a = b_a - \Theta^{-1}\nabla_a\Theta. \tag{1.6.3}$$

For reasons that will later become apparent, we also define another 1-form as

$$h_a := \Theta b_a = f_a + \nabla_a\Theta. \tag{1.6.4}$$

We now introduce coordinates x^μ and frame field $e^a_{\mathbf{a}}$, which is orthonormal with respect to the conformal metric g and we define $\eta_{\mathbf{ij}} := g_{ab}e^a_{\mathbf{i}}e^b_{\mathbf{j}}$. We then have

$$c^\mu_{\mathbf{a}} := e_{\mathbf{a}}(x^\mu) = \widehat{\nabla}_{\mathbf{a}}x^\mu, \qquad \widehat{\nabla}_{\mathbf{a}}e_{\mathbf{b}} = \widehat{\Gamma}_{\mathbf{ab}}{}^{\mathbf{c}}e_{\mathbf{c}}. \tag{1.6.5}$$

By writing (1.6.2) in our basis $e_{\mathbf{a}}$ and contracting with $e^b_{\mathbf{b}}e^c_{\mathbf{c}}$, we find

$$f_{\mathbf{a}} = \frac{1}{4}\widehat{\Gamma}_{\mathbf{ab}}{}^{\mathbf{b}}.$$

We are now in a position to start writing down the field equations.

The first two are Cartan's two structure equations [68], where the torsion-free equation is given by

$$\left[\widehat{\nabla}_a, \widehat{\nabla}_b\right]x^\mu = 0, \tag{1.6.6}$$

and the curvature equation is given by

$$\left[\widehat{\nabla}_a, \widehat{\nabla}_b\right]e_{\mathbf{c}} = \widehat{R}_{ab\mathbf{c}}{}^{\mathbf{d}}e_{\mathbf{d}}. \tag{1.6.7}$$

Contracting these equations with $e^a_{\mathbf{a}} e^b_{\mathbf{b}}$ and using the decomposition of the Riemann tensor (1.4.1) yields the two equations

$$e_{\mathbf{a}}(c^\mu_{\mathbf{b}}) - e_{\mathbf{b}}(c^\mu_{\mathbf{a}}) = \widehat{\Gamma}_{\mathbf{ab}}{}^{\mathbf{c}} c^\mu_{\mathbf{c}} - \widehat{\Gamma}_{\mathbf{ba}}{}^{\mathbf{c}} c^\mu_{\mathbf{c}}, \tag{1.6.8}$$

$$\begin{aligned} e_{\mathbf{a}}(\widehat{\Gamma}_{\mathbf{bc}}{}^{\mathbf{d}}) - e_{\mathbf{b}}(\widehat{\Gamma}_{\mathbf{ac}}{}^{\mathbf{d}}) &= \widehat{\Gamma}_{\mathbf{ab}}{}^{\mathbf{e}} \widehat{\Gamma}_{\mathbf{ec}}{}^{\mathbf{d}} - \widehat{\Gamma}_{\mathbf{ba}}{}^{\mathbf{e}} \widehat{\Gamma}_{\mathbf{ec}}{}^{\mathbf{d}} - \widehat{\Gamma}_{\mathbf{bc}}{}^{\mathbf{e}} \widehat{\Gamma}_{\mathbf{ae}}{}^{\mathbf{d}} + \widehat{\Gamma}_{\mathbf{ac}}{}^{\mathbf{e}} \widehat{\Gamma}_{\mathbf{be}}{}^{\mathbf{d}} \\ &\quad + C_{\mathbf{abc}}{}^{\mathbf{d}} - 2\eta_{\mathbf{c}[\mathbf{a}} \hat{P}_{\mathbf{b}]}{}^{\mathbf{d}} + 2\delta_{[\mathbf{a}}{}^{\mathbf{d}} \hat{P}_{\mathbf{b}]\mathbf{c}} - 2\hat{P}_{[\mathbf{ab}]} \delta_{\mathbf{c}}{}^{\mathbf{d}}. \end{aligned} \tag{1.6.9}$$

The next equation comes from the Bianchi identity for the vacuum metric $\widetilde{g}$,

$$\widetilde{\nabla}_{[e} \widetilde{R}_{ab]c}{}^{d} = \widetilde{\nabla}_{[e} C_{ab]c}{}^{d} = 0. \tag{1.6.10}$$

Rewriting this in terms of the conformal connection and gravitational tensor gives the simple equation

$$\nabla_e K_{abc}{}^{e} = 0. \tag{1.6.11}$$

Written in terms of the Weyl connection, we find

$$\widehat{\nabla}_e K_{abc}{}^{e} = f_e K_{abc}{}^{e}. \tag{1.6.12}$$

The final task is to look at the Bianchi equations for the Weyl connection. The second Bianchi identity is

$$\widehat{\nabla}_{[e} \widehat{R}_{ab]c}{}^{d} = 0, \tag{1.6.13}$$

which, when contracted once, gives

$$\widehat{\nabla}_e \widehat{R}_{abc}{}^{e} + \widehat{\nabla}_a \widehat{R}_{bc} - \widehat{\nabla}_b \widehat{R}_{ac} = 0. \tag{1.6.14}$$

Decomposing the Riemann tensor using (1.4.1), the first term can be written as

$$\widehat{\nabla}_e \widehat{R}_{abc}{}^{e} = \widehat{\nabla}_e C_{abc}{}^{e} - 2g_{c[a} \widehat{\nabla}^e \widehat{P}_{b]e} + 2\widehat{\nabla}_{[a} \widehat{P}_{b]c} - 2\nabla_c \widehat{P}_{[ab]}. \tag{1.6.15}$$

From the decomposition of the Riemann tensor, we find a relationship between the Ricci tensor and Schouten tensor, namely

$$\widehat{R}_{ac} = -2\widehat{P}_{ac} - g_{ac}\widehat{P} - 2\widehat{P}_{[ac]}. \tag{1.6.16}$$

Using (1.6.15) and (1.6.16) in the once-contracted Bianchi identity (1.6.14) gives us

$$\widehat{\nabla}_e C_{abc}{}^{e} - 2g_{c[a} \left(\widehat{\nabla}^e \widehat{P}_{b]e} - \widehat{\nabla}_{b]} \widehat{P} + 2f_{b]} \widehat{P} \right) - 2\widehat{\nabla}_{[a} \widehat{P}_{b]c} - 2\widehat{\nabla}_c \widehat{P}_{[ab]} - 2\widehat{\nabla}_a \widehat{P}_{[bc]} - 2\widehat{\nabla}_b \widehat{P}_{[ca]} = 0. \tag{1.6.17}$$

This can be simplified by looking at the once-contracted first Bianchi identity

$$2\widehat{R}_{ac} + \widehat{R}_{cab}{}^{b} = 0,$$

along with the expression

$$\left[\widehat{\nabla}_a, \widehat{\nabla}_b\right] g_{cd} = -2\widehat{R}_{ab(cd)} = -4\widehat{\nabla}_{[a} f_{b]} g_{cd}.$$

Combining these gives us the relationship

$$\widehat{R}_{[ab]} = 4\widehat{\nabla}_{[a} f_{b]}. \tag{1.6.18}$$

Expanding out the right-hand side and using $\widehat{R}_{[abc]}{}^{d} = 0$ yields the useful equation

$$\widehat{\nabla}_{[a}\widehat{P}_{bc]} = 0. \tag{1.6.19}$$

Using this we can simplify (1.6.17) to

$$\widehat{\nabla}_e C_{abc}{}^{e} - 2g_{c[a}\left(\widehat{\nabla}^e \widehat{P}_{b]e} - \widehat{\nabla}_{b]}\widehat{P} + 2f_{b]}\widehat{P}\right) - 2\widehat{\nabla}_{[a}\widehat{P}_{b]c} = 0.$$

Transvecting this with g^{bc} we obtain

$$4\left(\widehat{\nabla}^e \widehat{P}_{ae} - \widehat{\nabla}_a \widehat{P} + 2f_a \widehat{P}\right) = 4\widehat{\nabla}^e\left(\widehat{P}_{ae} - g_{ae}\widehat{P}\right) = 0,$$

and thus we arrive at the equation

$$\widehat{\nabla}_e C_{abc}{}^{e} - 2\widehat{\nabla}_{[a}\widehat{P}_{b]c} = 0.$$

Replacing the Weyl tensor with the gravitational tensor and using its equation (1.6.12), we get the final equation

$$\widehat{\nabla}_a \widehat{P}_{bc} - \widehat{\nabla}_b \widehat{P}_{ac} = \left(\widehat{\nabla}_e \Theta + \Theta f_e\right) K_{abc}{}^{e} = h_e K_{abc}{}^{e}. \tag{1.6.20}$$

We can now write down the full set of conformal field equations expressed with a Weyl connection:

$$e_{\mathbf{a}}(c^{\mu}_{\mathbf{b}}) - e_{\mathbf{b}}(c^{\mu}_{\mathbf{a}}) = \widehat{\Gamma}_{\mathbf{ab}}{}^{\mathbf{c}} c^{\mu}_{\mathbf{c}} - \widehat{\Gamma}_{\mathbf{ba}}{}^{\mathbf{c}} c^{\mu}_{\mathbf{c}}, \tag{1.6.21a}$$

$$\begin{aligned} e_{\mathbf{a}}(\widehat{\Gamma}_{\mathbf{bc}}{}^{\mathbf{d}}) - e_{\mathbf{b}}(\widehat{\Gamma}_{\mathbf{ac}}{}^{\mathbf{d}}) = {} & \left(\widehat{\Gamma}_{\mathbf{ab}}{}^{\mathbf{e}} - \widehat{\Gamma}_{\mathbf{ba}}{}^{\mathbf{e}}\right)\widehat{\Gamma}_{\mathbf{ec}}{}^{\mathbf{d}} - \widehat{\Gamma}_{\mathbf{bc}}{}^{\mathbf{e}}\widehat{\Gamma}_{\mathbf{ae}}{}^{\mathbf{d}} + \widehat{\Gamma}_{\mathbf{ac}}{}^{\mathbf{e}}\widehat{\Gamma}_{\mathbf{be}}{}^{\mathbf{d}} \\ & + \Theta K_{\mathbf{abc}}{}^{\mathbf{d}} - 2\eta_{\mathbf{c}[\mathbf{a}}\widehat{P}_{\mathbf{b}]}{}^{\mathbf{d}} + 2\delta_{[\mathbf{a}}{}^{\mathbf{d}}\widehat{P}_{\mathbf{b}]\mathbf{c}} - 2\widehat{P}_{[\mathbf{ab}]}\delta_{\mathbf{c}}{}^{\mathbf{d}}, \end{aligned} \tag{1.6.21b}$$

$$\widehat{\nabla}_a \widehat{P}_{bc} - \widehat{\nabla}_b \widehat{P}_{ac} = h_e K_{abc}{}^{e}, \tag{1.6.21c}$$

$$\nabla_e K_{abc}{}^{e} = 0. \tag{1.6.21d}$$

1.6.2 The Conformal Gauss Gauge (CGG)

In deriving the set of equations (1.6.21), we have artificially introduced gauge freedom via the conformal metric and Weyl connection. By analogy to the MCFE, we are lacking an equation for the conformal factor Θ. Now however, we have the additional problem of not having an equation for the 1-form f_a. These gauge freedoms are fixed using properties of the conformal structure only. The gauge imposed in this section is known as the Conformal Gauss Gauge (CGG). In the below, an underline is used to denote quantities defined on an initial surface which have indices $1, 2, 3$.

We fix the frame and coordinates as follows: Choose an initial space-like hypersurface $\widetilde{S}$ of the vacuum solution $(\widetilde{M}, \widetilde{g})$. Then on $\widetilde{S}$, choose a conformal factor $\underline{\Theta}$, a 1-form $\underline{b}_a$, coordinates $\underline{x}^\mu$, and a frame $\underline{e}_{\mathbf{a}}$ which is orthonormal with respect to the conformal metric $\underline{g}_{ab} = \underline{\Theta}^2 \underline{\widetilde{g}}_{ab}$ and such that $\underline{e}_{\mathbf{0}}$ is normal to $\widetilde{S}$. Then the initial data $\{\underline{u}^a := \underline{e}_{\mathbf{0}},\ \underline{b}_a\}$ define through each point of $\widetilde{S}$ a unique conformal geodesic. Provided sufficiently smooth initial data, this congruence is smooth and caustic free in a local neighbourhood $U \subset M$ of $\widetilde{S}$. The 1-form b_a in U then defines a unique Weyl connection such that the conformal geodesic equations reduce to equations (1.3.5a). The frame is extended to U by transport along the conformal geodesics with equation (1.3.3). The conformal factor can then by chosen such that $g(e_{\mathrm{i}}, e_{\mathrm{j}}) = \eta_{\mathrm{ij}}$ in U. The coordinates are extended to U by setting x^0 to be the parameter of the conformal geodesics s, and dragging the spatial coordinates along the geodesics.
In this gauge, we find the simplifications

$$u^a \widehat{\nabla}_a x^\alpha = 0, \quad u^a \widehat{\nabla}_a s = 1, \qquad\qquad \alpha = 1, 2, 3. \tag{1.6.22}$$

From the equations $g_{ab} = \Theta^2 \widetilde{g}_{ab}$ and $\widehat{\nabla}_a \widetilde{g}_{bc} = -2 b_a \widetilde{g}_{bc}$ we obtain

$$\dot{\Theta} = u^e b_e \Theta, \tag{1.6.23}$$

where we have defined an over-dot as $u^a \nabla_a$. This could then be used as an equation for the conformal factor. Using this and the conformal geodesic equations, we could also find an equation for the 1-form h_a. Supplementing the system with these equations would then give us a complete system. However, something surprising happens when looking at successive

derivatives of the conformal factor. One in fact finds

$$\dddot{\Theta} = 0. \tag{1.6.24}$$

Defining the scalars

$$U = \Theta^2 \widetilde{g}_{ab} u^a u^b, \quad Z = \Theta b_a u^a, \quad H = \Theta^{-1}(\widetilde{g}^{ab} b_a b_b - \frac{1}{3}\lambda), \tag{1.6.25}$$

we find an explicit formula for the conformal factor, namely

$$\Theta(s) = \underline{\Theta} + \underline{Z} s + \frac{1}{4}\underline{H}\,\underline{U} s^2. \tag{1.6.26}$$

This is an amazing achievement, as we now know the conformal factor, and hence know the location of the conformal infinity, *a-priori*! One can see the quadratic nature which ties in with the standard conformal diagrams of various asymptotically simple space-times (see section 7.1). This now raises the question, can we find an explicit formula for h_a as well?

To look into this, we write down the conformal geodesic equation for the 1-form with respect to the physical geometry to find

$$\frac{\mathrm{d}}{\mathrm{d}s} b_{\mathbf{b}} = -(u^a b_a) b_{\mathbf{b}} + \frac{1}{2}\Theta H \widetilde{g}_{ab} u^a e^b_{\mathbf{b}}.$$

Using $u^a = e_{\mathbf{0}}$ and (1.6.23) we can write down

$$\frac{\mathrm{d}}{\mathrm{d}s}(\Theta b_{\mathbf{b}}) = \frac{1}{2} H\, \eta_{\mathbf{0b}}.$$

Noting that $\dot{H} = 0$, we find the remarkable result that

$$h_{\mathbf{0}}(s) = \frac{1}{2}\underline{H} s + \underline{h}_{\mathbf{0}}, \qquad h_{\mathbf{b}}(s) = \underline{h}_{\mathbf{b}}, \qquad \mathbf{b} = 1, 2, 3. \tag{1.6.27}$$

This is good news. We now have an explicit expression for the 1-form h_a as well as Θ. One may then think about using the relationship (1.6.3) to obtain an explicit formula for f_a as well. This is unfortunately not possible, as one must also know the frame components $c^{\mu}_{\mathbf{a}}$, which are of course unknowns in our system.

The equations for Θ and h_a together with equations (1.6.21) are known as the GCFE. The "General" refers to the fact that we have used the full gauge freedom of the conformal structure. We now have a system which expresses (1.1.1) in a conformal setting that is regular in

the limit $\Theta \to 0$ and *where we know* Θ *a-priori*.

The conformal geodesics in this gauge are potentially less likely to develop caustics than metric geodesics used in the Gauss gauge. This was shown explicitly by Friedrich in [52], where he finds that a CGG can globally cover the Schwarzschild space-time. We make use of this later in section 8.1.

To conclude this section, we collect the implications of the CGG on our system.

$$\begin{aligned} u^a\widehat{\nabla}_a x^i = 0,\, u^a\widehat{\nabla}_a s = 1 &\implies u^\mu = \delta^\mu_0, \\ u^a = e_{\mathbf{0}} &\implies u^{\mathbf{a}} = \delta^{\mathbf{a}}_0, \quad c^\mu_{\mathbf{0}} = \delta^\mu_0, \\ u^a\widehat{\nabla}_a e_{\mathbf{b}} = 0 &\implies \widehat{\Gamma}_{\mathbf{0b}}{}^{\mathbf{c}} = 0, \\ f_{\mathbf{a}} = \frac{1}{4}\widehat{\Gamma}_{\mathbf{ab}}{}^{\mathbf{b}} &\implies f_{\mathbf{0}} = 0, \\ u^a\widehat{P}_{ab} = 0 &\implies \widehat{P}_{\mathbf{0b}} = 0. \end{aligned} \tag{1.6.28}$$

Chapter 2

The GCFE in our formalisms

2.1 The space-spinor formalism

Due to its compact form, the calculus of space-spinors [120] is a very enticing formalism in which to write the GCFE. We will use definitions similar to that used in the series of papers by Frauendiener [37, 38, 40] throughout.

First, we define a time-like vector field t^a, normalised with respect to the conformal metric g by $t^a t_a = 2$. Writing t^a in terms of spinors, one immediately finds the relationship

$$t_{AA'} t_B{}^{A'} = t_{A'(A} t_{B)}{}^{A'} + \frac{1}{2} t_{CA'} t^{CA'} \varepsilon_{AB} = \varepsilon_{AB},$$

which justifies the choice of normalisation constant. One can now use this vector field as a map from the complex spin-space $\bar{S}^{A'}$ onto the spin-space S^A, i.e. we can convert primed indices to unprimed ones. This map is given by

$$\alpha_{A'} \mapsto t_A{}^{A'} \alpha_{A'} =: \alpha_A. \tag{2.1.1}$$

For example, a spinor $\alpha_a = \alpha_{AA'}$ can be mapped to $\alpha_{AB} := t_B{}^{A'} \alpha_{AA'}$. The result can be decomposed into two terms

$$\alpha_{AB} = \alpha_{(AB)} + \frac{1}{2} \varepsilon_{AB} \alpha_E{}^E, \qquad \text{with} \quad \alpha_E{}^E = \alpha_{EA'} t^{EA'}.$$

This shows us that the trace term corresponds to the part of the spinor that has values in the direction of $t^{AA'}$. Thus finding irreducible decompositions of space-spinors is the same as

performing a 3+1 splitting. This is incredibly useful for deriving evolution and constraint equations.

We also define a complex conjugation map on the unprimed spin-space via

$$\alpha_A \mapsto \hat{\alpha}_A := t_A{}^{A'}\bar{\alpha}_{A'}. \tag{2.1.2}$$

This map has the property that for a spinor of rank n we obtain

$$\widehat{\hat{\alpha}}_{AB\cdots D} = (-1)^n \alpha_{AB\cdots D}.$$

We define a rank-2 spinor as real iff it is equal to the negative of its complex conjugate, in accordance with the reality of the SL(2,$\mathbb{C}$) spinors. Since for any two real rank-2 spinors α_{AB} and β_{CD} their outer product should also be real, a rank-4 spinor is real if it is equal to its complex conjugate.

We can now split the covariant derivative ∇ into spatial and temporal parts using the mapping $t_B{}^{A'}\nabla_{AA'}$ and its subsequent decomposition. This gives us two new derivative operators

$$D = t^a\nabla_a, \quad D_{AB} = t_{(A}{}^{B'}\nabla_{B)B'} \implies \nabla_{AA'} = \frac{1}{2}t_{AA'}D - t^B{}_{A'}D_{AB}. \tag{2.1.3}$$

Two fundamental spinor fields can now be defined as the derivatives of t^a with respect to these new derivative operators. We have

$$\chi_{CD} := t_D{}^{C'}Dt_{CC'}, \qquad \chi_{ABCD} := t_D{}^{C'}D_{AB}t_{CC'}. \tag{2.1.4}$$

Geometrically, the spinor field χ_{AB} corresponds to the acceleration vector of t^a while χ_{ABCD} is related to the geometry of the distribution defined by $t_a = 0$ and for a time-like vector field t^a satisfying the hypersurface orthogonal property, it corresponds to the extrinsic curvature. They have the reality properties

$$\hat{\chi}_{AB} = -\chi_{AB}, \qquad \hat{\chi}_{ABCD} = \chi_{ABCD}. \tag{2.1.5}$$

Note that these new derivatives operators are real in the sense that they map real spinors to real spinors, but they do not commute with our definition of complex conjugation, i.e.

$$D\hat{\alpha}_C = D(\bar{\alpha}_{A'}t_C{}^{A'}) = t_C{}^{A'}D\bar{\alpha}_{A'} + \bar{\alpha}_{A'}\,Dt_C{}^{A'} = \widehat{D\alpha_C} + \hat{\alpha}_A\,\chi_C{}^A.$$

A similar equation holds for χ_{ABCD}. Hence we introduce new derivative operators

$$\partial\alpha_C = D\alpha_C - \frac{1}{2}\chi_C{}^D\alpha_D, \qquad \partial_{AB}\alpha_C = D_{AB}\alpha_C - \frac{1}{2}\chi_{ABC}{}^D\alpha_D, \tag{2.1.6}$$

adjusted to commute with complex conjugation. We now have

$$\partial_{AB}\hat{\alpha}_C = -\widehat{\partial_{AB}\alpha_C}, \qquad \partial\hat{\alpha}_C = \widehat{\partial\alpha_C}. \tag{2.1.7}$$

Note that the correction term χ_{AB} or χ_{ABCD} corrects only one index. So replacing the action of D or D_{AB} on a rank-n spinor with ∂ or ∂_{AB} respectively, result in n correction terms. For example,

$$\partial\alpha_{AB} = D\alpha_{AB} - \frac{1}{2}\chi_A{}^C\alpha_{CB} - \frac{1}{2}\chi_B{}^C\alpha_{AC}.$$

The spinor equivalent of a frame is aptly called a spin-frame, and is usually denoted by the two spinors o^A and ι^A along with there primed counterparts. A list of the relationships between the spin-frame and the associated null tetrad and orthonormal frame is given in appendix A.1. These relations will be made us of extensively throughout the remainder of this document.

2.2 The GCFE in the space-spinor formalism

Here we convert the tensorial GCFE into the space-spinor language. A spinor representation of parts of the GCFE has been given in [53] and [48]. However here we present the entire GCFE in the space-spinor formalism.

The idea is to use quantities of the conformal metric connection (with the exception of the Weyl connection's Schouten tensor) as the unknowns, then split them into evolution and constraint equations by decomposing the fields. Once this is done the CGG is imposed and we obtain a complete system of evolution and constraint equations. This is an arduous, tedious process to say the least. We will not go into the details but rather give a brief summary and refer the reader to the "equation road map" in appendix B.3 as a reference to the big picture and appendix B.1 for the full derivation.

The standard procedure is:

- Replace $\widehat{\nabla}$'s with ∇'s using the standard transformation law,
- convert the tensor fields to space-spinor fields and decompose ∇ into D and D_{AB},
- convert D and D_{AB} into ∂ and ∂_{AB},
- decompose the equations into irreducible pieces to obtain evolution and constraint equations.

Denoting the space-spinor version of the Schouten tensor of the Weyl connection as P_{ABCD} (dropping the hat to avoid confusion with complex conjugation) and noting that this has no symmetries, but satisfies the reality condition

$$\widehat{P}_{ACBD} = P_{CADB} \Leftrightarrow P_{ABCD} = P_{BADC}, \tag{2.2.1}$$

we apply our procedure to equation (1.6.21c)

$$\widehat{\nabla}_a \hat{P}_{bc} - \widehat{\nabla}_b \hat{P}_{ac} = \left(\widehat{\nabla}_e \Theta + \Theta f_e\right) K_{abc}{}^e,$$

as an example. Introducing spinors we obtain for the left hand side of this equation

$$\widehat{\nabla}_{AA'} \hat{P}_{BB'CC'} - \widehat{\nabla}_{BB'} \hat{P}_{AA'CC'}.$$

Now we replace $\widehat{\nabla}_{AA'}$ with $\nabla_{AA'}$, drop the hat on $\hat{P}_{BB'CC'}$ and replace $\nabla_{AA'}$ with $\frac{1}{2} t_{AA'} D - t_{A'}{}^B D_{AB}$ to obtain

$$\begin{aligned}\frac{1}{2} t_{AA'} D P_{BB'CC'} - t_{A'}{}^E D_{AE} P_{BB'CC'} - \frac{1}{2} t_{BB'} D P_{AA'CC'} + t_{B'}{}^E D_{BE} P_{AA'CC'} \\ + f_{CB'} P_{AA'BC'} + f_{BC'} P_{AA'CB'} - f_{CA'} P_{BB'AC'} - f_{AC'} P_{BB'CA'}.\end{aligned}$$

Now we multiply with $t_E{}^{A'} t_F{}^{B'} t_G{}^{C'}$ and obtain

$$\begin{aligned}&\frac{1}{2}\varepsilon_{AE} D P_{BFCG} - \frac{1}{2}\varepsilon_{AE} P_{BDCG} \chi_F{}^D - \frac{1}{2}\varepsilon_{AE} P_{BFCD} \chi_G{}^D + D_{AE} P_{BFCG} - P_{BDCG} \chi_{AEF}{}^D \\ &- P_{BFCD} \chi_{AEG}{}^D - \frac{1}{2}\varepsilon_{BF} D P_{AECG} + \frac{1}{2}\varepsilon_{BF} P_{ADCG} \chi_E{}^D + \frac{1}{2}\varepsilon_{BF} P_{AECD} \chi_G{}^D - D_{BF} P_{AECG} \\ &+ P_{ADCG} \chi_{BFE}{}^D + P_{AECD} \chi_{BFG}{}^D + f_{CF} P_{AEBG} + f_{BG} P_{AECF} - f_{CE} P_{BFAG} - f_{AG} P_{BFCE}.\end{aligned}$$

By construction this expression is skew under the simultaneous interchange of $AE \leftrightarrow BF$. In order to separate this expression into a piece which contains no time derivatives and a piece

with the time derivatives we need to symmetrise it jointly over AE and BF to obtain constraints while contraction over AE and symmetrising over BF or vice-versa yields evolution equations. We first contract over AE and symmetrise over BF and obtain

$$DP_{(BF)CG} - P_{(B|DCG|}\chi_{F)}{}^{D} - P_{(BF)CD}\chi_{G}{}^{D} - D_{BF}P_{E}{}^{E}{}_{CG} + P_{EDCG}\chi_{BF}{}^{ED} + P_{E}{}^{E}{}_{CD}\chi_{BFG}{}^{D} + P_{E}{}^{E}{}_{(B|G}f_{C|F)} + P_{E}{}^{E}{}_{C(B}f_{F)G} - P_{(BF)EG}f_{C}{}^{E} + P_{(BF)CE}f^{E}{}_{G}.$$

Replacing the D operators with the ∂ ones, we find

$$\partial P_{(BF)CG} - P_{(B|DCG|}\chi_{F)}{}^{D} - P_{(BF)CD}\chi_{G}{}^{D} - \partial_{BF}P_{E}{}^{E}{}_{CG} + P_{EDCG}\chi_{BF}{}^{ED} + P_{E}{}^{E}{}_{CD}\chi_{BFG}{}^{D} + P_{E}{}^{E}{}_{(B|G}f_{C|F)} + P_{E}{}^{E}{}_{C(B}f_{F)G} - P_{(BF)EG}f_{C}{}^{E} + P_{(BF)CE}f^{E}{}_{G} + \frac{1}{2}\chi_{(B}{}^{E}P_{|E|F)CG} + \frac{1}{2}\chi_{(B}{}^{E}P_{F)ECG} + \frac{1}{2}\chi_{C}{}^{E}P_{(BF)EG} + \frac{1}{2}\chi_{G}{}^{E}P_{(BF)CE} - \frac{1}{2}\chi_{BFE}{}^{H}P_{H}{}^{E}{}_{CG} + \frac{1}{2}\chi_{BF}{}^{E}{}_{H}P_{E}{}^{H}{}_{CG} - \frac{1}{2}\chi_{BFC}{}^{H}P_{E}{}^{E}{}_{HG} - \frac{1}{2}\chi_{BFG}{}^{H}P_{E}{}^{E}{}_{CH}.$$

Contracting over BF and symmetrising AE yields the same equation except that (BF) is replaced with (AE). Symmetrising over both pairs we obtain

$$D_{AE}P_{(BF)CG} - P_{(B|DCG}\chi_{AE|F)}{}^{D} - P_{(BF)CD}\chi_{AEG}{}^{D} - D_{BF}P_{(AE)CG} + P_{(A|DCG}\chi_{BF|E)}{}^{D} + P_{(AE)CD}\chi_{BFG}{}^{D} + P_{(AE)(B|G)}f_{C|F)} + P_{(AE)C(B}f_{F)G} - P_{(BF)(A|G}f_{C|E)} - P_{(BF)C(A}f_{E)G}.$$

This expression is still skew under the simultaneous interchange over $AE \leftrightarrow BF$ so we can write it in the form

$$\varepsilon_{AB}T_{EFCG} + \varepsilon_{EF}T_{ABCG},$$

where $T_{ABCG} = T_{BACG}$. In order to determine T_{ABCG} we contract over EF and symmetrise over AB and obtain

$$- D_{A}{}^{E}P_{(BE)CG} + P_{(B|DCG}\chi_{A|}{}^{F}{}_{F)}{}^{D} + P_{(BF)CD}\chi_{A}{}^{F}{}_{G}{}^{D} - D_{B}{}^{E}P_{(AE)CG} + P_{(A|DCG}\chi_{B|}{}^{F}{}_{F)}{}^{D} + P_{(AF)CD}\chi_{B}{}^{F}{}_{G}{}^{D} - \frac{1}{2}P_{A}{}^{F}{}_{(B|G}f_{C|F)} - \frac{1}{2}P^{F}{}_{A(B|G}f_{C|F)} - \frac{1}{2}P_{A}{}^{F}{}_{C(B}f_{F)G} - \frac{1}{2}P^{F}{}_{AC(B}f_{F)G} - \frac{1}{2}P_{B}{}^{F}{}_{(A|G}f_{C|F)} - \frac{1}{2}P^{F}{}_{B(A|G}f_{C|F)} - \frac{1}{2}P_{B}{}^{F}{}_{C(A}f_{F)G} - \frac{1}{2}P^{F}{}_{BC(A}f_{F)G}.$$

Replacing the D operators with the ∂ ones, we find

$$- \partial_{A}{}^{E}P_{(BE)CG} + P_{(B|DCG}\chi_{A|}{}^{F}{}_{F)}{}^{D} + P_{(BF)CD}\chi_{A}{}^{F}{}_{G}{}^{D} - \partial_{B}{}^{E}P_{(AE)CG} + P_{(A|DCG}\chi_{B|}{}^{F}{}_{F)}{}^{D} + P_{(AF)CD}\chi_{B}{}^{F}{}_{G}{}^{D} - \frac{1}{2}P_{A}{}^{F}{}_{(B|G}f_{C|F)} - \frac{1}{2}P^{F}{}_{A(B|G}f_{C|F)} - \frac{1}{2}P_{A}{}^{F}{}_{C(B}f_{F)G} - \frac{1}{2}P^{F}{}_{AC(B}f_{F)G} - \frac{1}{2}P_{B}{}^{F}{}_{(A|G}f_{C|F)} - \frac{1}{2}P^{F}{}_{B(A|G}f_{C|F)} - \frac{1}{2}P_{B}{}^{F}{}_{C(A}f_{F)G} - \frac{1}{2}P^{F}{}_{BC(A}f_{F)G} - \frac{1}{2}\chi_{A}{}^{E}{}_{(B}{}^{H}P_{|H|E)CG} - \frac{1}{2}\chi_{A}{}^{E}{}_{(B}{}^{H}P_{E)HCG} - \frac{1}{2}\chi_{A}{}^{E}{}_{C}{}^{H}P_{(BE)HG} - \frac{1}{2}\chi_{A}{}^{E}{}_{G}{}^{H}P_{(BE)CH} - \frac{1}{2}\chi_{B}{}^{E}{}_{(A}{}^{H}P_{|H|E)CG} - \frac{1}{2}\chi_{B}{}^{E}{}_{(A}{}^{H}P_{E)HCG} - \frac{1}{2}\chi_{B}{}^{E}{}_{C}{}^{H}P_{(AE)HG} - \frac{1}{2}\chi_{B}{}^{E}{}_{G}{}^{H}P_{(AE)CH}.$$

Now looking at the right hand side of the equation we are converting to space-spinors

$$\left(\widehat{\nabla}_e\Theta + \Theta f_e\right) K_{abc}{}^e$$

in terms of spinors and multiplying with $t_E{}^{A'} t_F{}^{B'} t_G{}^{C'}$ we find

$$-\varepsilon_{EF} h^D{}_G \psi_{ABCD} - \varepsilon_{AB} h_C{}^D \hat{\psi}_{DEFG}.$$

Here, we have introduced the rescaled Weyl spinor

$$\psi_{ABCD} = \Theta^{-1}\Psi_{ABCD},$$

and we observe that h_{AB} is *not* symmetric. Following the above, we contract over AE and symmetrise over BF

$$h^D{}_G \psi_{BCDF} - h_C{}^D \hat{\psi}_{BDFL}.$$

Then we symmetrise over both pairs and contract over EF, giving

$$-h^D{}_G \psi_{ABCD} - h_C{}^D \hat{\psi}_{ABDG}.$$

Hence equating these terms we find an evolution equation for $P_{(AB)CD}$

$$\begin{aligned}
&\partial P_{(AB)CD} - \partial_{AB} P_E{}^E{}_{CD} = P_{(A|FCD|}\chi_{B)}{}^F + P_{(AB)CF}\chi_D{}^F - P_{EFCD}\chi_{AB}{}^{EF} - P_E{}^E{}_{CF}\chi_{ABD}{}^F \\
&- P_E{}^E{}_{(A|D} f_{C|B)} - P_E{}^E{}_{C(A} f_{B)D} + P_{(AB)ED} f_C{}^E - P_{(AB)CE} f^E{}_D - \frac{1}{2}\chi_{(A}{}^E P_{|E|B)CD} - \frac{1}{2}\chi_{(A}{}^E P_{B)ECD} \\
&- \frac{1}{2}\chi_C{}^E P_{(AB)ED} - \frac{1}{2}\chi_D{}^E P_{(AB)CE} + \frac{1}{2}\chi_{ABE}{}^H P_H{}^E{}_{CD} - \frac{1}{2}\chi_{AB}{}^E{}_H P_E{}^H{}_{CD} + \frac{1}{2}\chi_{ABC}{}^H P_E{}^E{}_{HD} \\
&+ \frac{1}{2}\chi_{ABD}{}^H P_E{}^E{}_{CH} + h^F{}_D \psi_{ABCF} - h_C{}^F \hat{\psi}_{ABDF},
\end{aligned} \tag{2.2.2}$$

and a constraint equation

$$\begin{aligned}
&\partial_A{}^E P_{(BE)CD} + \partial_B{}^E P_{(AE)CD} = P_{(B|FCD}\chi_{A|}{}^E{}_{E)}{}^F + P_{(BE)CF}\chi_A{}^E{}_D{}^F + P_{(A|FCD}\chi_{B|}{}^E{}_{E)}{}^F \\
&+ P_{(AE)CF}\chi_B{}^E{}_D{}^F - \frac{1}{2}P_A{}^E{}_{(B|D} f_{C|E)} - \frac{1}{2}P^E{}_{A(B|D} f_{C|E)} - \frac{1}{2}P_A{}^E{}_{C(B} f_{E)D} - \frac{1}{2}P^E{}_{AC(B} f_{E)D} \\
&- \frac{1}{2}P_B{}^E{}_{(A|D} f_{C|E)} - \frac{1}{2}P^E{}_{B(A|D} f_{C|E)} - \frac{1}{2}P_B{}^E{}_{C(A} f_{E)D} - \frac{1}{2}P^E{}_{BC(A} f_{E)D} - \frac{1}{2}\chi_A{}^E{}_{(B}{}^F P_{|F|E)CD} \\
&- \frac{1}{2}\chi_A{}^E{}_{(B}{}^F P_{E)FCD} - \frac{1}{2}\chi_A{}^E{}_C{}^F P_{(BE)FD} - \frac{1}{2}\chi_A{}^E{}_D{}^F P_{(BE)CF} - \frac{1}{2}\chi_B{}^E{}_{(A}{}^F P_{|F|E)CD} \\
&- \frac{1}{2}\chi_B{}^E{}_{(A}{}^F P_{E)FCD} - \frac{1}{2}\chi_B{}^E{}_C{}^F P_{(AE)FD} - \frac{1}{2}\chi_B{}^E{}_D{}^F P_{(AE)CF} - h^E{}_D \psi_{ABCE} - h_C{}^E \hat{\psi}_{ABDE}.
\end{aligned} \tag{2.2.3}$$

Notice that we only get an evolution equation for $P_{(AB)CD}$. This turns out to be enough once we choose and impose our gauge, as it implies that $P_{ABCD} = P_{BACD}$.

To derive the remaining gauge-related equations that are not in appendix B.1, we must first set up the CGG using our space-spinors. We fix coordinates and a spin-frame that are adapted to the congruence of conformal geodesics. We choose the spatial coordinates to be constant along the geodesics and the time coordinate to be the parameter along the curves. Then we fix the time-like vector field t^a to be proportional to the tangent vector u^a of the curves. We adjust the spin-frame so that $t_{AA'} = o_A o_{A'} + \iota_A \iota_{A'}$. Then we have

$$\hat{o}_A = \iota_A, \qquad \hat{\iota}_A = -o_A.$$

Next we define the frame components

$$\partial x^\mu =: c^\mu, \qquad \partial_{AB} x^\mu =: c^\mu_{AB}. \tag{2.2.4}$$

We choose the time-like frame vector to be parallel to the tangent vector of the conformal geodesics so that

$$u^a = e^a_{\mathbf{0}},$$

The gauge conditions imply

$$c^\mu = \sqrt{2}\delta^\mu_0. \tag{2.2.5}$$

Furthermore, we define the spinor fields

$$\partial o_A = \gamma_A \implies \partial \iota_A = \hat{\gamma}_A, \qquad \partial_{AB} o_C = \gamma_{ABC} \implies \partial_{AB} \iota_C = -\hat{\gamma}_{ABC}. \tag{2.2.6}$$

Since these derivatives preserve ε_{AB} the spinor fields satisfy the relations

$$\gamma_C \iota^C = \hat{\gamma}_C o^C, \qquad \gamma_{ABC} \iota^C = -\hat{\gamma}_{ABC} o^C.$$

The parallel transport of the spin-frame along the curves is given by $t^a \widehat{\nabla}_a o_C = 0$, which we write as

$$t^a \widehat{\nabla}_a o_C = t^a \nabla_a o_C - t^{AA'} f_{CA'} o_A = \partial o_C + \frac{1}{2} \chi_C{}^B o_B - t^{AA'} f_{CA'} o_A = 0.$$

This and the analogous equation for ι_C yield the equations

$$\gamma_C + \frac{1}{2}\left(\chi_C{}^B - 2 f_C{}^B\right) o_B - \frac{1}{2} f o_C = 0,$$
$$\hat{\gamma}_C + \frac{1}{2}\left(\chi_C{}^B - 2 f_C{}^B\right) \iota_B - \frac{1}{2} f \iota_C = 0.$$

Subtracting the complex conjugate of the second from the first equation and observing the reality properties of the quantities gives the condition

$$\gamma_C = \frac{f}{2} o_C.$$

The complex conjugate of this equation is

$$\hat{\gamma}_C = \frac{f}{2} \iota_C.$$

But $\gamma_1 = \iota^A \partial o_A = o^A \partial \iota_A = \hat{\gamma}_0$, which means

$$\gamma_1 = \frac{1}{2} f = \hat{\gamma}_0 = -\frac{1}{2} f,$$

which can only be true if $f = 0$. Thus, the gauge conditions imply

$$f = 0, \qquad \chi_{AB} = 2 f_{AB}, \qquad \gamma_C = 0. \tag{2.2.7}$$

The last consequence of the gauge conditions is

$$t^{AA'} \hat{P}_{AA'BB'} = 0, \tag{2.2.8}$$

which when translated into the space-spinor language implies

$$P_{ABCD} = P_{BACD}. \tag{2.2.9}$$

Now that we have our gauge quantities, we can apply our procedure to (1.6.21a) to obtain evolution and constraint equations for $c^{\mu}_{AB'}$, noting that c^{μ} is known from our choice of gauge.

The last and most complicated equation to deal with is (1.6.21b). The full derivation is in appendix B.1 so I will give a short summary. It helps to look at appendix B.3 to keep track of things. First, think of the equation written like $[\widehat{\nabla}_a, \widehat{\nabla}_b] o_C = \textit{curvature}$. The time-space projection gives an evolution equation for χ_{ABCD} and an expression for the commutator $[\partial, \partial_{AB}]$. The space-space projection gives a constraint equation for χ_{ABCD} and an expression for the commutator $\partial_{E(A} \partial^{E}{}_{B)}$. Action of these commutators on o_A give evolution and constraint equations for γ_{ABC}, while action on the ε_{AB} give evolution and constraint equations for f_{AB}.

Imposing the gauge conditions on the evolution equations and the constraint equations yields a closed system of equations for the unknowns

$$P_{ABCD}, \quad \psi_{ABCD}, \quad \chi_{ABCD}, \quad f_{AB}/\chi_{AB}, \quad c^{\mu}_{AB}, \quad \gamma_{ABC}, \tag{2.2.10}$$

where Θ and h_{AB} are determined *a-priori* from initial data.

The evolution equations are

$$\partial P_{ABCD} = -\chi_{ABEF}P^{EF}{}_{CD} + \psi_{ABCE}h^{E}{}_{D} - \hat{\psi}_{ABDE}h_{C}{}^{E}, \tag{2.2.11a}$$

$$\partial\psi_{ABCD} = 2\partial_{(A}{}^{E}\psi_{BCD)E} - 2\chi_{(A}{}^{E}\psi_{BCD)E} + 3\chi_{(A}{}^{E}{}_{B}{}^{F}\psi_{CD)EF} - \chi_{E(A}{}^{EF}\psi_{BCD)F}, \tag{2.2.11b}$$

$$\partial\chi_{ABCD} = -\chi_{AB}{}^{EF}\chi_{EFCD} - 2P_{AB(CD)} + \Theta\psi_{ABCD} + \Theta\hat{\psi}_{ABCD}, \tag{2.2.11c}$$

$$\partial f_{AB} = -\chi_{ABEF}f^{EF} + P_{ABC}{}^{C}, \tag{2.2.11d}$$

$$\begin{aligned}\partial\gamma_{ABC} = {} & -\chi_{AB}{}^{EF}\gamma_{EFC} - o_{(A}\chi_{B)CDE}f^{DE} + \frac{1}{2}o_{C}\chi_{ABEF}f^{EF} + \chi_{ABE(C}f_{D)}{}^{E}o^{D} \\ & + \frac{1}{2}P_{ABE}{}^{E}o_{C} + \varepsilon_{C(A}P_{B)DE}{}^{E}o^{D} - \frac{1}{2}\Theta\psi_{ABCD}o^{D} + \frac{1}{2}\Theta\hat{\psi}_{ABCD}o^{D},\end{aligned} \tag{2.2.11e}$$

$$\partial c^{0}_{AB} = -\frac{1}{\sqrt{2}}\chi_{AB} - \chi_{AB}{}^{CD}c^{0}_{CD}, \tag{2.2.11f}$$

$$\partial c^{i}_{AB} = -\chi_{AB}{}^{CD}c^{i}_{CD}, \qquad i = 1, 2, 3. \tag{2.2.11g}$$

The constraint equations are

$$\partial_{(A}{}^{E}P_{B)ECD} = -\frac{1}{2}f_{CE}P_{(A}{}^{E}{}_{B)D} - \frac{1}{2}f_{DF}P_{(A}{}^{E}{}_{|C|B)} - \frac{1}{2}\left(f_{D(A}P_{B)}{}^{E}{}_{CE} + f_{C(A}P_{B)}{}^{E}{}_{ED}\right)$$
$$+\frac{1}{2}P_{(A}{}^{E}{}_{|C|}{}^{F}\chi_{B)EDF} - \frac{1}{2}P_{(A}{}^{EF}{}_{|D|}\chi_{B)ECF} + \frac{1}{2}\psi_{ABCE}h^{E}{}_{D} + \frac{1}{2}\hat{\psi}_{ABDE}h_{C}{}^{E}, \tag{2.2.12a}$$

$$\partial^{CD}\psi_{ABCD} = -\chi^{CE}{}_{E}{}^{D}\psi_{ABCD} - \chi^{CDE}{}_{(A}\psi_{B)CDE}, \tag{2.2.12b}$$

$$\partial_{(A}{}^{E}\chi_{B)ECD} = -\frac{1}{2}f_{CD}\chi_{(A}{}^{E}{}_{B)E} - \frac{1}{2}f_{C(A}\chi_{B)}{}^{E}{}_{DE} - \frac{1}{2}\varepsilon_{C(A}f^{EF}\chi_{B)DEF} - \frac{1}{2}\varepsilon_{D(A}f^{EF}\chi_{B)ECF}$$
$$+\frac{1}{2}\varepsilon_{C(A}P_{B)DE}{}^{E} + \frac{1}{2}\varepsilon_{D(A}P_{B)CE}{}^{E} + \frac{1}{2}\Theta\psi_{ABCD} - \frac{1}{2}\Theta\hat{\psi}_{ABCD}, \tag{2.2.12c}$$

$$\partial_{(A}{}^{E}f_{B)E} = \frac{1}{2}P_{E(A}{}^{E}{}_{B)} - \frac{1}{2}P_{(A}{}^{E}{}_{B)E}, \tag{2.2.12d}$$

$$\partial_{(A}{}^{E}\gamma_{B)EC} = \frac{1}{4}f_{AB}f_{CD}o^{D} + \frac{1}{2}\chi_{(A}{}^{E}{}_{|C|}{}^{D}\chi_{B)EFD}o^{F} - \frac{1}{8}\left(P_{AC(BD)} + P_{BC(AD)}\right)o^{D}$$
$$-\frac{1}{8}\left(P_{AD(BC)} + P_{BD(AC)}\right)o^{D} + \frac{1}{4}\left(P_{A}{}^{D}{}_{BD} + P_{B}{}^{D}{}_{AD}\right)o_{C} + \frac{1}{8}\left(P_{A}{}^{D}{}_{(CD)}o_{B} + P_{B}{}^{D}{}_{(CD)}o_{A}\right)$$
$$-\frac{1}{8}\left(\varepsilon_{AC}P_{B}{}^{E}{}_{(DE)} + \varepsilon_{BC}P_{A}{}^{E}{}_{(DE)}\right)o^{D} - \frac{1}{2}o^{D}\partial_{D(A}f_{B)C} + \frac{1}{2}o_{(A}\partial_{B)}{}^{E}f_{CE}, \tag{2.2.12e}$$

$$\partial^{C}{}_{(A}c^{0}_{B)C} = -\frac{1}{\sqrt{2}}\chi_{(A}{}^{C}{}_{B)C}, \tag{2.2.12f}$$

$$\partial^{C}{}_{(A}c^{i}_{B)C} = 0, \tag{2.2.12g}$$

and the expressions for h_a and Θ are as we have found in the tensorial case;

$$\Theta(s) = \underline{\Theta} + \underline{Z}s + \frac{1}{4}\underline{H}\,\underline{U}s^{2}, \tag{2.2.13}$$

$$h_{\mathbf{0}}(s) = \frac{1}{2}\underline{H}s + \underline{h}_{\mathbf{0}}, \qquad h_{\mathbf{b}}(s) = \underline{h}_{\mathbf{b}}, \qquad \mathbf{b} = 1, 2, 3, \tag{2.2.14}$$

where s is the affine parameter of the conformal geodesics. Although the explicit expression for h_{AB} is given in terms of its tensor formulation for simplicity, one can easily derive from this the spinor components. For example,

$$h_{01} = \frac{1}{\sqrt{2}}\left(e^{a}_{\mathbf{0}} + e^{a}_{\mathbf{1}}\right)h_a = \frac{1}{\sqrt{2}}\left(h_{\mathbf{0}} + h_{\mathbf{1}}\right),$$

and similarly for the other components.

The final steps involve writing out the above equations in components, which for obvious reasons we will not list here. We label the spinor components using conventions set out in appendix A.1.9. When written out in full the system above consists of 47 complex-functions with a set of 39 complex constraint equations.

2.3 Spin-weighted spherical harmonics, integer spin

There are many interesting space-times that have a submanifold with topology $\mathbb{S}^2$, such as conformal infinity $\mathscr{I}$ of asymptotically simple space-times and Friedmann-Robertson-Walker (FRW) space-times to name just a few. It is advantageous for our numerical schemes (see section 5.4) to assume that our space-time manifold is of the form $M = M_2 \times \mathbb{S}^2$. However this topology causes issues as it cannot globally be covered by a regular coordinate patch. This problem is usually referred to as "the pole problem". A way to resolve this is by use of spin-weighted spherical harmonics.

Spin-weighted spherical harmonics ${}_s\mathrm{Y}_{lm}(\theta,\phi)$, first defined in [87] to describe asymptotic behaviour of the gravitation field, are a generalisation of the standard spherical harmonics $\mathrm{Y}_{lm}(\theta,\phi)$ defined on the unit 2-sphere. They are used as a complete orthogonal basis to represent square-integrable functions defined on $\mathbb{S}^2$. This has many advantages for numerical codes that we will make use of and so we introduce them into our system in the next section. First, we give their derivation and an overview of their properties.

Looking at the metric for the unit 2-sphere written as

$$g = -\mathrm{d}\theta^2 - \sin^2\theta \mathrm{d}\phi^2,$$

in order to be compatible with our signature (+,-,-,-), we define a null-basis on the unit 2-sphere by [1]

$$M^a = \frac{1}{\sqrt{2}}\Big(\partial_\theta - \frac{i}{\sin\theta}\partial_\phi\Big),$$

along with its complex-conjugate $\bar{M}^a$ which satisfy the relations

$$M^a M_a = 0, \qquad \bar{M}^a M_a = -1.$$

[1] Following conventions of [13] for compatibility of their code later on.

Then we have that

$$g_{ab} = -2\bar{M}_{(a}M_{b)}.$$

This metric has two distinct connection coefficients in the coordinate frame, namely $-\sin\theta\cos\theta$ and $\cot\theta$. The $\cot\theta$ connection coefficient clearly demonstrates issues that may appear at the poles and this is the part of the connection we will want to "hide" from our GCFE system. It is clear that we have a gauge freedom of the form $M^a \to e^{i\alpha(\theta,\phi)}M^a$ which preserves the metric. Then a scalar f which transforms under this gauge transformation as

$$f \to e^{is\alpha(\theta,\phi)}f,$$

is said to be *spin-weighted* with *spin-weight* s. Immediately we see that M^a has spin-weight $+1$ and $\bar{M}^a$ has spin-weight -1. Of course not all functions will be properly spin-weighted, i.e.

$$\bar{M}^a\delta M_a \to e^{-i\alpha(\theta,\phi)}\bar{M}^a\delta M_a - \delta e^{-i\alpha(\theta,\phi)},$$

where we have defined

$$\delta := M^a\nabla_a, \qquad \delta' := \bar{M}^a\nabla_a, \tag{2.3.1}$$

and ∇ is the covariant derivative on the unit sphere. There is also the problem that action of δ, δ' on spin-weighted functions may not give back a properly spin-weighted function. The idea to fix this is to absorb the connection coefficients on the unit sphere without proper spin-weight (i.e. the $\cot\theta$) into new derivative operators. We define the new operators to be

$$\eth f = \sqrt{2}\Big(\delta f - saf\Big), \qquad \eth' f = \sqrt{2}\Big(\delta' f + s\bar{a}f\Big), \tag{2.3.2}$$

where a is related to the connection coefficients on the unit sphere that are not properly spin-weighted. The action of their commutator on a spin-s function f is given simply as

$$\Big[\eth, \eth'\Big]f = -2sf. \tag{2.3.3}$$

Now we find that the action of $\eth, \eth'$ on properly spin-weighted functions preserves the spin-weighted property, but changes the spin. Action on a spin-s function by $\eth$ raises the spin by one and action by $\eth'$ lowers the spin by one. Action of $\eth, \eth'$ on the spin-weight 0 spherical harmonics Y_{lm} give us the *spin-weighted spherical harmonics* ${}_sY_{lm}$. They are

$$\begin{aligned}\eth\ {}_sY_{lm}(\theta,\phi) &= -\sqrt{(l-s)(l+s+1)}\ {}_{s+1}Y_{lm}(\theta,\phi),\\ \eth'\ {}_sY_{lm}(\theta,\phi) &= \sqrt{(l+s)(l-s+1)}\ {}_{s-1}Y_{lm}(\theta,\phi).\end{aligned} \tag{2.3.4}$$

We can use the spin-weight s spherical harmonics as a complete orthogonal basis for spin-weight s square-integrable functions on $\mathbb{S}^2$, i.e. we can write any smooth square-integrable spin-weight s function f as an infinite series of spin-weighted spherical harmonics

$$f(\theta,\phi) = \sum_{l=|s|}^{\infty} \sum_{m=-l}^{l} a_{lm}\ {}_s\mathrm{Y}_{lm}(\theta,\phi), \tag{2.3.5}$$

where the a_{lm} are complex coefficients called *spectral coefficients*.

The fantastic feature of spin-weighted spherical harmonics that we will make use of is that we can rework our system (2.2.11), (2.2.12) by implementing the new derivative operators (2.3.2) to get properly spin-weighted equations. There are only three unknowns which are not properly spin-weighted and they decouple from the spin-weighted system. These are superfluous for looking at gravitational radiation and other interesting phenomena, but can always be computed from solutions to the spin-weighted system if one desires.

2.4 Implementation of the $\eth$ operators

In order for us to implement this in our system, we must specialise to space-times with this spherical topology. That is, we want the surfaces s = constant, ρ = constant to be 2-spheres. This specialisation is incorporated into how we expand the derivative operator ∂_{AB}. Currently the expansion of ∂_{AB} looks like

$$\partial_{AB} = c^0_{AB}\frac{\partial}{\partial x^0} + c^1_{AB}\frac{\partial}{\partial x^1} + c^2_{AB}\frac{\partial}{\partial x^2} + c^3_{AB}\frac{\partial}{\partial x^3}. \tag{2.4.1}$$

We now suppose, and will assume for the rest of the document, that the CGG has the coordinate system $\{s,\rho,\theta,\phi\}$. This is to make the distinction between the coordinates used in the CGG gauge and other frequently used coordinates such as t and r. Following notation given in [99] we can write the derivative operators tangent to the unit 2-sphere in terms of the unit-sphere $M^a, \bar{M}^a$ as in (2.3.1). Then we rewrite the expansion of ∂_{AB} as

$$\partial_{AB} = c^0_{AB}\partial_s + c^1_{AB}\partial_\rho - \Big(\frac{1}{R}\iota_A\iota_B + 2Xo_{(A}\iota_{B)} + Yo_Ao_B\Big)\delta + \Big(\frac{1}{R}o_Ao_B - 2\bar{X}o_{(A}\iota_{B)} + \bar{Y}\iota_A\iota_B\Big)\delta', \tag{2.4.2}$$

where R is the conformal factor for the 2-sphere so that $m_a = RM_a$ and X and Y are complex functions. The new function X corresponds to the case where derivatives in the e_1-direction

pick up derivatives tangent to the sphere and Y corresponds to the derivatives in the direction of the space-time m^a and $\bar{m}^a$ picking up both δ and δ' terms. It is worth noting that with this representation of the equations, our basis is of the form $\{e_{\mathbf{0}}, e_{\mathbf{1}}, m, \bar{m}\}$.

In order to compute new equations replacing those of c^2_{AB} and c^3_{AB} we look at the commutators $[\partial, \partial_{AB}]$ and $\partial_{E(A}\partial^{E}{}_{B)}$ acting on both the coordinates and the spin-frame[2]. We note that all of the commutators of the coordinate derivatives vanish, except

$$[\delta, \delta']f = a\delta f - \bar{a}\delta' f,$$

remembering a is a quantity encoding the connection coefficient of the unit 2-sphere that is not properly spin-weighted. In terms of spinor quantities, a is related to γ_{21}, its conjugate γ_{01} and γ_{11}. These have no well-defined spin-weight and hence, following the procedure in [99], must be eliminated from our system. The approach to do this is the following:

- Write down all the equations obtained from action of the commutators on the coordinates.
- Replace δ and δ' derivatives with $\eth$ and $\eth'$ derivatives.
- Pick out equations involving $a, \gamma_{01}, \gamma_{11}$ and γ_{21}.
- Use these equations to replace γ_{01}, γ_{11} and γ_{21} with $a, \bar{a}$ plus other terms.
- Use (2.3.2) to replace δ, δ' derivatives with $\eth, \eth'$ derivatives and $a, \bar{a}$ terms.

This process should then cancel the $a's$ and give spin-weighted equations. The action of the time-space commutator on the coordinates gives the new evolution equations

$$\partial_t R = \frac{1}{\sqrt{2}} R\chi_{02} + \sqrt{2}R^2 X\chi_{01} + \frac{1}{\sqrt{2}} R^2 Y\chi_{00}, \tag{2.4.3}$$

$$\partial_t X = \frac{1}{\sqrt{2}R}\chi_{12} + \sqrt{2}X\chi_{11} + \frac{1}{\sqrt{2}} Y\chi_{10}, \tag{2.4.4}$$

$$\partial_t Y = -\frac{1}{\sqrt{2}R}\chi_{22} - \sqrt{2}RX\chi_{21} - \frac{1}{\sqrt{2}} Y\chi_{20}, \tag{2.4.5}$$

[2] $\partial_{E(A}\partial^{E}{}_{B)}$ is the only irreducible component of $[\partial_{AB}, \partial_{CD}]$.

and their complex conjugates. As the conformal factor R is real, we take its evolution equation above, add its complex conjugate and divide by two to get

$$\partial_t R = \frac{R}{2\sqrt{2}}\Big(\chi_{02} + \chi_{20} + 2RX\chi_{01} - 2R\bar{X}\chi_{21} + RY\chi_{00} + R\bar{Y}\chi_{22}\Big), \tag{2.4.6}$$

which will be used as its evolution equation. The difference

$$\chi_{02} - \chi_{20} + 2R\Big(X\chi_{01} + \bar{X}\chi_{21}\Big) + R\Big(Y\chi_{00} - \bar{Y}\chi_{22}\Big) = 0, \tag{2.4.7}$$

is used as a constraint.

The action of the space-space commutator on the coordinates gives us replacement rules for the non-spin-weighted γ's:

$$\gamma_{01} = -\frac{\bar{Y}}{2}a - \frac{1}{2R}\bar{a} + \text{other terms}, \tag{2.4.8a}$$

$$\gamma_{11} = -\frac{\bar{X}}{2}a + \frac{X}{2}\bar{a} + \text{other terms}, \tag{2.4.8b}$$

$$\gamma_{21} = -\frac{1}{2R} - \frac{Y}{2} + \text{other terms}, \tag{2.4.8c}$$

where the "other terms" involve ρ and $\eth, \eth'$ derivatives of $R, X, \bar{X}, Y, \bar{Y}$ and algebraic terms involving components of χ_{ABCD}, the spin-weighted components of γ_{ABC} and the frame components. We also obtain the constraints

$$\begin{aligned}&\Big(c^1{}_2 + \frac{1}{2}RYc^1{}_0\Big)\partial_r X + \frac{1}{2}RYc^1{}_2\partial_r\bar{X} + c^1{}_1\partial_r Y - \frac{3}{2\sqrt{2}}Y\eth X - \frac{1}{2\sqrt{2}}RY^2\eth\bar{X} + \frac{1}{\sqrt{2}}X\eth Y\\ &+\Big(\frac{1}{\sqrt{2R}} + \frac{1}{2\sqrt{2}}RY\bar{Y}\Big)\eth' X + \frac{1}{2\sqrt{2}}Y\eth'\bar{X} + \frac{1}{\sqrt{2}}\bar{X}\eth' Y + \text{algebraic terms} = 0,\end{aligned} \tag{2.4.9a}$$

$$\begin{aligned}&\frac{2}{R}c^1{}_1\partial_r R - Rc^1{}_0 R\partial_r X + Rc^1{}_2\partial_r\bar{X} + \frac{\sqrt{2}}{R}X\eth R + \frac{1}{\sqrt{2}}\eth X - \frac{1}{\sqrt{2}}RY\eth\bar{X} + \frac{\sqrt{2}}{R}\bar{X}\eth' R\\ &\qquad - \frac{1}{\sqrt{2}}R\bar{Y}\eth' X + \frac{1}{\sqrt{2}}\eth'\bar{X} + \text{algebraic terms} = 0,\end{aligned} \tag{2.4.9b}$$

where "algebraic terms" contain components of χ_{ABCD}, the spin-weighted components of γ_{ABC} and the frame components.

The idea is then to rewrite our equations by replacing γ_{01}, γ_{11} and γ_{21} by the above expressions and replacing derivatives δ and δ' by (2.3.2). It is found, with the exception of

constraints derived from (2.2.12e), that the a terms coming from the γ replacements and the δ replacements cancel exactly, leaving proper spin-weighted equations as expected. We drop equations (2.2.11g) and (2.2.12g) for $i = 2, 3$, which are no longer in our system due to (2.4.1) and instead use evolution equations (2.4.4), (2.4.6) and constraint equations (2.4.7), (2.4.9a) and (2.4.9b).

The constraints derived from (2.2.12e) still contain expressions like $\delta(a)$ coming from the equations which involve derivatives of γ_{01}, γ_{11} and γ_{21} and we have no way yet of replacing them. An equation that can be used to replace this is found by looking at the definition for the curvature on the unit 2-sphere,

$$[\nabla_a, \nabla_b]v_c = -R_{abc}{}^d v_d,$$

where ∇ is the covariant derivative on the sphere. The only non-zero curvature component comes from transvection with $M^a, \bar{M}^b$ and must be the Gaussian curvature up to a constant, which is of course equal to one for the unit 2-sphere. Writing this in terms of δ, δ' derivatives gives us the relationship

$$\delta a + \delta' \bar{a} = -(2a\bar{a} + 1). \tag{2.4.10}$$

Using this equation in the constraints for γ_{ABC} we find that terms of the form $\delta a, \delta' \bar{a}$ and $a\bar{a}$ all cancel, leaving only terms linear in a and $\bar{a}$. These of course must also vanish. By using the new constraints derived in this section appropriately, we see this is in fact the case.

Now we have a system of evolution and constraint equations involving the $\eth, \eth'$ operators that are properly spin-weighted by not involving $\gamma_{01}, \gamma_{11}, \gamma_{21}$ or a and $\bar{a}$. They give rise to a 3+1 system of equations.

For completeness we list them here. Our evolution system is given by

$$\partial P_{ABCD} = -\chi_{ABEF}P^{EF}{}_{CD} + \psi_{ABCE}h^{E}{}_{D} - \hat{\psi}_{ABDE}h_{C}{}^{E}, \tag{2.4.11a}$$

$$\partial\psi_{ABCD} = 2\partial_{(A}{}^{E}\psi_{BCD)E} - 2\chi_{(A}{}^{E}\psi_{BCD)E} + 3\chi_{(A}{}^{E}{}_{B}{}^{F}\psi_{CD)EF} - \chi_{E(A}{}^{EF}\psi_{BCD)F}, \tag{2.4.11b}$$

$$\partial\chi_{ABCD} = -\chi_{AB}{}^{EF}\chi_{EFCD} - 2P_{AB(CD)} + \Theta\psi_{ABCD} + \Theta\hat{\psi}_{ABCD}, \tag{2.4.11c}$$

$$\partial f_{AB} = -\chi_{ABEF}f^{EF} + P_{ABC}{}^{C}, \tag{2.4.11d}$$

$$\begin{aligned}\partial\gamma_{ABC} = {} & -\chi_{AB}{}^{EF}\gamma_{EFC} - o_{(A}\chi_{B)CDE}f^{DE} + \frac{1}{2}o_{C}\chi_{ABEF}f^{EF} + \chi_{ABE(C}f_{D)}{}^{E}o^{D} \\ & + \frac{1}{2}P_{ABE}{}^{E}o_{C} + \varepsilon_{C(A}P_{B)DE}{}^{E}o^{D} - \frac{1}{2}\Theta\psi_{ABCD}o^{D} + \frac{1}{2}\Theta\hat{\psi}_{ABCD}o^{D},\end{aligned} \tag{2.4.11e}$$

$$\partial c^{0}_{AB} = -\frac{1}{\sqrt{2}}\chi_{AB} - \chi_{AB}{}^{CD}c^{0}_{CD}, \tag{2.4.11f}$$

$$\partial c^{1}_{AB} = -\chi_{AB}{}^{CD}c^{1}_{CD}, \tag{2.4.11g}$$

$$\partial_{t}R = \frac{1}{\sqrt{2}}R\chi_{02} + \sqrt{2}R^{2}X\chi_{01} + \frac{1}{\sqrt{2}}R^{2}Y\chi_{00}, \tag{2.4.11h}$$

$$\partial_{t}X = \frac{1}{\sqrt{2}R}\chi_{12} + \sqrt{2}X\chi_{11} + \frac{1}{\sqrt{2}}Y\chi_{10}, \tag{2.4.11i}$$

$$\partial_{t}Y = -\frac{1}{\sqrt{2}R}\chi_{22} - \sqrt{2}RX\chi_{21} - \frac{1}{\sqrt{2}}Y\chi_{20}. \tag{2.4.11j}$$

The constraint equations are

$$\partial_{(A}{}^{E}P_{B)ECD} = -\frac{1}{2}f_{CE}P_{(A}{}^{E}{}_{B)D} - \frac{1}{2}f_{DF}P_{(A}{}^{E}{}_{|C|B)} - \frac{1}{2}\left(f_{D(A}P_{B)}{}^{E}{}_{CE} + f_{C(A}P_{B)}{}^{E}{}_{ED}\right) + \frac{1}{2}P_{(A}{}^{E}{}_{|C|}{}^{F}\chi_{B)EDF} - \frac{1}{2}P_{(A}{}^{EF}{}_{|D|}\chi_{B)ECF} + \frac{1}{2}\psi_{ABCE}h^{E}{}_{D} + \frac{1}{2}\hat{\psi}_{ABDE}h_{C}{}^{E}, \tag{2.4.12a}$$

$$\partial^{CD}\psi_{ABCD} = -\chi^{CE}{}_{E}{}^{D}\psi_{ABCD} - \chi^{CDE}{}_{(A}\psi_{B)CDE}, \tag{2.4.12b}$$

$$\partial_{(A}{}^{E}\chi_{B)ECD} = -\frac{1}{2}f_{CD}\chi_{(A}{}^{E}{}_{B)E} - \frac{1}{2}f_{C(A}\chi_{B)}{}^{E}{}_{DE} - \frac{1}{2}\varepsilon_{C(A}f^{EF}\chi_{B)DEF} - \frac{1}{2}\varepsilon_{D(A}f^{EF}\chi_{B)ECF} + \frac{1}{2}\varepsilon_{C(A}P_{B)DE}{}^{E} + \frac{1}{2}\varepsilon_{D(A}P_{B)CE}{}^{E} + \frac{1}{2}\Theta\psi_{ABCD} - \frac{1}{2}\Theta\hat{\psi}_{ABCD}, \tag{2.4.12c}$$

$$\partial_{(A}{}^{E}f_{B)E} = \frac{1}{2}P_{E(A}{}^{E}{}_{B)} - \frac{1}{2}P_{(A}{}^{E}{}_{B)E}, \tag{2.4.12d}$$

$$\partial_{(A}{}^{E}\gamma_{B)EC} = \frac{1}{4}f_{AB}f_{CD}o^{D} + \frac{1}{2}\chi_{(A}{}^{E}{}_{|C|}{}^{D}\chi_{B)EFD}o^{F} - \frac{1}{8}\left(P_{AC(BD)} + P_{BC(AD)}\right)o^{D} - \frac{1}{8}\left(P_{AD(BC)} + P_{BD(AC)}\right)o^{D} + \frac{1}{4}\left(P_{A}{}^{D}{}_{BD} + P_{B}{}^{D}{}_{AD}\right)o_{C} + \frac{1}{8}\left(P_{A}{}^{D}{}_{(CD)}o_{B} + P_{B}{}^{D}{}_{(CD)}o_{A}\right) - \frac{1}{8}\left(\varepsilon_{AC}P_{B}{}^{E}{}_{(DE)} + \varepsilon_{BC}P_{A}{}^{E}{}_{(DE)}\right)o^{D} - \frac{1}{2}o^{D}\partial_{D(A}f_{B)C} + \frac{1}{2}o_{(A}\partial_{B)}{}^{E}f_{CE}, \tag{2.4.12e}$$

$$\partial^{C}{}_{(A}c^{0}_{B)C} = -\frac{1}{\sqrt{2}}\chi_{(A}{}^{C}{}_{B)C}, \tag{2.4.12f}$$

$$\partial^{C}{}_{(A}c^{1}_{B)C} = 0, \tag{2.4.12g}$$

$$\left(c^{1}{}_{2} + \frac{1}{2}RYc^{1}{}_{0}\right)\partial_{r}X + \frac{1}{2}RYc^{1}{}_{2}\partial_{r}\bar{X} + c^{1}{}_{1}\partial_{r}Y - \frac{3}{2\sqrt{2}}Y\eth X - \frac{1}{2\sqrt{2}}RY^{2}\eth\bar{X} + \frac{1}{\sqrt{2}}X\eth Y + \left(\frac{1}{\sqrt{2R}} + \frac{1}{2\sqrt{2}}RY\bar{Y}\right)\eth' X + \frac{1}{2\sqrt{2}}Y\eth'\bar{X} + \frac{1}{\sqrt{2}}\bar{X}\eth' Y + \text{algebraic terms} = 0, \tag{2.4.12h}$$

$$\frac{2}{R}c^{1}{}_{1}\partial_{r}R - Rc^{1}{}_{0}R\partial_{r}X + Rc^{1}{}_{2}\partial_{r}\bar{X} + \frac{\sqrt{2}}{R}X\eth R + \frac{1}{\sqrt{2}}\eth X - \frac{1}{\sqrt{2}}RY\eth\bar{X} + \frac{\sqrt{2}}{R}\bar{X}\eth' R - \frac{1}{\sqrt{2}}R\bar{Y}\eth' X + \frac{1}{\sqrt{2}}\eth'\bar{X} + \text{algebraic terms} = 0. \tag{2.4.12i}$$

We will henceforth refer to the system (2.4.11), (2.4.12) as the *GCFE system*.

2.5 The metric

It is useful to see the representation of the metric in terms of the coordinate frame. We compute this by noting that the inverse metric can be written as

$$g^{ab} = e_0^a e_0^b - e_1^a e_1^b - m^a \bar{m}^b - \bar{m}^a m^b,$$

with the frame vectors expanded as

$$\begin{aligned}
e_0^a &= \partial_t, \\
e_1^a &= \sqrt{2}\Big(c^0{}_1 \partial_t + c^1{}_1 \partial_r + X\delta + \bar{X}\delta'\Big), \\
m^a &= -c^0{}_0 \partial_t - c^1{}_0 \partial_r + \frac{1}{R}\delta - \bar{Y}\delta', \\
\bar{m}^a &= c^0{}_2 \partial_t + c^1{}_2 \partial_r - Y\delta + \frac{1}{R}\delta'.
\end{aligned}$$

Combining these we find the inverse metric has the form

$$\begin{pmatrix}
1 - 2\,(c^0{}_1)^2 + 2\,c^0{}_0 c^0{}_2 & c^0{}_2 c^1{}_0 - 2\,c^0{}_1 c^1{}_1 + c^0{}_0 c^1{}_2 & -R^{-1}c^0{}_2 - 2\,c^0{}_1 X - c^0{}_0 Y & R^{-1}c^0{}_0 - 2\,c^0{}_1 \bar{X} + c^0{}_2 \bar{Y} \\
c^0{}_2 c^1{}_0 - 2\,c^0{}_1 c^1{}_1 + c^0{}_0 c^1{}_2 & -2\,(c^1{}_1)^2 + 2\,c^1{}_0 c^1{}_2 & -R^{-1}c^1{}_2 - 2\,c^1{}_1 X - c^1{}_0 Y & R^{-1}c^1{}_0 - 2\,c^1{}_1 \bar{X} + c^1{}_2 \bar{Y} \\
-R^{-1}c^0{}_2 - 2\,c^0{}_1 X - c^0{}_0 Y & -R^{-1}c^1{}_2 - 2\,c^1{}_1 X - c^1{}_0 Y & -2\,X^2 + 2\,R^{-1}Y & -R^{-2} - 2\,X\bar{X} - Y\bar{Y} \\
R^{-1}c^0{}_0 - 2\,c^0{}_1 \bar{X} + c^0{}_2 \bar{Y} & R^{-1}c^1{}_0 - 2\,c^1{}_1 \bar{X} + c^1{}_2 \bar{Y} & -R^{-2} - 2\,X\bar{X} - Y\bar{Y} & -2\,\bar{X}^2 + 2\,R^{-1}\bar{Y}
\end{pmatrix}. \tag{2.5.1}$$

Of course the metric with indices downstairs is quite messy, so we omit it. However we do note that $g_{00} = 1$ as a result of our gauge.

Chapter 3

The spin-2 system for ψ_{ABCD}

The aim of this section is to analyse the equation

$$\nabla_{A'}{}^{E}\psi_{ABCE} = 0,$$

which governs the evolution of the gravitational spinor ψ_{ABCD} and constrains it on each $s =$ constant hypersurface. We may refer to this equation as the spin-2 zero rest-mass field equation or just the spin-2 equation as, although coming from a vacuum Bianchi identity, it is the same equation as for a spin-2 zero rest-mass field. We first show that the resulting evolution equations and subsidiary system are symmetric hyperbolic. We specify what surfaces to take as the boundaries and calculate the characteristic modes of both systems. Maximally dissipative boundary conditions are then used as a way of imposing stable boundary conditions for the ingoing modes of ψ_{ABCD}. Lastly, we present a procedure of fixing the free data for the ingoing modes of ψ_{ABCD} such that the ingoing modes of the subsidiary system are killed and hence do not propagate into the domain of the solution.

3.1 Symmetric hyperbolicity

It is well known that the field equation for the gravitational spinor admits a symmetric hyperbolic system of PDEs (see for example [53], [49]). In order to derive boundary conditions for this system it is convenient to first put it in symmetric hyperbolic form. This is realised

by writing the equations obtained from the components of (2.2.11b)[1] in the form

$$A^{\mu}\partial_{\mu}u = Bu + f(x^{\mu}), \tag{3.1.1}$$

where A^{μ} are 5×5 hermitian matrices and u is a vector containing the components of ψ_{ABCD}. The spin-2 zero rest-mass equation written in the space-spinor formalism is

$$\Lambda_{ABCD} := \partial\psi_{ABCD} - 2\partial_{A}{}^{E}\psi_{BCDE} + 2\chi_{(A}{}^{E}\psi_{BCD)E} - 3\chi_{D}{}^{E}{}_{(A}{}^{F}\psi_{BC)EF} + \chi_{DE}{}^{EF}\psi_{ABCF}, \tag{3.1.2}$$

from which we can extract an evolution system by taking the totally symmetric part. Written in this way we find that A^{μ} are hermitian if we multiply each evolution equation by an appropriate number. Noting that the reality condition on the frame components translates to $\widehat{c^{0}{}_{0}} = -c^{0}{}_{2}$, $\widehat{c^{0}{}_{1}} = c^{0}{}_{1}$ and similarly for $c^{1}{}_{AB}$, the first two matrices are

$$A^{0} = \begin{pmatrix} 1-\sqrt{2}\,c^{0}{}_{1} & \sqrt{2}\,c^{0}{}_{0} & 0 & 0 & 0 \\ -\sqrt{2}\,c^{0}{}_{2} & 4-2\sqrt{2}\,c^{0}{}_{1} & 3\sqrt{2}\,c^{0}{}_{0} & 0 & 0 \\ 0 & -3\sqrt{2}\,c^{0}{}_{2} & 6 & 3\sqrt{2}\,c^{0}{}_{0} & 0 \\ 0 & 0 & -3\sqrt{2}\,c^{0}{}_{2} & 4+2\sqrt{2}\,c^{0}{}_{1} & \sqrt{2}\,c^{0}{}_{0} \\ 0 & 0 & 0 & -\sqrt{2}\,c^{0}{}_{2} & 1+\sqrt{2}\,c^{0}{}_{1} \end{pmatrix}, \tag{3.1.3}$$

$$A^{1} = \begin{pmatrix} -\sqrt{2}\,c^{1}{}_{1} & \sqrt{2}\,c^{1}{}_{0} & 0 & 0 & 0 \\ -\sqrt{2}\,c^{1}{}_{2} & -2\sqrt{2}\,c^{1}{}_{1} & 3\sqrt{2}\,c^{1}{}_{0} & 0 & 0 \\ 0 & -3\sqrt{2}\,c^{1}{}_{2} & 0 & 3\sqrt{2}\,c^{1}{}_{0} & 0 \\ 0 & 0 & -3\sqrt{2}\,c^{1}{}_{2} & 2\sqrt{2}\,c^{1}{}_{1} & \sqrt{2}\,c^{1}{}_{0} \\ 0 & 0 & 0 & -\sqrt{2}\,c^{1}{}_{2} & \sqrt{2}\,c^{1}{}_{1} \end{pmatrix}. \tag{3.1.4}$$

The characteristic speeds of each of the components of ψ_{ABCD} in the ρ-direction are calculated by use of the metric derived in the previous section 2.5. As expected, the speeds of ψ_0 and ψ_4 are null while the others are time-like. One also sees that for an appropriate choice of initial data, namely that $c^{0}{}_{AB} = 0$, we get that $A^{0} = A^{\mu}\delta^{0}{}_{\mu}$ is positive-definite in a neighbourhood of the initial surface. Hence we have hyperbolicity and our system has thus been shown to be symmetric hyperbolic.

[1] Note that these will not be the evolution equations for our system, as one gets time derivatives from both ∂ and ∂_{AB} derivatives, hence A^{0} is not diagonal.

These will clearly not be the equations used in the numerical evolution of the system as A^0 is not diagonal, and hence we have not solved for the time derivatives of the fields. However this can be accomplished by diagonalising A^0 and the resulting equations will be used as the evolution equations for the components of ψ_{ABCD}.

3.2 Maximally dissipative boundary conditions

Now comes the question of what surfaces to take for the boundaries. In general we have a full 3+1 problem, but we have restricted the spatial topology to be of the form $M_1 \times \mathbb{S}^2$. Thus the only boundary conditions needed are for M_1 which is related to the coordinate ρ. The obvious choice then is to take $\rho =$ constant surfaces, as these will be the easiest from the point of view of the numerics as the boundary will not move over time on the computational domain. Recall that our spatial coordinates are constant along the conformal geodesics used to define our gauge, and hence the boundaries will be conformal geodesics.

Now that we have decided on what surfaces to take as the boundaries, we need to find a way to impose stable boundary conditions there. The standard method of fixing boundary conditions for ψ_{ABCD} is to use maximally dissipative boundary conditions. These boundary conditions are found by looking at energy estimates of the system and choosing boundary conditions so that no energy comes in from the boundary. These conditions are used successfully at an analytical level in the Friedrich-Nagy gauge [58] and for the GCFE with Anti-de Sitter space-time in [48]. In order to derive these boundary conditions, we must first simultaneously diagonalise the A^0 and A^1 matrices. This is done so that we can decouple the time derivatives of the ψ_{ABCD} fields propagating normal to the boundary. This procedure is accomplished by:

- Computing the five distinct eigenvalues λ_i and eigenvectors of $(A^0)^{-1}A^1$. This can be done without computing $(A^0)^{-1}$ using the equations

$$\det(A^1 - \lambda A^0) = 0, \qquad A^1 x = \lambda A^0 x.$$

- Normalising the eigenvectors by treating A^0 as a norm, i.e. $x^* A^0 x = 1$ (where $*$ denotes conjugate-transpose).

- Using appropriately ordered eigenvectors as columns of a matrix T, defining $v = Tu$ and multiplying (3.1.1) by T^*, one obtains $(T^* A^\mu T)\partial_\mu v = RHS$ so that

$$T^* A^0 T = \begin{pmatrix} 1 & 0 & 0 & 0 & 0 \\ 0 & 1 & 0 & 0 & 0 \\ 0 & 0 & 1 & 0 & 0 \\ 0 & 0 & 0 & 1 & 0 \\ 0 & 0 & 0 & 0 & 1 \end{pmatrix}, \qquad T^* A^1 T = \begin{pmatrix} -\alpha & 0 & 0 & 0 & 0 \\ 0 & -\beta & 0 & 0 & 0 \\ 0 & 0 & 0 & 0 & 0 \\ 0 & 0 & 0 & \beta & 0 \\ 0 & 0 & 0 & 0 & \alpha \end{pmatrix}. \tag{3.2.1}$$

We can then associate the transformed ψ_{ABCD} components $\widetilde{\psi}_0$ and $\widetilde{\psi}_1$ as outgoing and $\widetilde{\psi}_3$ and $\widetilde{\psi}_4$ as ingoing with respect to the left boundary and vice-versa for the right ($\rho \geq 0$). The zero in the middle of $T^* A^1 T$ indicates that $\widetilde{\psi}_2$ propagates along the boundary and hence will not need a boundary condition.

Looking now at the left boundary, the homogeneous boundary conditions are of the form

$$\begin{pmatrix} 0 \\ 0 \end{pmatrix} = \begin{pmatrix} \widetilde{\psi}_3 \\ \widetilde{\psi}_4 \end{pmatrix} - H \begin{pmatrix} \widetilde{\psi}_0 \\ \widetilde{\psi}_1 \end{pmatrix}, \tag{3.2.2}$$

where H is a 2×2 matrix satisfying

$$H^* H \leq I_2, \tag{3.2.3}$$

where I_2 is the identity matrix. The restriction on H imposes the condition that the energy entering the system is less than the energy which is leaving. The inhomogeneous boundary conditions are given by

$$\begin{pmatrix} q_3 \\ q_4 \end{pmatrix} = \begin{pmatrix} \widetilde{\psi}_3 \\ \widetilde{\psi}_4 \end{pmatrix} - H \begin{pmatrix} \widetilde{\psi}_0 \\ \widetilde{\psi}_1 \end{pmatrix}, \tag{3.2.4}$$

where the q_i are free boundary data. The simplest case is where $H = 0$, which says that energy leaving the system through the left boundary does not get partially reflected back in, it just passes through the boundary and leaves the system. We use this choice for the rest of the document.

The above can easily be converted to the right boundary by simply switching $\widetilde{\psi}_3$ with $\widetilde{\psi}_1$ and $\widetilde{\psi}_4$ with $\widetilde{\psi}_0$ and having different free data q_0 and q_1. This gives us boundary conditions for

v, but we must convert them to boundary conditions for our original ψ's contained in u via the transformation matrix T. Then the left boundary conditions (3.2.4) will look something like

$$q_3 = (T_{30}\psi_0 + T_{31}\psi_1 + T_{32}\psi_2 + T_{33}\psi_3 + T_{34}\psi_4),$$
$$q_4 = (T_{40}\psi_0 + T_{41}\psi_1 + T_{42}\psi_2 + T_{43}\psi_3 + T_{44}\psi_4),$$

where $T_{ij},\ i,j = 0,1,2,3,4$ are components of the matrix T. It is important to realise that the ψ's that are used in the GCFE system will in general have different propagation directions to the $\widetilde{\psi}$'s, and the purpose of doing the above is to obtain a stable way of imposing boundary conditions for them. By choosing initial data ${c^0}_{AB} = 0$ we find that the propagation directions of the ψ's are initially the same as the $\widetilde{\psi}$'s, i.e. on the left boundary ψ_3 and ψ_4 are ingoing, ψ_2 propagates along the boundary and ψ_0 and ψ_1 are outgoing. Then on the left boundary the equations immediately above are solved simultaneously for ψ_3 and ψ_4 so that the boundary data does not contain any ingoing modes.

The approach aforementioned is for the case of two ingoing, one tangential and two outgoing modes. Our boundaries are given by $\rho =$ constant surfaces which lie along conformal geodesics by their definition. This implies that our boundaries will tend to "bend" over time, in the sense that the conformal geodesics will take different paths in the space-time. Also worth noting, the spatial frame vectors used in the system $\{e_1, m, \bar{m}\}$ will in general stop being tangent to the surfaces of constant s due to the s-derivative operator appearing in the expansion of ∂_{AB} and the surfaces $s =$ constant will "tilt" due to having different accelerations along different conformal geodesics. All of these things affect the propagation directions and speeds of the ψ's on the boundaries, see Figure 3.1. Due to our conformal geodesics being always time-like, we will never see a change in sign of the characteristic speed of ψ_0 and ψ_4 which propagate along null lines. However we must take care to monitor the propagation directions of ψ_1, ψ_2 and ψ_3 on our boundaries. Clearly ψ_2 will be the most sensitive to a bending boundary as a slight change in the ρ-direction will stop it from propagating along the boundary and it will instead be either ingoing or outgoing.

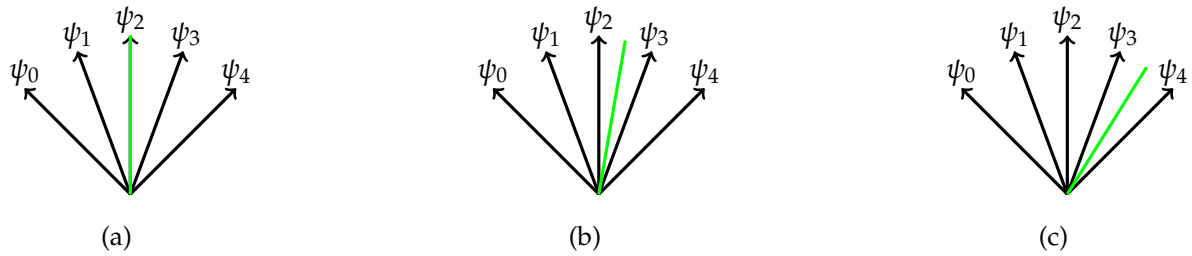

Figure 3.1: The effect of the conformal geodesic bending over-time on the characteristics of ψ_{ABCD}. The green line indicates the rightmost boundary (i.e. a conformal geodesic) of the system. There are two ingoing modes in (a), three in (b) and four in (c).

To show how to handle this, suppose we are looking at the right-most boundary (largest ρ, $\rho \geq 0$) and initially we have that ψ_0 and ψ_1 are ingoing, ψ_2 is propagates along the boundary and ψ_3 and ψ_4 are outgoing. As mentioned above, we initially choose simple boundary data of the form

$$\widetilde{\psi}_0 = q_0, \qquad \widetilde{\psi}_1 = q_1.$$

These two equations will in general be functions of all the ψ_{ABCD} components and so we must solve them together for ψ_0 and ψ_1 so their right-hand-sides contain no ingoing modes. Then if the boundary bends such that ψ_2 becomes outgoing, we need not do anything. However if the boundary bends so that ψ_2 becomes ingoing, then we must do something.

We can obtain a boundary condition for ψ_2 by imposing the condition

$$\widetilde{\psi}_2 = q_2,$$

which reflects the extra degree of freedom on the boundary. However now that ψ_2 is ingoing, it can no longer be on the right-hand-side of the boundary conditions for ψ_0 and ψ_1. So we need to re-solve the now three boundary equations together so that they do not contain the new ingoing mode ψ_2 on the right-hand-side, as well as ψ_0 and ψ_1. This clearly gives new boundary conditions for ψ_0 and ψ_1 as well as an additional one for ψ_2.

Suppose now that the boundary bends even more so that ψ_3 also becomes ingoing. We repeat the above procedure, solving now a system of four equations for the correct boundary

data so that the only ψ_{ABCD} component on the right-hand-sides is ψ_4.

3.3 Handling constraint propagation

From the previous section, we have two free functions to specify on each boundary initially. However this procedure in no way guarantees that the constraints will be satisfied there. As the constraint equations coming from the spin-2 zero rest-mass equation are PDEs, if they are violated on the boundary they may propagate into the interior region and destroy constraint propagation there. Although we have not explicitly written down the subsidiary system, many of the constraint propagation equations in the subsidiary system are written in terms of the spin-2 zero rest-mass constraints. Thus if they are violated, they will cause other constraints to be violated too. In order to see how this works in more detail, we need to analyse the subsidiary system.

The principle part of the subsidiary system for the spin-2 zero rest-mass equation is given by

$$\partial Z_{AB} = -\partial^{C}{}_{(A} Z_{B)C}, \tag{3.3.1}$$

where we have defined

$$Z_{AB} := \partial^{CD}\psi_{ABCD} + \chi^{CE}{}_{E}{}^{D}\psi_{ABCD} + \chi^{CDE}{}_{(A}\psi_{B)CDE}. \tag{3.3.2}$$

By writing (3.3.1) in components we obtain three equations, which when written in the form (3.1.1) give us the matrices

$$A^0 = 2\begin{pmatrix} \sqrt{2} - c^0{}_1 & c^0{}_0 & 0 \\ -c^0{}_2 & 2\sqrt{2} & c^0{}_0 \\ 0 & -c^0{}_2 & \sqrt{2} + c^0{}_1 \end{pmatrix}, \qquad A^1 = 2\begin{pmatrix} -c^1{}_1 & c^1{}_0 & 0 \\ -c^1{}_2 & 0 & c^1{}_0 \\ 0 & -c^1{}_2 & c^1{}_1 \end{pmatrix}. \tag{3.3.3}$$

Clearly this system is symmetric hyperbolic, and hence we can derive maximally dissipative boundary conditions. By following the same procedure as for the ψ_{ABCD} evolution system, we find that for each boundary there is an ingoing mode, an outgoing mode and one which propagates along the boundary. So at each boundary we obtain one boundary condition which we choose again to be maximally dissipative. This confirms that if we violate the

constraints at the boundary the error will in fact propagate into the interior.

So how do we prescribe boundary data for the ψ_{ABCD} system on the boundary in such a way that the constraints still propagate? With respect to the GCFE, this question has only been answered by Friedrich for the case of Anti-de Sitter [48] where the special choice of the boundary being at $\mathscr{I}$ was taken. He then modified the evolution system by adding constraints in such a way that it remained symmetric hyperbolic as well as the subsidiary system consisting only of Ordinary Differential Equations (ODEs). This then avoids the problem of ingoing modes in the subsidiary system all together. This process however is very specialised due the unique properties of having $\mathscr{I}$ as the boundary. Here, we will try and kill the ingoing mode by appropriate choice of boundary data for the ψ_{ABCD} system.

The most physically interesting quantities to prescribe at the boundary are the gravitational waves described by ψ_0 resp. ψ_4. One may then ask whether it is possible to leave their prescription free, while fixing the remaining freedom in choosing ψ_1 resp. ψ_3 in such a way that the ingoing mode of the subsidiary system is zero. This is in fact possible, as we will shortly see.

The way to do this on the right boundary (the left is analogous) for the case of ψ_0, ψ_1 ingoing, ψ_3, ψ_4 outgoing and ψ_2 propagating along the boundary is to derive an ODE for the free data q_1 as follows:

- Treat the prescription of ψ_0 as being free, i.e. the boundary data q_0 is a free spin-2 function. Then the derivatives of ψ_0 tangent to the boundary are also known on the boundary.
- Take a time derivative of the boundary equations for ψ_0 and ψ_1 and replace all of the time derivatives with their evolution equations. This will, in particular, leave the equation containing terms involving $\partial_s q_1, \partial_\rho \psi_0$ and $\partial_\rho \psi_1$.
- Solve these equations simultaneously for $\partial_\rho \psi_0$ and $\partial_\rho \psi_1$.
- Replace $\partial_\rho \psi_0$ and $\partial_\rho \psi_1$ in the boundary equation for the ingoing subsidiary mode with

the above.

- Solve this equation for $\partial_s q_1$.

The resulting equation is free of $\partial_\rho \psi_0$ and $\partial_\rho \psi_1$ terms which are technically not known on the boundary (although numerically these can always be approximated). This gives us an ODE for q_1 on the boundary that should kill the ingoing mode from the subsidiary system. Note that it is fine for this equation to contain ingoing modes because the right-hand-side is computed after the boundary data have been assigned, i.e. when $\partial_s q_1$ is computed all of the functions in the system are already known on the boundary.

By choosing q_0 freely and q_1 as above we have shown that the ingoing mode of the subsidiary system is killed so that the constraints will hopefully propagate.

The final remark here is how to extend this approach to incorporate the potential bending of the boundaries. One notes that the propagation speeds and directions of ψ_2 and Z_1 are in fact the same. Similarly for Z_0, ψ_1 and Z_2, ψ_3. On the right boundary, this means that as soon as ψ_2 becomes ingoing, so will a mode from the subsidiary system. Later, if ψ_3 becomes ingoing, then so does the final mode in the subsidiary system. Hence at any point in time on the boundary we will have n ingoing modes from the ψ_{ABCD} evolution system and $n-1$ ingoing modes from the ψ_{ABCD} subsidiary system. This means we can always choose q_0 freely and choose the remaining free data to kill the ingoing modes of the subsidiary system.

The results of this approach on the numerical level are presented in sections 6.4 and 9.3.

3.4 Frame rotation simplification

The analysis of the spin-2 zero rest-mass system's maximally dissipative boundary conditions is complicated in general due to the existence of the six frame components from c^0_{AB} and c^1_{AB}. The crux of the problem is the inversion of the transformation matrix that relates the original equations with the diagonalised ones. Although we managed to handle the

rather large expressions, it is likely possible that we could modify the CGG to help matters. By changing the frame transport equation in (1.3.5c) so that the frame is *not* parallely propagated along the conformal geodesics we could rotate the frame so that certain frame components remain zero. This would of course introduce new variables into the system whose job it is to rotate the frame to maintain killing these components. This would make most equations longer, but would simplify the boundary analysis. However as we manage to handle the boundary analysis as is, we leave this as a comment.

Chapter 4

Checking the equations

Since the derivation of the GCFE in the space-spinor formalism was so tedious, one needs to perform checks for correctness. In this section we outline the analytical checks performed to ensure this. Firstly we note that the derivation was done by hand initially, and hence subject to human error. Thus we also used a Mathematica package xAct [81], which handles symbolic manipulation of tensors and spinors, to verify our hand-written calculations. This package was especially useful for writing the unknowns (2.2.10) with respect to the spin-frame, i.e.

$$f_{AB} = f_0\, \iota_A\iota_B - 2f_1\, o_{(A}\iota_{B)} + f_2\, o_A o_B,$$

and thus giving us the component representation of the equations with ease.

4.1 Constraint propagation/Subsidiary system

It is well known that the constraint equations derived from the GCFE propagate, in the sense that time-derivatives of the constraints are combinations of the constraints themselves (and potentially spatial derivatives of them). Constraint propagation at the numerical level is another story entirely, and is still not very well understood [54]. A good consistency check is to reproduce that the time derivative of the constraints are combinations of the constraints themselves. This is accomplished by taking a time derivative with ∂ of the constraints (2.2.12), using our expression for $[\partial, \partial_{AB}]$[1] to switch the order of the derivatives, re-

[1] This was given in appendix B.1.

placing the time derivatives of the fields using evolution equations, and then replacing the spatial derivatives with the constraints. This is a purely mechanical process as given spatial derivatives of say f_{AB}, one can write them in irreducible parts. The parts corresponding to a constraint equation from (2.2.12d) can be replaced, while the others *must* vanish. This results in propagation equations only involving combinations of the constraints, which vanish when the constraints vanish and thus show propagation. This has been confirmed for each of the constraints listed above.

It is worth mentioning that the only subsidiary equation which has spatial derivatives is that of the constraint arising from the spin-2 zero rest-mass equation for ψ_{ABCD} which is of the form (3.3.1). This means that this is the only equation that potentially has constraint violating modes that may propagate into the interior of the computational domain from the boundaries.

4.2 Computing exact space-times in the CGG

Now that we have our system and performed a few checks, we compute known exact solutions in the CGG and show they satisfy our system. In general this will not be possible analytically, but it is possible for some simple space-times which are still general enough to be a decent test.

The following is the procedure used to rewrite an arbitrary metric $\widetilde{g}_{ab}$ with coordinates $\{t, r, \tilde{\theta}, \tilde{\phi}\}$ in the CGG. I will leave this short, and discuss some details below.

1 Compute the Christoffel symbols and curvature quantities of $\widetilde{g}_{ab}$ in the coordinate basis.

2 Solve the conformal geodesic equations

$$v^a \widehat{\nabla}_a v^b = 0 \quad \Longleftrightarrow \quad v^a \widetilde{\nabla}_a v^b = -2(b_a u^a)\, v^b + (v_a v^a)\, b^b,$$
$$v^a \widehat{P}_{ab} = 0 \quad \Longleftrightarrow \quad v^a \widetilde{\nabla}_a b_b = (v^a b_a) b_b - \frac{1}{2} b^e b_e\, v_b + v^a P_{ab},$$

for tangent vector v^a, 1-form b_a and in terms of a parameter s. In general this will leave

eight degrees of freedom, namely the values of v^a and b_a on the initial surface $\underline{v}^a$ and $\underline{b_a}$.

3 Choose a function t_0 which may be dependent on the spatial coordinates which describes the initial hypersurface $s = 0$.

4 Choose as a new temporal coordinate the parameter s of the geodesic, and new spatial coordinates which are constant along the geodesics. The obvious choice are their values at $s = 0$. The new coordinate system is then $\{s, \rho, \theta, \phi\}$.

5 Generalise from one geodesic to a congruence, hence the initial data $\underline{v}^a, \underline{b}_a$ become functions of the new spatial coordinates. At this stage how the geodesics are initially oriented with respect to the initial hypersurface can be fixed.

6 Transform the metric $\widetilde{g}_{ab}$, tangent vector v^a and 1-form b_a to the new coordinate system.

7 Specify an orthogonal frame with $e_{\mathbf{0}} = v^a$, where each vector has the same length, and that is parallely transported along the geodesics with respect to the Weyl connection, i.e. satisfies

$$v^a \widehat{\nabla}_a e^b_{\mathbf{b}} = 0 \iff v^a \widetilde{\nabla}_a e^b_{\mathbf{b}} = -b_a v^a \, e^b_{\mathbf{b}} - b_a e^a_{\mathbf{b}} \, v^b + (v_a e^a_{\mathbf{b}}) \, b^b.$$

8 The frame defines a unique metric in the conformal class in which it becomes orthonormal. This gives us a conformal factor, defined as

$$\Theta^2 \widetilde{g}(e_{\mathbf{a}}, e_{\mathbf{b}}) = \eta_{\mathbf{ab}}.$$

This conformal factor gives us a new metric $g_{ab} := \Theta^2 \widetilde{g}_{ab}$.

9 Compute the connection coefficients and curvature quantities of g_{ab} with respect to the frame $e_{\mathbf{a}}$ and compute the spinor components of (2.2.10) from them and the frame components.

First note that in **2**, the conformal geodesic equations can be solved using any metric in the conformal class (see section 1.3). This can dramatically alter the differential equations that

one needs to solve. In particular if one solves the conformal geodesic equations with respect to the Einstein Cylinder metric, which gives relatively simple equations, then one has the conformal geodesics for all three spaces of constant curvature.

When computing the spinor components in **9**, one just needs to use the equations relating the orthonormal frame $\{e_{\mathbf{a}}\}$ and spin-frame $\{o, \iota\}$ to relate tensor components to our space-spinor ones. These relations are given by the equations (A.1.6) and (A.1.7).

The Schouten spinor in our system is associated with the Weyl connection, not the conformal connection. Since one has the conformal connection, one could compute the conformal Schouten tensor and then use the appropriate conformal transformation law to obtain the Weyl Schouten tensor. However it is easiest to use the conformal transformation law between $\widehat{P}_{ab}$ and $\widetilde{P}_{ab}$ (1.4.7). One then enforces the vacuum equation (1.1.1) to eliminate the physical Schouten tensor. This saves having to compute Ricci curvature from the potentially large and nasty looking conformal metric.

By following the above procedure with Minkowski space written as

$$\widetilde{g}_{ab} = \mathrm{d}t^2 - \mathrm{d}r^2 - r^2(\mathrm{d}\theta^2 + \sin^2\theta\ \mathrm{d}\phi^2),$$

and Anti-de Sitter, written as

$$\widetilde{g}_{ab} = \frac{1}{\cos^2 r}\Big(\mathrm{d}t^2 - \mathrm{d}r^2 - \sin^2 r(\mathrm{d}\theta^2 + \sin^2\theta\ \mathrm{d}\phi^2)\Big),$$

we were able to show that the resulting fields[2] satisfied the evolution and constraint equations identically where the gauge was chosen to be adapted to spherically symmetric conformal geodesics. A more detailed description of the Anti-de Sitter case is described in section 6.1.

[2]The expressions for the components of our system are horrible, thus we leave them out.

Part II

The numerical implementation of the IBVP for the GCFE

Chapter 5

Numerical methods

5.1 Numerical preliminaries

The aim of this section is to formulate a numerical implementation of the Initial Boundary Value Problem (IBVP) for the GCFE system. The idea is to choose some initial space-like hypersurface and prescribe on it data for the unknowns (2.2.10) so that the constraints (2.4.12) are satisfied. Then we evolve the initial data using the evolution equations (2.4.11) and choose boundary conditions in such a way that the constraints remain satisfied during the evolution. First, a short overview of the numerical methods used will be presented before going into more detail in the subsequent sections.

We must first discretise the continuous version of the equations in order to evolve the system on the computer using various numerical methods. We will discretise our system using the *method of lines*. This is done by approximating the spatial derivatives so that on the level of the discretised system, we have a system of ODEs. In full generality, we have three spatial directions that need discretising, two of which are tangent to unit 2-spheres[1] while the other is normal to them. The spatial derivatives $\eth, \eth'$ can be approximated using the so-called *pseudo-spectral methods*, which involve transforming to spectral space where the derivative is calculated very quickly and accurately, then transforming back. The radial direction will be approximated using straightforward *finite difference* methods. Using these approximation

[1] This is because we introduced the unit-sphere derivative operators δ, δ' and subsequently $\eth, \eth'$.

methods to extract a semi-discrete system of ODEs, we use for the temporal discretisation the standard *fourth-order explicit Runge-Kutta* scheme. In order to impose stable boundary conditions, we utilise the *simultaneous-approximation-term* (SAT) method, which works very well with certain finite difference operators.

The first step to take is to discretise the three-dimensional hypersurfaces of constant time and the time direction itself. The spatial directions can be discretised by choosing the computational domain to be the multi-dimensional interval $[\rho_0, \rho_N] \times [0, \pi] \times [0, 2\pi]$ (for $\{\rho, \theta, \phi\}$ respectively) where the left and right boundaries are ρ_0 and ρ_N respectively. Each direction can be split into $N + 1$ equi-distant grid points so that, taking the ρ-direction as an example, $\rho_i = \rho_0 + ih_\rho$, for $i = 0, 1, \cdots, N$ where h_ρ is the step-size. The time direction is also discretised into equi-distant points where the step-size is chosen to be related to the step-size in the ρ-direction by $h_s = C\ h_\rho$, where C is the Courant number which is used to satisfy the so-called Courant-Friedrichs-Lewy (CFL) condition [24] which is required for a stable evolution. For the rest of this document this value is fixed as 0.5.

There are many different kinds of finite differencing operators. Of particular use are a subset of them called *Summation-By-Parts* (SBP) operators, first defined in 1974 by Kreiss and Scherer (republished article [72]) and subsequently [73]. In the continuous case one can use integration-by-parts to obtain energy estimates that can then be used to prove wellposedness of the system. Summation-by-parts is the discrete analogue of integration-by-parts, and hence can give a discrete energy estimate for the system. This is then used to prove numerical stability results for these operators. Their convergence order near the boundary is generally a few smaller than the interior. However when one increases the grid resolution, "near the boundary" becomes a smaller and smaller subset of the domain. They have been used widely in the numerical relativity community, see for example [70, 74, 75, 91, 116] and more recently [10, 11, 12, 29, 42].

Although the general idea is the same, there are many kinds of algorithms for spectral and pseudo-spectral methods. Of late there have been fast C-codes developed by Huffenberger

and Wandelt [66], which have recently been optimised for the axially-symmetric case by Beyer, Escobar and Frauendiener [13]. The general method has very good convergence properties, namely exponential for smooth enough functions. They also require a much smaller number of grid points compared to finite difference operators for a similar order of accuracy. We will be using these methods which exploit the relationship between the Wigner d-functions and spin-s spherical harmonics, given originally in [63].

Finally we need a stable way of implementing boundary conditions for the gravitational spinor components. The *Simultaneous-Approximation-Term* (SAT) method is one way of doing this, given originally by Carpenter, Nordström and Gottlieb in [21]. This method seems to work very well with SBP operators. In particular, it has been shown that the numerical stability properties of the SBP operators remain when using the SAT method on the boundary. This is by no means a trivial condition. The SAT method involves adding a weighted penalty term to the evolution equations that require boundary conditions. This then drives the functions to the desired value on the boundary with a speed determined by a parameter τ.

The SAT method has been used successfully in a variety of numerical relativity codes that also implement the SBP operators, see [22, 28, 75, 116] and more recently [42, 64] and the series by Beyer et al. starting with [10].

The Python package COFFEE (COnFormal Field Equation Evolver), developed by the relativity group at the University of Otago will be used to incorporate all of the aforementioned numerical schemes. This package has been thoroughly tested and has been used in a variety of papers [10, 11, 12, 42].

5.2 First derivative SBP finite difference operators

In this section we give the details for SBP finite difference operators that approximate a first order derivative operator. The equations we are interested in are the PDEs coming from the field equation for the gravitational spinor, which are advection equations. The

spatial derivative operators $\frac{\partial}{\partial\rho}$ will be approximated using finite differencing. To make the discussion simpler, we look at the scalar 1D advection equation[2]

$$u_s = \alpha u_\rho, \qquad \text{in } [0,\infty)\times[\rho_0,\rho_N], \tag{5.2.1}$$

where s and ρ are real numbers in their respective intervals, α is a non-zero constant and at each $s=$ constant surface u is a differentiable function in the space of real square-integrable functions $L^2[\rho_0,\rho_N]$. We define

$$(u,v) := \int_{\rho_0}^{\rho_N} uv\mathrm{d}\rho,$$

so that the L_2-norm of u is given as

$$\|u\| := \sqrt{\int_{\rho_0}^{\rho_N}(u,u)\mathrm{d}\rho}.$$

The energy estimate for the system is computed by looking at the time derivative of the square of the L_2-norm of u. Using integration by parts and (5.2.1) we find

$$\frac{\mathrm{d}}{\mathrm{d}s}\|u\|^2 = \alpha\Big((u,u_\rho)+(u_\rho,u)\Big) = \alpha\Big(u(s,\rho_N)^2 - u(s,\rho_0)^2\Big). \tag{5.2.2}$$

The idea of this process is to try and keep the right-hand-side non-positive, and a simple way to ensure this for $\alpha>0$ is to set the boundary condition $u(s,\rho_N)=0$ and leave $u(s,\rho_0)$ free, and vice-versa with $\alpha<0$. The idea now is to discretise the ρ-derivative operator so that we get a similar energy estimate for the discretised equation. We discretise u into $N+1$ equidistant points which we shall denote by $v := \{v_0, v_1, \cdots, v_N\}$ and define the discretised norm as $\|v\|_H := v^T H v$, where H is a positive-definite symmetric $(N+1)\times(N+1)$ matrix. Then the derivative operator is defined as $D := H^{-1}Q$ for some $(N+1)\times(N+1)$ matrix Q with constant entries and the discretised equation becomes

$$v_s = \alpha D v.$$

The energy estimate for the discretised equation is

$$\frac{\mathrm{d}}{\mathrm{d}s}\|v\|_H^2 = \frac{\mathrm{d}}{\mathrm{d}s}\Big(v^T H v\Big) = \alpha v^T\Big(Q^T(H^{-1})^T H + Q\Big)v = \alpha v^T\Big(Q^T+Q\Big)v, \tag{5.2.3}$$

[2]We leave out an initial condition as this is not relevant for our discussion.

using that H is symmetric. Then in order to obtain a similar form to (5.2.2), we restrict Q by requiring

$$Q + Q^T = diag(-1, 0, \cdots, 0, 1). \tag{5.2.4}$$

Then the discretised energy estimate becomes

$$\frac{\mathrm{d}}{\mathrm{d}t}\|v\|_H^2 = \alpha\Big(v_N^2 - v_0^2\Big), \tag{5.2.5}$$

which is clearly the discretised equivalent of (5.2.2).

Any finite difference operator $D := H^{-1}Q$ satisfying (5.2.4) as well as $H = H^T$ is said to have the *summation-by-parts* property. It has been shown in [72] and [73] that this property guarantees numerical stability. There is still a large degree of freedom in fixing the H matrix, i.e. choosing some norm that the energy estimate is done with-respect-to. The three commonly considered cases are the full norm, restricted full norm and diagonal norm. These additional restrictions do not of course fix H uniquely. In [28] they prescribe addition optimisation criteria that is used to further restrict H, such as minimisation of the bandwidth, truncation error on the boundary points, spectral radius or a combination of these. For all of our simulations, we use a method given by Strand in [121] which is fourth order in the interior and third order on the boundary.

5.3 The SAT method

Here we describe the SAT method [21] that will be used to implement boundary conditions for (5.2.1). As we are taking $\rho =$ constant surfaces for our boundaries, which are made up of 2-spheres, we essentially end up with a one-dimensional problem and so the problem (5.2.1) is an adequate example. From section 3.2 we know that in the simplest case we must specify boundary data for ψ_0, ψ_1 on the right boundary (ρ_N) and ψ_3, ψ_4 on the left boundary (ρ_0). To showcase the SAT method it will be enough to look at the case where we must prescribe data on the right boundary, with the left boundary case following analogously. We then want to solve (5.2.1) subject to the Dirichlet boundary condition

$$u(s, \rho_N) = g_N(s). \tag{5.3.1}$$

The SAT method involves adding a penalty term to the right-hand-side of the evolution equation (i.e. of (5.2.1)) on the boundary which drives the solution to the prescribed boundary value. The rate at which the solution is driven to the boundary value is determined by a parameter denoted as τ, which we introduce shortly. Using the boundary condition, the energy estimate (5.2.2) becomes

$$\frac{\mathrm{d}}{\mathrm{d}s}\|u\|^2 = \alpha\Big(g_N(s)^2 - u(s,\rho_0)^2\Big). \tag{5.3.2}$$

We then modify D (as defined in the previous section) to obtain the new equation for v

$$v_s = \alpha H^{-1}Qv - \tau\alpha H^{-1}\Big(E_N v - e_N g_N(s)\Big),$$

where τ is called the penalty parameter, $E_N = diag(0,0,\cdots,0,1)$ is an $(N+1)\times(N+1)$ matrix and $e_N = (0,0,\cdots,0,1)$. If we choose $\tau \geq 1$ then this method is proven to be stable. The energy estimate with the SAT method imposed is

$$\frac{\mathrm{d}}{\mathrm{d}s}\|v\|_H^2 = \alpha\Big[g_N(s)^2 - v_0^2 - \tau\Big(v_N - g_N(s)\Big)^2\Big]. \tag{5.3.3}$$

As the last term is always non-positive (for $\alpha > 0$), our energy estimate is unaffected and we maintain the *summation-by-parts property*. For the remainder of this document, we choose $\tau = 1$.

5.4 Pseudo-spectral methods

The final task is to choose a method of approximating $\eth, \eth'$. The idea we will make use of is to transform a function to spectral space using the forward transform

$${}_s a_{lm} = \int_{S^2} f(\theta,\phi)\ {}_s\bar{Y}_{lm}(\theta,\phi)\mathrm{d}\Omega, \tag{5.4.1}$$

using some quadrature rule on S^2 to evaluate the integral, given that we know the ${}_sY_{lm}$ (this of course needs to be truncated at some maximum mode $l = L$ to obtain a finite representation for when this is implemented on the computer). We then have the representation of the function expressed in terms of spin-weighted spherical harmonics. The relationships (2.3.4) to compute the action of $\eth, \eth'$ on the spin-weighted spherical harmonics can now be used, remembering that the ${}_s a_{lm}$ are just complex numbers. This gives a set of ${}_{s\pm1}a_{lm}$ for the basis

${}_{s\pm1}Y_{lm}$ which is the derivative we want represented in spectral space. Using the backward transform

$$f(\theta,\phi) = \sum_{l=|s|}^{L} \sum_{m=-l}^{l} {}_{s}a_{lm}\ {}_{s}Y_{lm}(\theta,\phi), \tag{5.4.2}$$

gives the derivative expression in our $\{e_{\mathbf{0}}, e_{\mathbf{1}}, m, \bar{m}\}$ basis.

The way we actually do this does follow the above, although we now replace the spin-weighted spherical harmonics with their expressions involving the *Wigner d-matrices* and write it in a way that is optimised to be computed as fast as possible. This method has fast algorithms for both the general case (Huffenberger and Wandelt [66]) and the axially-symmetric case (Beyer et al. [13]). In terms of time-complexity, the brute force approach of computing the spin-weighted spherical harmonics mentioned above is $O(L^4)$, while it is $O(L^3)$ for the general case using Huffenberger and Wandelt's algorithm and $O(L^2)$ when axial-symmetry is imposed on their method.

The relationship between the spin-weighted spherical harmonics and the Wigner d-functions is given by

$${}_{s}Y_{lm} = (-1)^{s}\sqrt{\frac{2l+1}{4\pi}}e^{im\phi}d^{l}_{m(-s)}(\theta). \tag{5.4.3}$$

The d-matrices are computed recursively by an algorithm introduced in [122]. Then defining

$$\Delta^{l}_{mn} = d^{l}_{mn}\Big(\frac{\pi}{2}\Big), \tag{5.4.4}$$

we can write the d-matrices as

$$d^{l}_{mn}(\theta) = i^{m-n}\sum_{q=-l}^{l}\Delta^{l}_{qm}e^{-iq\theta}\Delta^{l}_{qn}. \tag{5.4.5}$$

Then the forward and backward transforms of Huffenberger and Wandelt are given by

$${}_{s}a_{lm} = (-1)^{s}i^{m+s}\sqrt{\frac{2l+1}{4\pi}}\sum_{q=-l}^{l}\Delta^{l}_{qm}I_{qm}\Delta^{l}_{q(-s)}, \tag{5.4.6}$$

$${}_{s}f(\theta,\phi) = \sum_{m,n}e^{im\theta}e^{in\phi}G_{mn}, \tag{5.4.7}$$

where

$$I_{mn} = \int_2 e^{-im\theta} e^{-in\phi} f(\theta, \phi) \mathrm{d}\Omega, \tag{5.4.8}$$

$$G_{mn} = (-1)^s i^{n+s} \sum_l \sqrt{\frac{2l+1}{4\pi}} \Delta^l_{(-m)(-s)} \Delta^l_{(-m)n} \, {}_s a_{lm}. \tag{5.4.9}$$

The integral in the definition of I_{mn} can be computed very fast using a 2-dimensional Fast-Fourier Transform (FFT) with a modified version of $f(\theta, \phi)$. For a band-limited function (i.e. a function that has been truncated at some maximal mode $l = L$) the $(2L+1)^2$ integrals can be computed in $O(L^2 \log L)$ operations. The computation of the G_{mn} also takes $O(L^2 \log L)$ operations. This is the basic idea of the algorithm.

Chapter 6

Checking the numerics

Now that we have fully described the numerical schemes that we will use to evolve our system, we need to check that they are working correctly. We also need to check that the system is correct in the sense that it reproduces known exact solutions of the field equations. We use the axially-symmetric pseudo-spectral algorithm for all our simulations that have θ-dependence. We do not run full $3+1$ problems due to the computational time required.

6.1 Deriving an exact solution

The first thing to check is that our system reproduces an exact solution. To verify this we compute the exact analytic solution of Anti-de Sitter space-time in the CGG using the process outlined in section 4.2.

One can think of Anti-de Sitter space-time (see section 7.1 for an explanation of this space-time) as a conformal rescaling of the Einstein cylinder with metric

$$\widetilde{g} = \frac{1}{\cos^2 r}\Big[dt^2 - dr^2 - \sin^2 r\Big(\mathrm{d}\theta^2 + \sin^2\theta\ \mathrm{d}\phi^2\Big)\Big],$$

and cosmological constant $\lambda = -3$. This clearly shows that Anti-de Sitter space-time has conformal infinity at $r = \frac{\pi}{2}$.

In accordance with the CGG, we adapt our gauge to spherically-symmetric conformal geodesics $\gamma(s,\rho)$ and hence have four degrees of freedom in choosing the initial data for them; two for

the tangent vector to the conformal geodesics v^μ and two for the 1-form b_μ (recalling Greek indices indicate components in the coordinate basis). To first see roughly what this solution looks like, we choose the initial data on $t = 0 \Leftrightarrow s = 0$, as

$$v^0(0,\rho) = 1, \qquad v^1(0,\rho) = 0, \qquad b_0(0,\rho) = 0, \qquad b_1(0,\rho) = -\tan\rho, \tag{6.1.1}$$

so that one gets conformal geodesics that are spatially constant with respect to the $\{t, r, \theta, \phi\}$ coordinates. Then we only have $v^0(s)$ and $b_0(s)$ to worry about. They are given as

$$v^0(s) = \frac{1}{1 + (\frac{s}{2})^2}, \qquad b_0(s) = \frac{s}{2}. \tag{6.1.2}$$

This demonstrates a potential problem that is inherent in the class of metrics conformal to the Einstein Cylinder which is exemplified by the integral of $v^0(s)$, namely

$$t(s) = 2\arctan b_0(s).$$

The conformal geodesics which start at $t = 0$ only get to $t = \pi$ as $s \to \infty$. This is not an issue when looking at the conformal embeddings of Minkowski or de Sitter space-times in the Einstein Cylinder for example, as the conformal geodesics manage to globally cover the conformal embedding of de Sitter space-time while they cover all of Minkowski space-time bar future and past time-like infinity which occur at $t = \pm\pi$. However one can only cover a finite subset of the conformal embedding of Anti-de Sitter space-time, which is only compactified in the spatial direction.

Anti-de Sitter space-time in the CGG adapted to these spatially-constant conformal geodesics takes the form

$$\widetilde{g} = \frac{1}{\cos^2\rho}\Big[\frac{1}{[(\frac{s}{2})^2 + 1]^2}\mathrm{d}s^2 - \mathrm{d}\rho^2 - \sin^2\rho\Big(\mathrm{d}\theta^2 + \sin^2\theta\mathrm{d}\phi^2\Big)\Big],$$

with conformal factor

$$\Theta = \Big[\Big(\frac{s}{2}\Big)^2 + 1\Big]\cos\rho,$$

and conformal metric thus

$$g = \mathrm{d}s^2 - \Big[\Big(\frac{s}{2}\Big)^2 + 1\Big]^2\Big[\mathrm{d}\rho^2 + \sin^2\rho\Big(\mathrm{d}\theta^2 + \sin^2\theta\mathrm{d}\phi^2\Big)\Big].$$

The fields in the GCFE system derived from the conformal metric g (except R, the conformal factor for the 2-sphere) tend to zero over-time due to the slowing down of the conformal geodesics. This can be explained as follows: The way the CGG is defined is that the frame specified on the initial surface is parallely propagated along the conformal geodesics by the Weyl connection. The lengths of the frame vectors with respect to the physical metric will change as they travel along these curves. Hence this defines a conformal factor and hence a conformal metric along the conformal geodesics for which the frame becomes orthonormal. In the case presented here, we have that $\Theta \to \infty$ as $s \to \infty$, which implies that the frame vectors are shrinking with respect to the physical metric.

By computing the quantities of our system from the exact solution and plugging them into the GCFE system equations we find they are identically satisfied not only for the spatially-constant case, but with none of the free data specified for v^μ and b_μ, as must of course be the case.

Now we present more general free data other than the spatially-constant case to test the numerics. We fix $v^1(0,\rho)$ by requiring the geodesics to be orthogonal to the $t = 0 \Leftrightarrow s = 0$ initial surface by $v^1(0,\rho) = 0$. We choose $v^0(0,\rho) = 1$ and $b_1(0,\rho) = -\tan\rho$ as before but now we fix $b_0(0,\rho) = \rho$. This in particular, gives us a non-zero f_1. This particular choice of

free data gives us the exact solution of the GCFE system as

$$R = \alpha \sin\rho,$$

$$c^0{}_1 = -\frac{\sqrt{2}s^2}{\alpha}, \qquad c^1{}_1 = -\frac{2\sqrt{2}}{\alpha},$$

$$f_1 = \frac{2\sqrt{2}s}{\alpha},$$

$$h_{01} = \frac{\left(s + 2\rho + s\rho^2\right)\cos\rho + 2\sin\rho}{2\sqrt{2}}, \qquad h_{01} = \frac{-\left(s + 2\rho + s\rho^2\right)\cos\rho + 2\sin\rho}{2\sqrt{2}},$$

$$\gamma_{20} = \hat{\gamma}_{01} = \frac{\left(s + \cot\rho\right)}{\sqrt{2}\,\alpha},$$

$$\chi_{02} = \chi_{20} = \frac{\left(s + 2\rho + s\rho^2\right)}{\sqrt{2}\,\alpha}, \qquad \chi_{11} = -\frac{\left(s + 2\rho + s\rho^2\right)}{2\sqrt{2}\,\alpha},$$

$$P_{011} = P_{200} = -\frac{1+\rho^2}{2\,\alpha},$$

$$P_{101} = \frac{3+\rho^2}{4\,\alpha}, \qquad P_{110} = \frac{-1+\rho^2}{4\,\alpha}, \tag{6.1.3}$$

with all other fields in the system zero and where we have defined

$$\alpha := 1 + s\rho + \left(\frac{s}{2}\right)^2(1+\rho^2).$$

6.2 Reproducing an exact solution

Now we test the numerical schemes employed in our code by reproducing Anti-de Sitter space-time using the initial data derived in the previous section. As Anti-de Sitter space-time is spherically symmetric we have a 1+1 problem, and hence are only concerned with the spatial dimension ρ. We discretise the ρ-direction with equi-distant points in the interval $[0.25, 1.25]$ with resolutions (i.e. how many sub intervals we split $[0.25, 1.25]$ into) $\{25, 50, 100, 200, 400\}$ and a time-step of 0.5 h_ρ, recalling that 0.5 is the choice for the Courant number C to satisfy the CFL condition and h_ρ is the step-size in the ρ-direction. In other

words, our time-step halves as we double the ρ-resolution.

First we look at convergence of the fields to their exact expressions and verify that they indeed converge, and at the correct order. Figure 6.1 shows the convergence of two fields in the system over time by looking at the L_2-norm of the difference between the simulation fields and their exact expressions on a $\log_{10}$ scale. This shows that even with a reasonably low resolution, we are almost at machine precision of around 1×10^{-16}. This is also the case for the remaining fields.

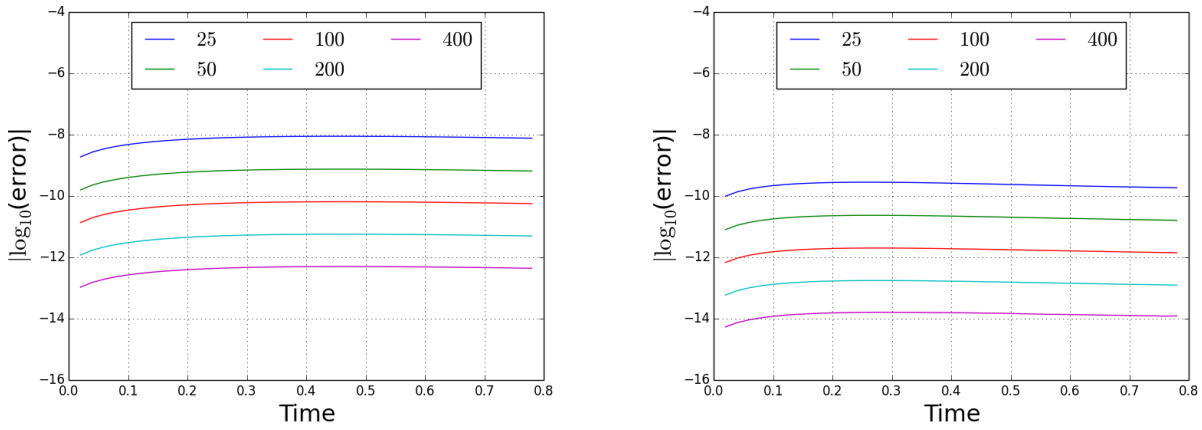

(a) χ_{11} (b) P_{110}

Figure 6.1: The convergence of χ_{11} and P_{110} to their exact expressions over time s for different ρ-resolutions.

To see that they are converging at the correct order, Figure 6.2 plots the convergence rate of a selection of functions in the system. The convergence rate is found by computing the absolute errors between the approximated values in the simulations and the exact value at a particular timeslice, then looking at the differences between them on a $\log_2$ scale.

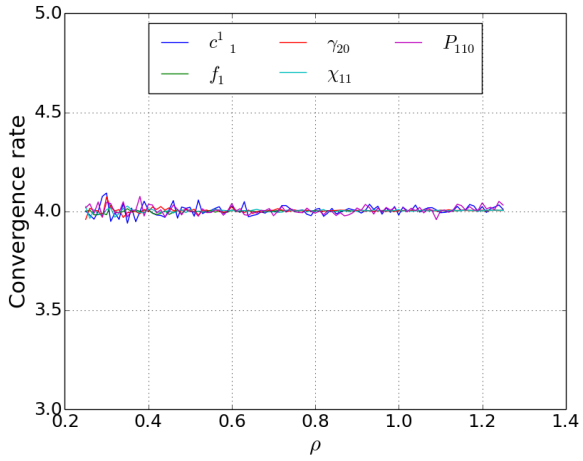

Figure 6.2: The convergence rate of a selection of fields at $s = 0.75$.

We do not need to show constraint propagation, as we know the exact solution satisfies the constraints identically, and we have shown that we approach the exact solution at the correct order as the resolution increases.

The plots for the remaining fields are very similar and hence we have shown that not only does the exact solution of Anti-de Sitter space-time satisfy our equations, but our numerics reproduce this solution given the appropriate initial data. This is the first step in a series of tests that need to be carried out in order for us to be confident that our system is working correctly.

6.3 Checking the numerical implementation of the $\eth$-operators

Now that we have seen that our system reproduces an exact solution in spherical symmetry, we generalise to axial-symmetry and show that the constraints propagate in a simple test case. Note that in all of our simulations that are not spherically-symmetric we will implement Orszag's two-thirds rule by truncating the modes of functions represented in the spin-weighted spherical harmonic basis at $L = \frac{2}{3}N_\theta$, where N_θ are the number of points taken in the θ-direction, following [19] (originally [90]) to try and suppress over-sampling/aliasing errors.

We choose our initial physical space-time to be Minkowski space-time and we choose a θ-dependent conformal factor. This way we can further test the evolution and constraint system, as well as our implementation of the pseudo-spectral methods.

More specifically, we choose the conformal factor initially as

$$\underline{\Theta} = 6\sqrt{\pi}\,{}_0Y_{00} + 8\sqrt{\frac{\pi}{5}}\,{}_2Y_{20} = 4 + 3\cos(2\theta), \tag{6.3.1}$$

so our initial metric takes the form

$$h = -\Big(4 + 3\cos(2\theta)\Big)^2\Big[\mathrm{d}\rho^2 + \rho^2\Big(\mathrm{d}\theta^2 + \sin^2\theta\mathrm{d}\phi^2\Big)\Big],$$

and choose χ_{ABCD} to vanish initially. We choose the initial data $\underline{H} = \underline{Z} = 0$ and hence we find [1]

$$\Theta(s) = \underline{\Theta}, \qquad h_{AB}(s) = 0. \tag{6.3.2}$$

Our initial choice of frame takes the form

$$\underline{e}_0 = \underline{\Theta}^{-1}\partial_s, \tag{6.3.3a}$$

$$\underline{e}_1 = \underline{\Theta}^{-1}\partial_\rho, \tag{6.3.3b}$$

$$\underline{m} = \frac{1}{\sqrt{2}\,\rho\,\underline{\Theta}}\Big(\partial_\theta - i\csc\partial_\phi\Big), \tag{6.3.3c}$$

where the frame vector m^a is noted to be a conformal rescaling of the unit-sphere M^a defined in section 2.3, with conformal factor $R = \rho\ \underline{\Theta}$ (i.e. $m^a = R^{-1}M^a$). This choice of initial data implies that initially the physical and Weyl connections are the same, and the fact that $h_{AB}(s) = 0$ tells us we are using metric geodesics for our gauge setup. The only non-zero

[1] This is clearly a very boring case as we do not even get to $\mathscr{I}$, however from the point of view of testing our code and system this is a nice, simple start.

initial data for our system are

$$R = \rho\,\underline{\Theta}, \qquad c^1{}_1 = \frac{1}{\sqrt{2}\,\underline{\Theta}}, \tag{6.3.4a}$$

$$\gamma_{10} = -\frac{\eth\, c^1{}_1}{2\,\rho}, \qquad \gamma_{20} = -\frac{1}{2\,\rho\,\underline{\Theta}}, \qquad \hat{\gamma}_{01} = -\frac{1}{2\,\rho\,\underline{\Theta}}, \qquad \hat{\gamma}_{11} = \frac{\eth' c^1{}_1}{2\,\rho}, \tag{6.3.4b}$$

$$f_0 = \frac{\eth\,\underline{\Theta}}{\sqrt{2}\,\rho\,\underline{\Theta}^2}, \qquad f_2 = -\frac{\eth'\underline{\Theta}}{\sqrt{2}\,\rho\,\underline{\Theta}^2}. \tag{6.3.4c}$$

As our space-time is conformal to Minkowski space-time, its Weyl spinor vanishes for all time. As this is the space-time we want to reproduce, we set all free boundary data to zero. The initial data (6.3.3), (6.3.4), and expressions for the conformal factor and rescaled 1-form (6.3.4) are then all that is required to start evolving our system.

Due to the expected exponential convergence rate of our numerical scheme for appropriately smooth square-integrable functions on $\mathbb{S}^2$, we need to look at how our initial data is represented in the spin-weighted spherical harmonic basis. This is because the coefficients ${}_s a_{l0}$ go to zero as $l \to \infty$ so fast that we may actually take too many points, which could cause problems. If we use too many, the increased resolution will just give us noise once the function is resolved (we say a function has resolved if its spectral coefficients have decayed to machine precision). This can give rise to aliasing errors and thus we want to try and minimise the amount of "leftover" coefficients we have. Although one must be careful as during the evolution, the non-linearity of the equations will of course excite higher frequency modes and hence we need to have enough room for these to accurately evolve as well. Adaptive mesh-refinement would then be an idea to fix this balancing problem. One could look at the magnitude of the coefficients at a particular timeslice and see if they get truncated before machine precision or not. If they are then add more points. If not then continue the evolution. However we find that for all the simulations in this thesis, this was not required.

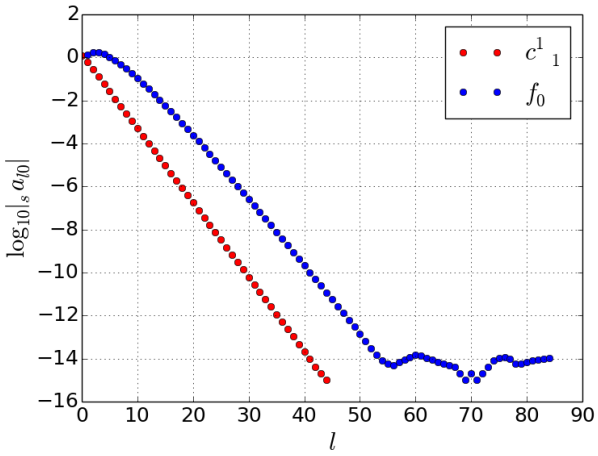

Figure 6.3: The convergence of initial data for $c^1{}_1$ and f_0 as $l \to \infty$.

We investigate how many grid points we need to initially get machine precision for our functions. Obviously the chosen conformal factor is represented exactly in the truncated spin-weighted spherical harmonic basis, so we look at the functions $c^1{}_1$ and f_0 as examples (see Figure 6.3). This clearly shows that the coefficients decay to zero exponentially, due to being straight lines in a semi-log plot. However looking closely, they only decay to machine precision when $l \approx 45$ and $l \approx 55$ for $c^1{}_1$ and f_0 respectively. Notice that once the spectral coefficients of $c^1{}_1$ reach machine precision they are set to exactly zero by the forward transform algorithm, which is not the case for f_1. This is a reasonably large number of points to take for pseudo-spectral methods, and one can narrow down the cause to taking a reciprocal of the conformal factor. This is because while a function f may be well represented in the spin-weighted spherical harmonic basis, the reciprocal f^{-1} may not be. This can be demonstrated by considering the function $1 - x$, which is represented exactly in the polynomial basis. However its reciprocal becomes the well-known series $1 + x + x^2 + \cdots$ which is not represented as well as the original function. This works out well for testing though, as we are able to see the convergence rate easier.

Now that we know that the spin-weighted spherical harmonic code seems to be working, we need to see how it fares in our system, i.e. we need to look at constraint propagation.

The constraints should approach machine precision at the correct order as our resolution increases and hence let us check that our numerical methods are working correctly. The initial data we have detailed in this section reduces the IVP for the GCFE system to a $2+1$ problem and hence we can increase the spatial resolution along either the ρ or θ-directions. It is rather messy looking at convergence plots plotted as 2-dimensional surfaces, so we will look separately at ρ-convergence along $\theta =$ constant and θ-convergence along $\rho =$ constant.

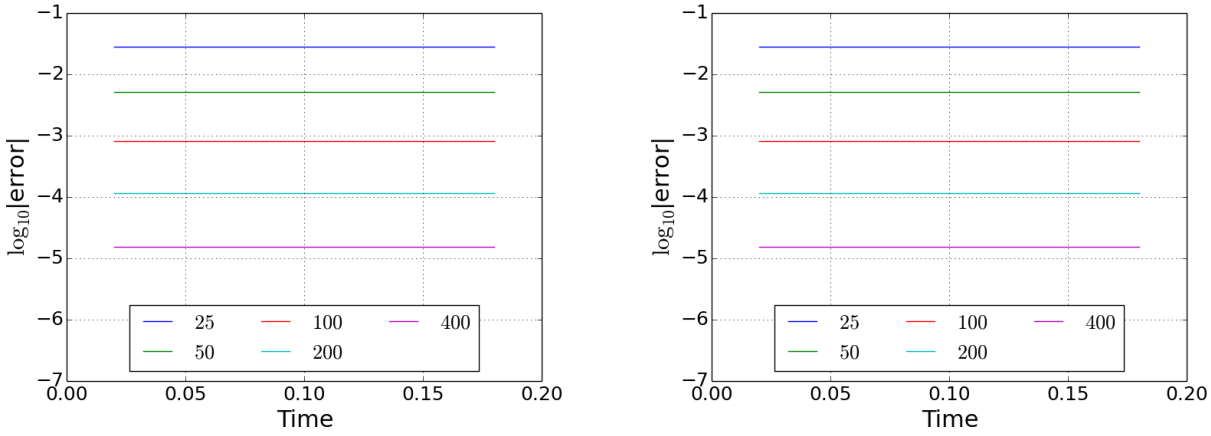

Figure 6.4: The convergence of a component of the ψ_{ABCD} constraint (2.4.12b) and f_{AB} constraint (2.4.12d) respectively over time s along $\theta = \frac{\pi}{2}$ with a θ-resolution of 128 for different ρ-resolutions.

We solve the equations numerically for ρ-resolutions of $\{25, 50, 100, 200, 400\}$ and θ-resolutions of $\{8, 16, 32, 64, 128\}$ (i.e. 25 simulations) on the 2-dimensional interval $[0.25, 1.25] \times [0, \pi]$ discretised into equi-distant points with time-steps of 0.5 h_ρ (recall that 0.5 is the Courant number) up until $s = 0.2$. Firstly, we look at ρ-convergence along the curve $\theta = \frac{\pi}{2}$. The resulting convergence plots for a component of the ψ_{ABCD} constraint (2.4.12b) and f_{AB} constraint (2.4.12d) respectively are shown in Figure 6.4, where we take the L_2-norm at each timeslice. These converge nicely, and by looking at Figure 6.5 converge at the correct order (recall the discussion around Figure 6.2 for how the convergence rate is computed). This is also the case for the other constraints in the system. The spikes near the boundary are due to

the finite differencing operator working differently near the boundary. These spikes reduce as we add more points.

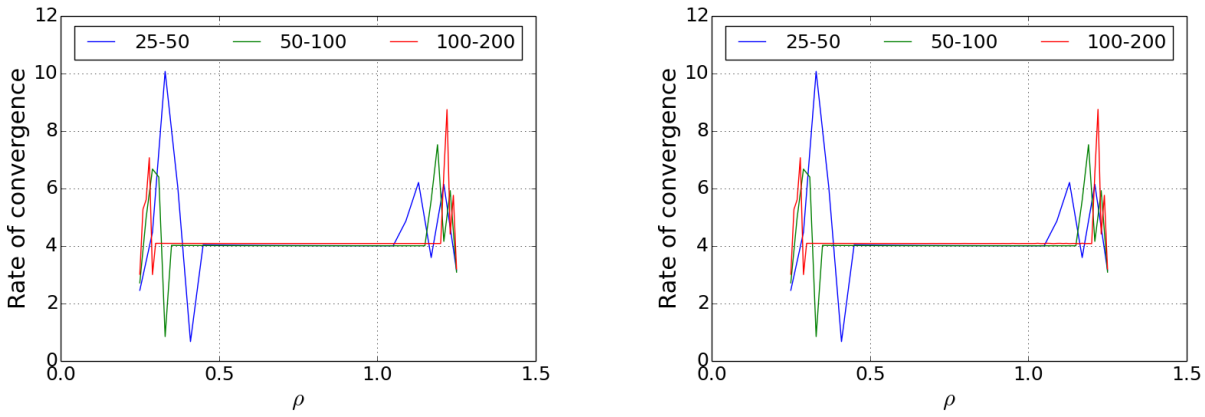

(a) (b)

Figure 6.5: The order of convergence of a component of the ψ_{ABCD} constraint (2.4.12b) and f_{AB} constraint (2.4.12d) respectively along $\theta = \frac{\pi}{2}$ at $s = 0.4$ with a θ-resolution of 128 and with an increasing ρ-resolution.

There are some constraints in the system which do not go to zero with increased ρ-resolution. This is due to the fact that the error is coming from the lack of θ-resolution. This is demonstrated nicely in Figure 6.6, which shows the convergence of a component of the γ_{ABC} constraint (2.4.12e). Clearly as you increase the ρ-resolution, the constraints do not approach machine-precision, but rather bunch up as seen by the curves of ρ-resolution 400 passing through the markers with ρ-resolution 25 for the same θ-resolution. However if we increase the θ-resolution, the constraint clearly starts approaching machine precision. This is due to the fact that some constraints in the system are more dependent on the θ-resolution than others.

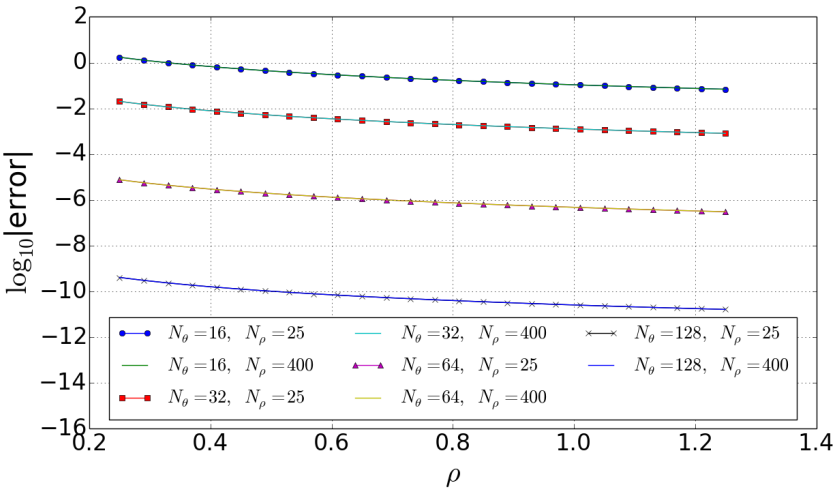

Figure 6.6: The convergence of a component of the γ_{ABC} constraint (2.4.12e) along $\theta = \frac{\pi}{2}$ at $s = 0.2$ with increasing ρ and θ-resolutions denoted by N_ρ and N_θ respectively.

Now we look more closely at the constraints along ρ = constant and how they behave when we increase the θ-resolution. It appears that the only constraints that depend heavily on the θ-resolution are the components of the γ_{ABC} constraint (2.4.12e). Looking at the same component of this constraint in Figure 6.7, we can see the convergence of the constraint with increased θ-resolution over both time and θ more clearly.

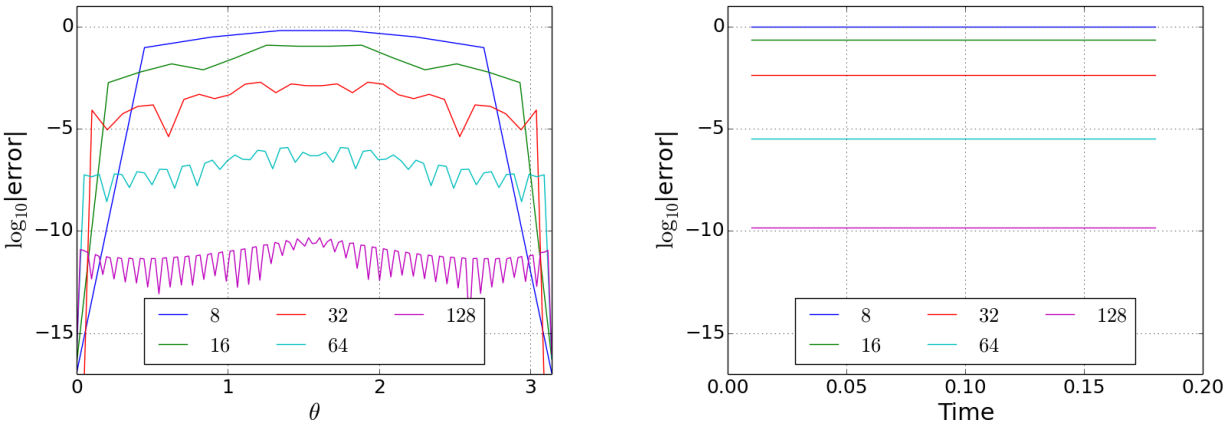

(a) $\rho = 1,\ s = 0.2$.

(b) $\rho = 1,\ \theta = \frac{\pi}{2}$.

Figure 6.7: The convergence of a component of the γ_{ABC} constraint (2.4.12e) along $\rho = 1$ over time s, and space at $s = 0.2$ with a ρ-resolution of 400 for different θ-resolutions.

Thus we have shown that our numerical schemes are stable in the 2+1 case and converge at the correct order.

6.4 Checking our boundary treatment

Now that the basic numerical methods as well as a large subset of our system have been verified to be working correctly (all except the ψ_{ABCD} contribution), we need to test our boundary implementation. In particular, we need to test whether with an appropriate choice of boundary data, we can kill the ingoing modes from the spin-2 zero rest-mass subsidiary system. We do this by choosing a very simple initial space-time and imposing appropriate boundary conditions to shoot in gravitational waves, represented by ψ_0 and ψ_4 (propagating in the ρ-direction from right to left and left to right respectively).

As in section 6.3 we decide to have Minkowski space-time initially. Although this time we choose initial data for Θ and h_a so that we get the expressions

$$\Theta(s) = 1, \qquad h_{AB}(s) = 0.$$

Again this is boring, but we are only interested in testing our boundary implementation.

This choice of 1-form h_a says that our gauge is adapted to metric geodesics. The reason for fixing Θ and h_a as above is so that the frame components $c^0{}_{AB}$ vanish for all time. This implies that there is no $\frac{\mathrm{d}}{\mathrm{d}s}$ contribution from the expansion of ∂_{AB} during the evolution, and so our spatial frame vectors will stay within $s =$ constant surfaces. This has the consequence of keeping the characteristic speeds of the ψ_{ABCD} system from changing sign, and hence we only need to implement the first and easiest part of our boundary treatment.

To explain why $c^0{}_{AB}$ remain zero for all time, first we write down the initial data. We have the standard representation of Minkowski space-time in spherical coordinates for our initial metric

$$h = -\mathrm{d}\rho^2 - \rho^2\Big(\mathrm{d}\theta^2 + \sin^2\theta \mathrm{d}\phi^2\Big),$$

and the only non-zero fields are

$$R = \rho, \qquad c^1{}_1 = \frac{1}{\sqrt{2}}, \qquad \gamma_{20} = \hat{\gamma}_{01} = -\frac{1}{\sqrt{2}\,\rho}.$$

Now we are in a position to see why $c^0{}_{AB}$ remains zero for all time. This can be seen from first looking at the evolution equation for P_{ABCD} in (2.4.11). As we know that P_{ABCD} and h_{AB} vanish initially, we have that the right-hand-side of the evolution equation also vanishes. Then as $h_{AB} = 0$ is satisfied for all time, it must be that $P_{ABCD} = 0$ for all time as well. Now looking at the evolution equation for f_{AB} in (2.4.11), noting that initially $f_{AB} = 0$ and using that $P_{ABCD} = 0$ for all time, we can conclude in the same way that $f_{AB} = 0$ for all time as well. Finally we can look at the evolution equation for $c^0{}_{AB}$ in (2.4.11). Since we know $c^0{}_{AB} = 0$ initially and $f_{AB} = 0$ for all time we conclude that $c^0{}_{AB} = 0$ for all time.

Now we know that $c^0{}_{AB} = 0$ we see what affect this has on the characteristic speeds of the spin-2 system. The characteristic speeds of the components of ψ_{ABCD} used in the evolution are given by

$$-\sqrt{2}c^1{}_1, \qquad -\frac{c^1{}_1}{\sqrt{2}}, \qquad 0, \qquad \frac{c^1{}_1}{\sqrt{2}}, \qquad \sqrt{2}c^1{}_1, \tag{6.4.1}$$

for $\psi_0, \cdots, \psi_4$ respectively. One sees by checking the value of $c^1{}_1$ over the course of the simulation that it does not change sign or go to zero and hence there are always two ingoing,

two outgoing and one tangential mode at each boundary.

We again discretise our spatial directions by choosing equi-distant points in the 2-dimensional interval $[0.25, 1.25] \times [0, \pi]$. As our boundary conditions, we shoot in a gravitational wave from each boundary by choosing the boundary data for $\psi_0[s, \rho, \theta]$ and $\psi_4[s, \rho, \theta]$ as

$$\psi_0[s, 1.25, \theta] = \begin{cases} 2\sqrt{\frac{2\pi}{15}}\, {}_2Y_{20} \sin^8(4\pi s), & s \leq \frac{1}{4} \\ 0 & s > \frac{1}{4} \end{cases},$$

$$\psi_4[s, 0.25, \theta] = \begin{cases} 2\sqrt{\frac{2\pi}{15}}\, {}_2Y_{20} \sin^8(4\pi s), & s \leq \frac{1}{4} \\ 0 & s > \frac{1}{4} \end{cases},$$

where the spin-weighted spherical harmonic ${}_2Y_{20}$ is $\sin^2\theta$ up to a constant when written in the usual polar coordinates. These are natural choices as the simpler we choose the functions in the spin-weighted spherical harmonic basis, the smaller the number of grid points we need to take in the θ-direction to represent them exactly. Although one needs to be careful as during the non-linear evolution the functions in the system will pick up higher order modes and hence a higher resolution may be required.

We adopt our boundary treatment outlined in section 3.3 which fixes the boundary conditions for ψ_1 on the rightmost boundary and ψ_3 on the leftmost boundary. Hence we have fixed all the free data on the boundaries: ψ_0, ψ_1 on the right and ψ_3, ψ_4 on the left. We evolve up until $s = 1$ with a θ-resolution of 32, ρ-resolutions of $\{25, 50, 100, 200, 400\}$ and use a time-step of 0.5 h_ρ (again recalling 0.5 represents the Courant number and h_ρ is the step-size in the ρ-direction). We find that this θ-resolution is enough to represent all the functions in our system on the spheres at machine precision.

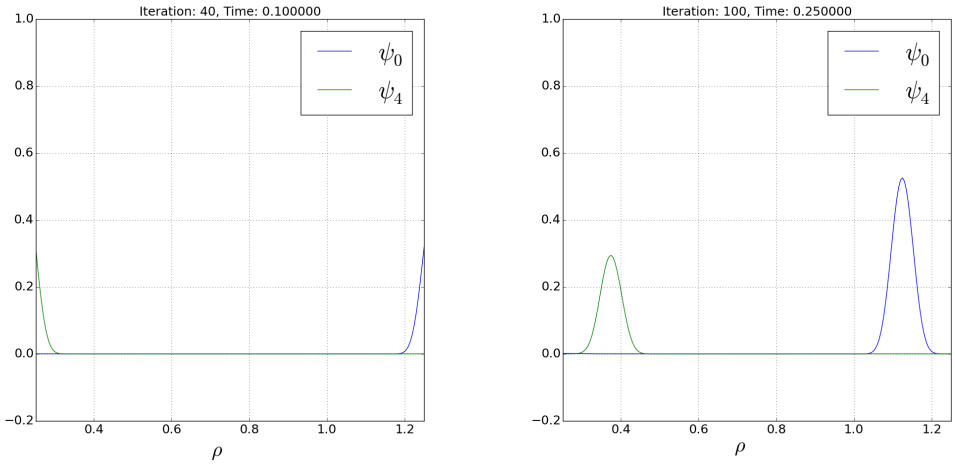

(a) $s = 0.1$ (b) $s = 0.25$

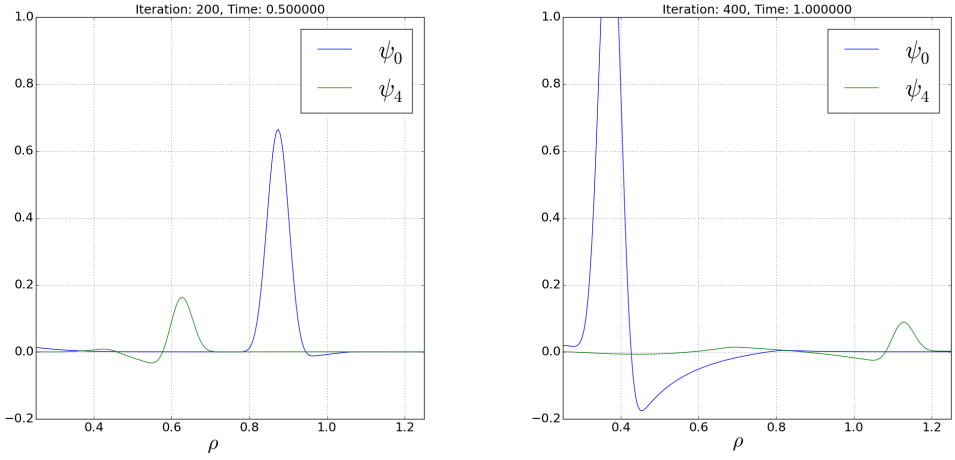

(c) $s = 0.5$ (d) $s = 1$

Figure 6.8: A sequence of simulation screen shots of two gravitational waves with Minkowskian initial data using our boundary treatment outlined in section 3.3.

First we look at the case without employing our subsidiary-mode-killing boundary treatment, to confirm that constraint violating modes are indeed propagated in from the boundary. We use the maximally dissipative boundary conditions but choose the free data (i.e. the "q") for ψ_1 on the right and ψ_3 on the left to be zero. Looking at a component of the ψ_{ABCD} constraint (2.4.12b) on the slices $s =$ constant, $\theta = \frac{\pi}{2}$ in Figure 6.9 we see that initially the constraints are converging. However as one evolves the system, the constraints

seem to start being violated. We know this constraint violating mode should propagate in a time-like manner from our analysis in section 3.3. This clearly is the case, as by comparison in Figure 6.8 our null-propagating gravitational waves are moving much faster. This lack of convergence is also seen in the other constraints of the system.

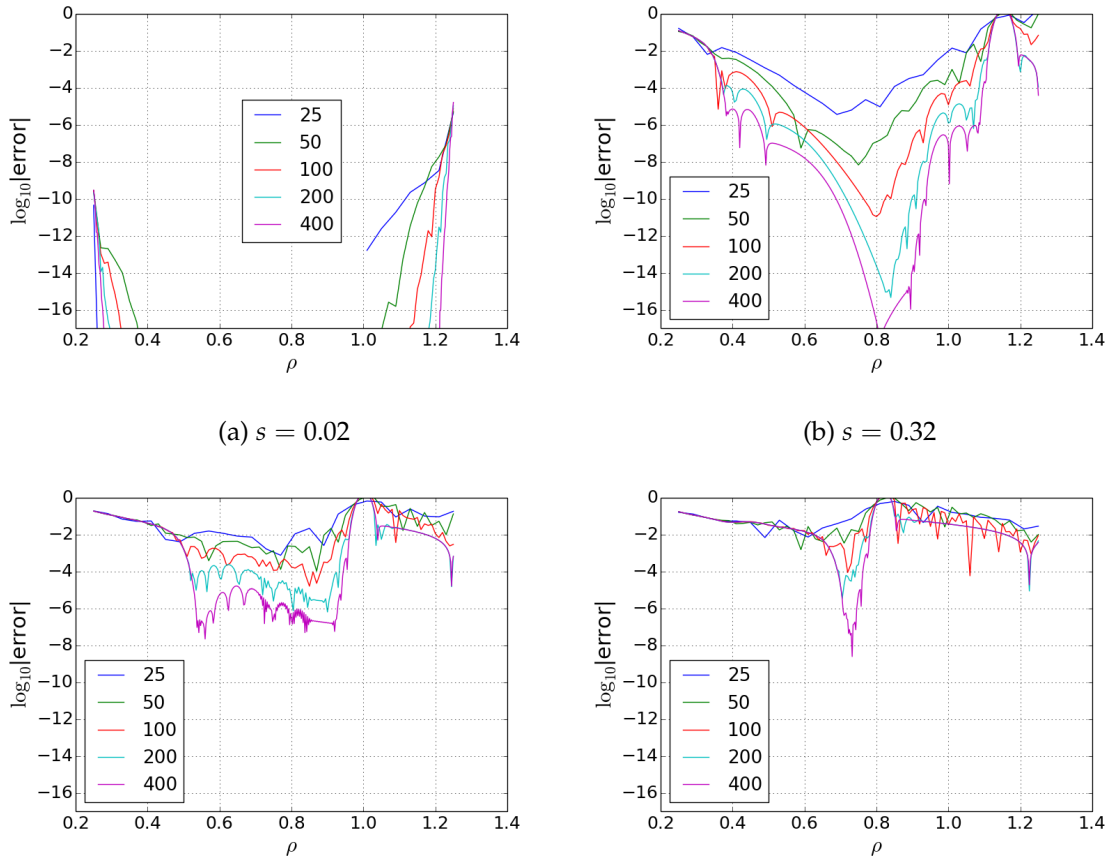

(a) $s = 0.02$ (b) $s = 0.32$

(c) $s = 0.62$ (d) $s = 0.98$

Figure 6.9: A sequence of convergence tests at s = constant, $\theta = \frac{\pi}{2}$ for a component of the ψ_{ABCD} constraint (2.4.12b) with increasing ρ-resolution for the case of two gravitational waves with Minkowskian initial data using boundary conditions that do not kill subsidiary modes.

Now let us see how well our subsidiary-mode-killing boundary conditions work. In Figure 6.10 we display the same constraint as in Figure 6.9 except with the "correct" boundary conditions. One can see that there is no longer a constraint violation propagating inward

from the boundary and the constraints converge across the entire grid.

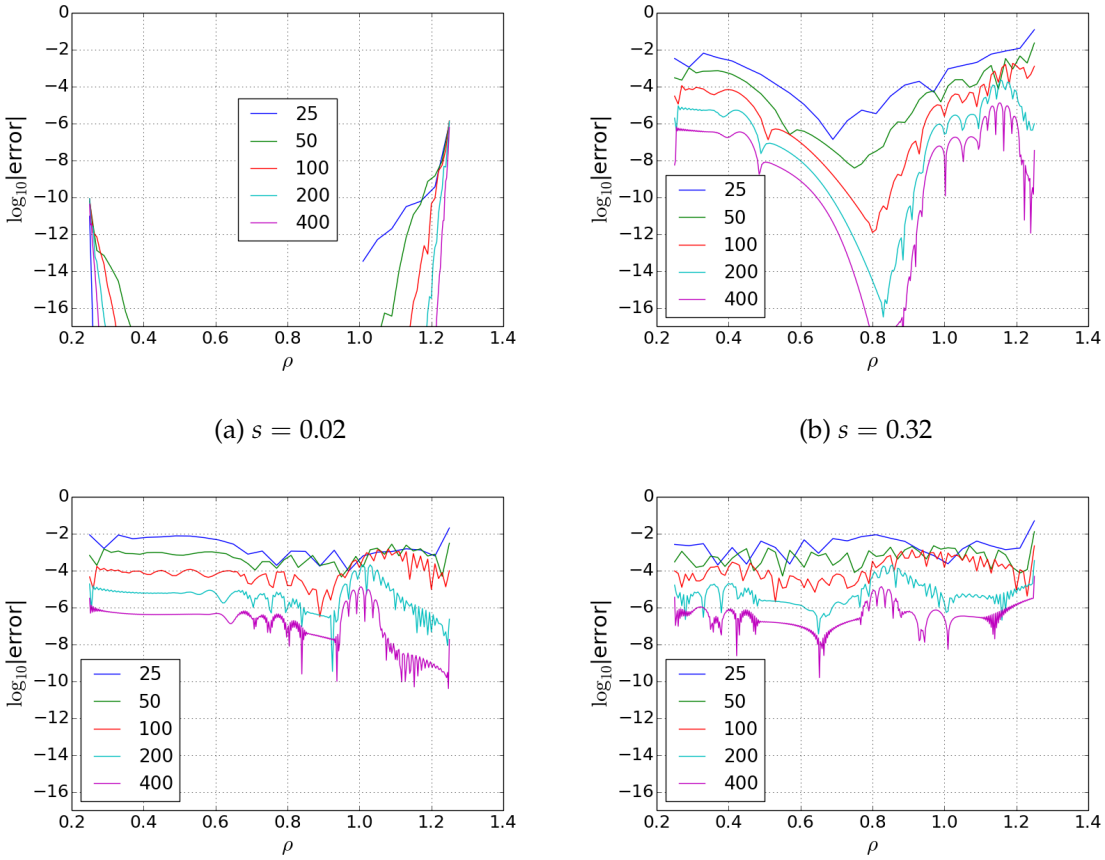

(a) $s = 0.02$

(b) $s = 0.32$

(c) $s = 0.62$

(d) $s = 0.98$

Figure 6.10: A sequence of convergence tests at $s = \text{constant}, \theta = \frac{\pi}{2}$ for a component of the ψ_{ABCD} constraint (2.4.12b) with increasing ρ-resolution for the case of two gravitational waves with Minkowskian initial data using boundary conditions that kill subsidiary modes.

Analogous plots are seen in all the other constraints, so the initial test looks very good. Although this was a very simple case, the premise of our boundary treatment method has been verified. The next step is to generalise this method to the case where the propagation directions of the ψ_{ABCD} modes change during the course of the evolution. We will not test this with a similar boring case, instead we will look at gravitational perturbations of the Schwarzschild space-time in section 9.

Part III

Global properties of black hole space-times

Chapter 7

Conformal structure

Now that we have checked the correctness of our system in section 6, we look at simple space-times and see how the system behaves close to and beyond conformal infinity. Some interesting cases are that of Schwarzschild, Schwarzschild-de Sitter and Schwarzschild-Anti-de Sitter space-times. These all have a different global structure and it is interesting to see how well we can numerically reproduce these. First we give a summary of the global structure of the three space-times of constant curvature satisfying Einstein's vacuum field equation (1.1.1), before generalising to their black hole equivalents.

7.1 Constant curvature space-times

The simplest place to start is Minkowski space-time, which we write in null coordinates as

$$\mathrm{d}s^2 = \mathrm{d}u\mathrm{d}v - \frac{1}{4}(u-v)^2\Big(\mathrm{d}\theta^2 + \sin^2\theta\mathrm{d}\phi^2\Big).$$

In order to try compactify the space-time, we need some sort of coordinate transformation that compactifies the range of u and v (which is of course $\mathbb{R}$) into a smaller, finite subset. The simplest function that has this property is probably $\tan u$ (resp. $\tan v$), which has range $\mathbb{R}$ but the domain can be chosen to be $[-\frac{\pi}{2}, \frac{\pi}{2}]$. Hence we define new coordinates as

$$p = \arctan u, \qquad q = \arctan v,$$

which give

$$\mathrm{d}s^2 = \sec^2 p \sec^2 q\Big[\mathrm{d}p\mathrm{d}q - \frac{1}{4}\sin^2(p-q)\Big(\mathrm{d}\theta^2 + \sin^2\theta\mathrm{d}\phi^2\Big)\Big].$$

We perform a final coordinate transformation

$$t = p + q, \qquad r = p - q,$$

noting the restrictions

$$-\pi < t + r < \pi, \qquad -\pi < t - r < \pi, \qquad r \geq 0. \tag{7.1.1}$$

We find that the whole of Minkowski space-time is embedded in the Einstein cylinder, whose metric is given by

$$\mathrm{d}s^2 = \mathrm{d}t^2 - \mathrm{d}r^2 - \sin^2 r\left(\mathrm{d}\theta^2 + \sin^2\theta \mathrm{d}\phi^2\right), \tag{7.1.2}$$

but without the coordinate restrictions (7.1.1).

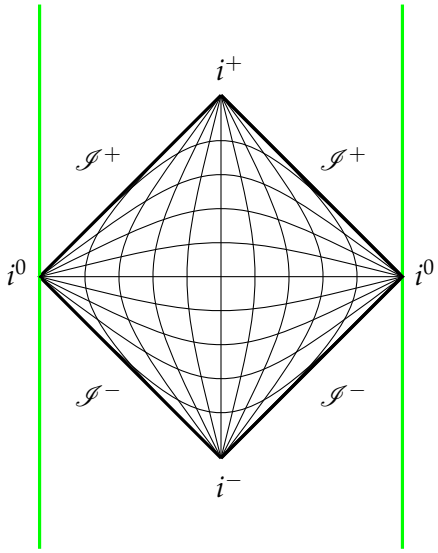

Figure 7.1: The global structure of Minkowski space-time embedded in the Einstein cylinder with suppressed spherical dimensions, where for illustration purposes we let the r-coordinate take negative values (otherwise we would only get half of this picture). The green lines represent the Einstein cylinder while the black represent the embedding of Minkowski space-time. Each point can be thought of as a 2-sphere with the exception of i^+, i^- and i^0 which are single points. The curves going to i^0 are given by $t =$ constant while the curves going to i^+ and i^- are given by $r =$ constant If only one spherical dimension is suppressed, the embedding should be thought of as the “diamond" patch” being wrapped around a cylinder so that i^0 on the left and right touch, as these are the same point.

The Einstein cylinder, which is topologically $\mathbb{R} \times \mathbb{S}^3$, was originally proposed by Einstein as a solution to his field equations that described a steady state universe. However after observations that the universe was expanding, the theory was thrown out. The Einstein cylinder has the mathematical property that it contains as submanifolds conformal rescalings of Minkowski, de Sitter and Anti-de Sitter space-times. It is conformally related to these by taking as conformal factor $\frac{1}{2}\sec(t+r)\sec(t-r)$, $\sec t$ and $\sec r$ respectively.

The conformal structure of Minkowski space-time is thus described by Figure 7.1 with the spherical dimensions suppressed. The global structure of Minkowski space-time is made up of space-like infinity i^0 which represents $r = \infty$ and is a point, $i^{\pm}$ are future and past time-like infinity respectively and represent $t = \pm\infty$ which are also points and $\mathscr{I}^{\pm}$ are future and past null-infinity and represent the start and end points of null rays. These are topologically $\mathbb{R} \times \mathbb{S}^2$ and are null-hypersurfaces.

De-Sitter space-time is generally stated as being the hyperboloid

$$-u^2 + v^2 + x^2 + y^2 + z^2 = \alpha^2$$

embedded in flat 5-dimensional space $\mathbb{R}^5$ with metric

$$\mathrm{d}s^2 = -\mathrm{d}u^2 + \mathrm{d}v^2 + \mathrm{d}x^2 + \mathrm{d}y^2 + \mathrm{d}z^2.$$

The resultant metric satisfies the 4-dimensional Einstein equation with (in our conventions) positive cosmological constant, has topology $\mathbb{R} \times \mathbb{S}^3$ and symmetry group $SO(4,1)$. In order to conformally compactify this space-time, one uses a similar approach to that for Minkowski space and finds the global structure depicted in Figure 7.2. In contrast to Minkowski space, de Sitter space has for the end points of time-like and null geodesics the submanifolds $\mathscr{I}^{\pm}$ given by $t =$ constant surfaces in the Einstein cylinder which are space-like.

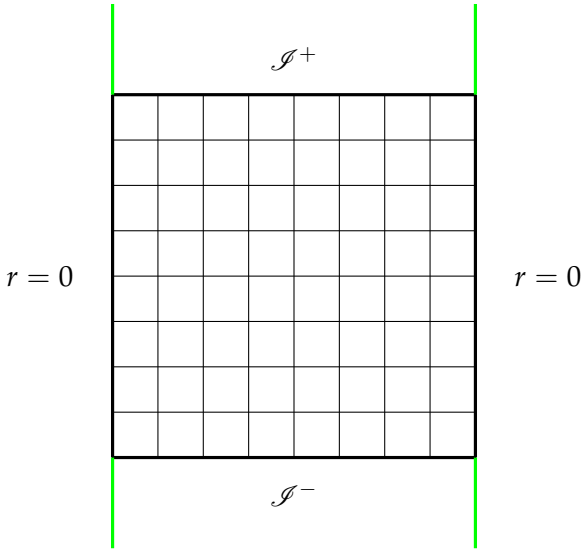

Figure 7.2: The global structure of de Sitter space-time embedded in the Einstein cylinder with suppressed spherical dimensions, where again the r-coordinate has been extended for illustration purposes (otherwise we would only get half of this picture). The green lines represent the Einstein cylinder while the black represent the embedding of de Sitter space-time. Each point can be thought of as a 2-sphere. The curves going to $r = 0$ are given by $t =$ constant while the curves going to $\mathscr{I}^+$ and $\mathscr{I}^-$ are given by $r =$ constant If only one spherical dimension is suppressed, the embedding should be thought of as a taking a complete section out of the Einstein cylinder, that is taking everything from $t = t_0$ to $t = t_1$. Hence de Sitter space-time has no time-like or null conformal boundaries.

The final space-time to consider is Anti-de Sitter space-time, which is defined in a similar way to de Sitter space-time. It is the hyperboloid

$$-u^2 - v^2 + x^2 + y^2 + z^2 = 1,$$

embedded in the flat 5-dimensional space $\mathbb{R}^5$ with metric

$$\mathrm{d}s^2 = -\mathrm{d}u^2 - \mathrm{d}v^2 + \mathrm{d}x^2 + \mathrm{d}y^2 + \mathrm{d}z^2.$$

The resultant metric satisfies the 4-dimensional Einstein equation with (in our conventions) negative cosmological constant, has topology $\mathbb{R}^3 \times \mathbb{S}^1$ and symmetry group $SO(3,2)$.

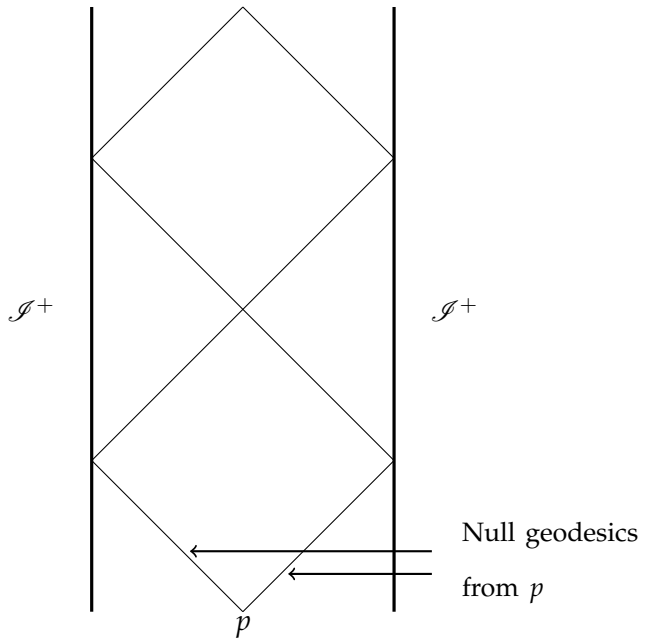

Figure 7.3: The global structure of Anti-de Sitter space-time embedded in the Einstein cylinder with suppressed spherical dimensions, again extending the r-coordinate for illustration purposes (otherwise we would get only half this picture). Null and space-like infinity are given by the submanifold $\mathscr{I}^+$ at $r = \frac{\pi}{2}$ which is a time-like surface. However as the time (vertical) direction is not compactified this diagram continues indefinitely. If only one spherical dimension is suppressed, the embedding should be thought of as taking one half of the Einstein cylinder $0 \leq r < \frac{\pi}{2}$.

Because the $\mathbb{S}^1$-part of the topology corresponds to the time direction, this space has closed time-like curves. However the standard procedure is to "unwrap" this by replacing $\mathbb{S}^1$ with its covering space $\mathbb{R}$. This gives a new space-time called "the universal covering space" which has topology $\mathbb{R}^4$ and this is what we shall henceforth refer to as Anti-de Sitter space-time.

Unlike the Minkowski and de Sitter space-times, Anti-de Sitter space is not compactified in time. This is obvious from observing the representation of Anti-de Sitter space as the Einstein cylinder metric (7.1.2) multiplied by $\sec^2 r$. From this representation one can easily see that is has for space-like and null infinity a submanifold of the Einstein cylinder given by

$r = \frac{\pi}{2}$ which is time-like.

An interesting note to make here is the significance of the symmetry group $SO(3,2)$ of Anti-de Sitter space-time to String theory. First proposed by Maldacena in his groundbreaking paper [77], the so-called AdS/CFT (Anti-de Sitter/Conformal Field Theory) correspondence relates a gravitational theory on n-dimensional Anti-de Sitter space-time to a $(n-1)$-dimensional conformal quantum field theory on its conformal boundary. The heart of the mathematics behind this can be displayed by noticing the homomorphism between the symmetry group of the 5-dimensional Anti-de Sitter space-time $SO(4,2)$ and the conformal group $C(3,1)$. It is a property of the 5-dimensional Anti-de Sitter space that its conformal boundary is locally Minkowski space, which of course has conformal group $C(3,1)$. Thus the homomorphism relates the interior space-time to the conformal boundary in a particular way that is made use of by Maldacena.

Another, more relevant point to make now that we know the global structure of these space-times is how conformal geodesics behave in them. This is of paramount importance to us as our gauge is adapted to them, so knowing how they behave will tell us what to expect during our evolution. In section 6.1 we solved the conformal geodesic equations for spherically symmetric solutions for the conformal class of metrics containing the Einstein cylinder. It was found that, no matter the choice of initial data, the geodesics would slow down and eventually stop as the geodesics parameter goes to infinity. This does not mean that the geodesic does not exist past this point, just that the parameter chosen does not cover anymore of the geodesic. This is potentially problematic as what if the geodesics stop before the conformal boundary has been covered? With respect to the representation of the Einstein cylinder (7.1.2), if we start the conformal geodesics orthogonal to $t = 0$, then as their parameter $s \to \infty$, $t \to \pi$. The end-point of the conformal geodesics therefore corresponds to the time-like infinities $i^{\pm}$ of Minkowski space. This would mean that one could get an arbitrarily large amount of $\mathscr{I}^{\pm}$ but the geodesics would asymptote to $t = \pi$. The null infinities $\mathscr{I}^{\pm}$ for de Sitter space-time appear at $t = \pm\frac{\pi}{2}$ and therefore one in principle should have no problem covering the entire space-time. However the real problems begin when looking at

Anti-de Sitter space-time, which is only compactified in the r-direction. This poses a serious problem. If one tries to compute a piece of the space-time beyond $-\pi < t < \pi$, one has to somehow "reset" the conformal geodesics parameter in order to keep it going. This is a problem that needs to be overcome if one wants to explore this space-time using the GCFE system, perhaps to investigate the non-linear instability that has been observed numerically using other methods [14, 15, 16, 20, 26, 27, 57].

7.2 Black hole space-times

In 1918 the Schwarzschild solution was generalised to include the cosmological constant. The so-called Kottler metric, which was first derived in the papers [71, 123, 124], takes the form

$$\widetilde{g} = \Big(1 - \frac{2m}{r} - \frac{\lambda}{3}r^2\Big)\mathrm{d}t^2 - \Big(1 - \frac{2m}{r} - \frac{\lambda}{3}r^2\Big)^{-1}\mathrm{d}r^2 - r^2\Big(\mathrm{d}\theta^2 + \sin^2\theta\mathrm{d}\phi^2\Big), \tag{7.2.1}$$

where λ is the cosmological constant. Clearly this reduces to the Schwarzschild solution for $\lambda = 0$ and perhaps not so clearly to the three space-times of constant curvature when $m = 0$. The space-time is called Schwarzschild-de Sitter or Schwarzschild-Anti-de Sitter space-time when λ is taken to be positive or negative respectively.

One can conformally compactify the Schwarzschild space-time by first writing it in terms of the so-called "tortoise coordinate", defined as

$$r_* := \int \Big(1 - \frac{2m}{r}\Big)^{-1}\mathrm{d}r = r + 2m\log\Big|\frac{r}{2m} - 1\Big|,$$

so that null-curves are given by constant u, v defined as

$$u := t - r, \qquad v := t + r.$$

In these null coordinates, the metric takes the form

$$\widetilde{g} = \Big(1 - \frac{2m}{r}\Big)\mathrm{d}u\mathrm{d}v - r^2\Big(\mathrm{d}\theta^2 + \sin^2\theta\mathrm{d}\phi^2\Big).$$

We define further coordinates

$$U := -\mathrm{e}^{-u/4m}, \qquad V := \mathrm{e}^{v/4m},$$

to obtain the Kruskal-Szekeres form of the metric

$$\widetilde{g} = \frac{32m^3}{r} e^{-r/2m} dU dV - r^2 \left(d\theta^2 + \sin^2\theta d\phi^2 \right), \tag{7.2.2}$$

which showcases the regularity of the solution at the event horizon $r_s := 2m$.

In order to see the conformal structure, we make one last coordinate transformation

$$\tilde{u} := 2 \arctan\left(\frac{U}{4m}\right), \qquad \tilde{v} := 2 \arctan\left(\frac{V}{4m}\right),$$

with the coordinates being restricted like

$$-\pi < \tilde{u} < \pi, \qquad -\pi < \tilde{v} < \pi, \qquad -\pi < \tilde{u} + \tilde{v} < \pi.$$

This representation admits the Penrose-Carter diagram Figure 7.4 shown below. Note that for the right-half of the diagram, we have $\mathscr{I}^+$ at $\tilde{v} = \pi$,$\mathscr{I}^-$ at $\tilde{u} = -\pi$ and the singularities at $r = 0$ are at $\tilde{u} + \tilde{v} = \pm\pi$.

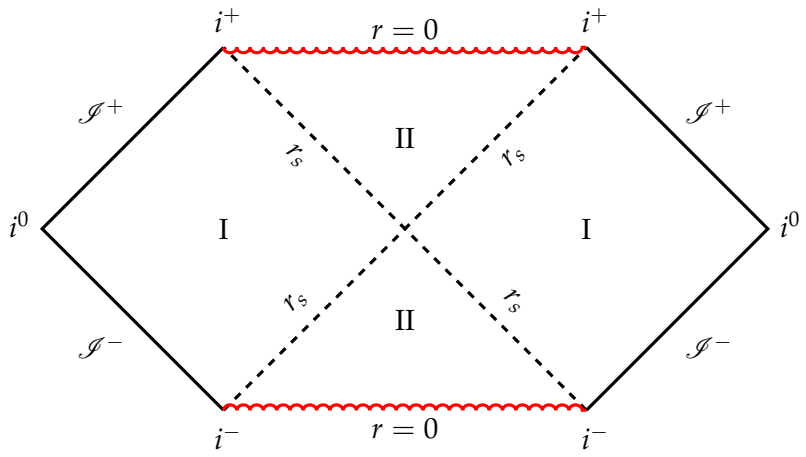

Figure 7.4: The global structure of the Schwarzschild solution. Each point represents a 2-sphere of radius r and 45 degree lines represent null curves.

This conformal diagram shows us that the Schwarzschild space-time is asymptotically Minkowskian, pictorially evident due to the sides of the diagram mimicking the Minkowski space-time's structure seen in Figure 7.1. It also shows us the space-like nature of the curvature singularity at $r = 0$ and the nature of the event horizon.

An important property of the space-times defined by fixing m and λ in (7.2.1) is the location of horizons, which are the surfaces where g_{00} vanish. With $\lambda = 0$ one gets a unique solution as $rg_{00} = r - 2m = 0$ is a linear equation. However by choosing $\lambda \neq 0$, one ends up solving the more complicated cubic equation

$$\frac{\lambda}{3}r^3 - r + 2m = 0. \tag{7.2.3}$$

Hence it is possible that the space-time may have up to three horizons. There is a useful dimensionless quantity $k := 9\lambda m^2$ which nicely breaks up the different solutions to (7.2.3). Assuming that $m \neq 0$ and $r > 0$, $k < 0$ gives one root, $k = 0$ also gives one root, $0 < k < 1$ gives two roots, $k = 1$ gives again one root and finally $k > 1$ gives no roots. Clearly $k = 0$ gives us the standard Schwarzschild solution with its one event horizon. The $k < 0$ case can only be obtained by having a negative λ, hence Schwarzschild-Anti-de Sitter space-time has only one horizon. However it appears that Schwarzschild-de Sitter space-time can have no, one or two horizons depending on the choice of k. To discuss these cases in more detail, we look at their conformal diagrams.

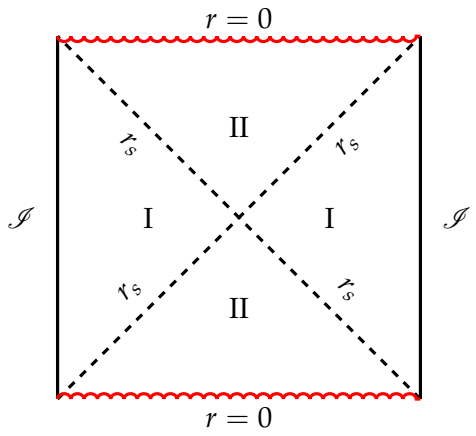

Figure 7.5: The global structure of the Schwarzschild-Anti-de Sitter solution. Each point represents a 2-sphere of radius r and 45 degree lines represent null curves.

By following a similar process to that of Schwarzschild space-time, one finds the conformal diagram of Schwarzschild-Anti-de Sitter space-time as shown in Figure 7.5. This is very interesting as all time-like observers will ultimately end up passing through the event horizon

and inevitably meeting the singularity that lurks inside. By making k larger negative, one sees that the location of the event horizon moves to smaller and smaller r-values.

There are multiple things going on for Schwarzschild-de Sitter space-time. Firstly, Figure 7.6 represents the case where $0 < k < 1$ and hence we have two horizons, called the event horizon r_s and cosmological horizon r_c. The event horizon hides the singularity from outside observers, while the cosmological horizon is the part of the space-time which signifies the end of the observable universe. Let us fix the value of $0 < k < 1$ for a moment. If we increase m and balance by decreasing λ, then r_s becomes larger while r_c gets smaller. Similarly if we increase λ while decreasing m, r_c becomes larger and r_s becomes smaller. The increase in m increasing r_s is obvious, while the increase in λ increasing r_c is due the increased expansion of the universe which the cosmological constant drives.

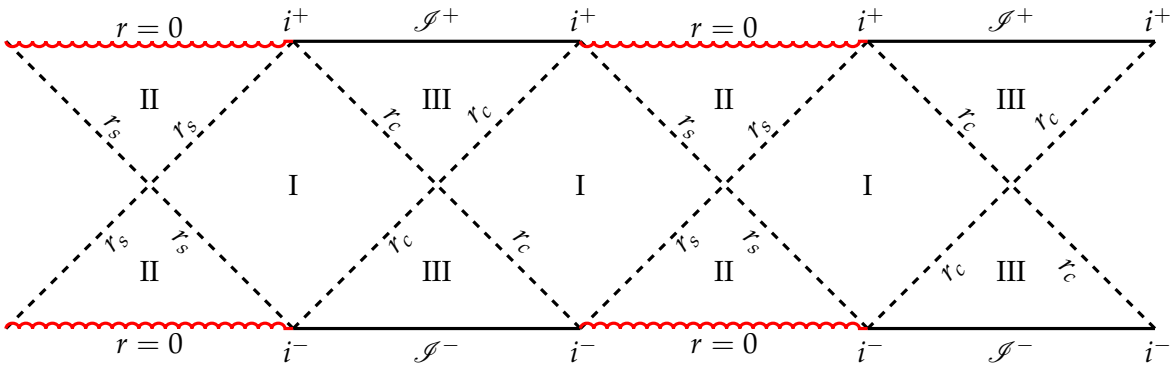

Figure 7.6: The global structure of the Schwarzschild-de Sitter solution with two horizons. Each point represents a 2-sphere of radius r except for $i^{\pm}$.

The space-time where $k = 1$ is called the extreme Schwarzschild-de Sitter space-time and has an interesting global structure, see Figure 7.7. In this space-time the event and cosmological horizons merge at $r = 3m$. Observers in the space-time described by (a) start at $\mathscr{I}^-$ and continue until they either go through the event horizon and fall into the singularity or stay outside and safely reach the point P. Observers in the space-time described by (b) emanate from either $r = 0$ or the point P, go through the horizon and either reach $\mathscr{I}^+$ or the point Q. These clearly are the space-times of a black hole and white hole respectively.

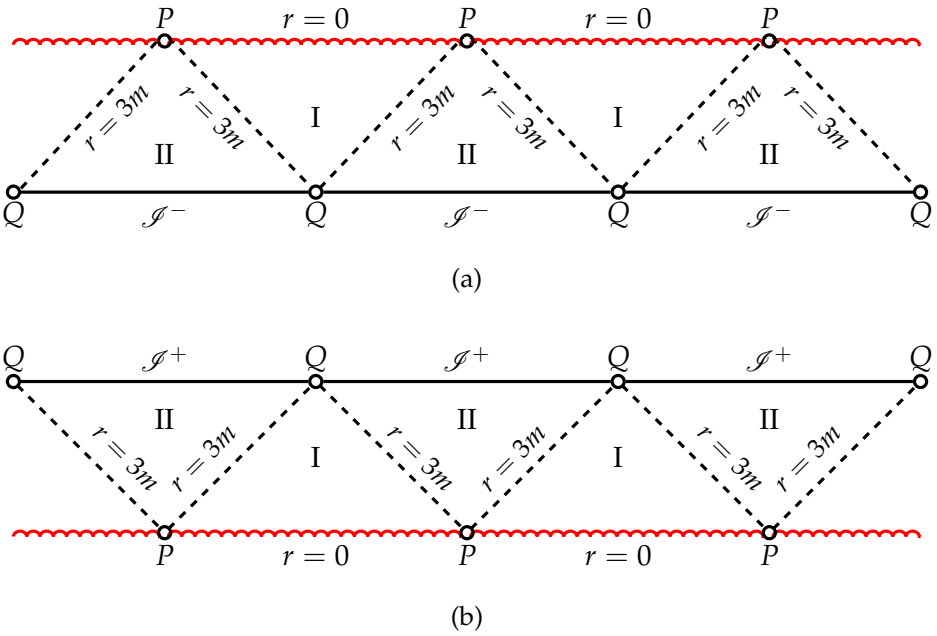

Figure 7.7: The global structure of the extreme Schwarzschild-de Sitter solution.

The space-time where $k > 1$ is called the hyperextremal Schwarzschild-de Sitter space-time and also has an interesting global structure, see Figure 7.8. This is the case where there are no horizons and hence the space-time contains a naked singularity, violating the weak cosmic censorship conjecture proposed by Penrose in 1969 [97]. Observers in (a) start on $\mathscr{I}^-$ and evolve inevitably into the singularity. The observers in (b) start on the singularity and evolve to $\mathscr{I}^+$. These are black and white holes respectively.

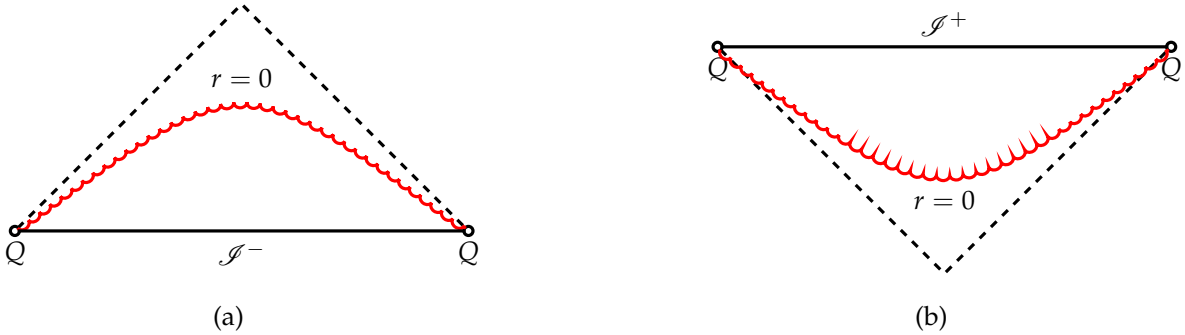

Figure 7.8: The global structure of the hyperextremal Schwarzschild-de Sitter solution. The dotted line is to emphasise the space-like nature of the singularity.

Chapter 8

Numerical emulation of black hole space-times

It has been shown by Friedrich [52] that there exists a specific choice for the CGG that globally covers the Schwarzschild-Kruskal space-time smoothly and without degeneracy. This involves writing the Schwarzschild metric in isotropic coordinates and choosing appropriate initial data for the conformal geodesics. This is an important result that exemplifies the CGG's superiority over the standard Gauss gauge, which is thought of only as a local gauge choice.

In this section we present how we (following Friedrich) set up the GCFE system to investigate null infinity of the Schwarzschild black hole and subsequently extend this procedure to the Schwarzschild-de Sitter and Schwarzschild-Anti-de Sitter black holes. We then numerically evolve the resulting initial data and see how our system behaves near the conformal boundary and the singularity.

8.1 Setting up the gauge

The first step we take is write (7.2.1) in isotropic coordinates, i.e. we want the metric in the form

$$\widetilde{g} = \Big(1 - \frac{2m}{r(\rho)} - \frac{\lambda}{3} r(\rho)^2\Big)\mathrm{d}t^2 - \alpha(\rho)^2\Big[\mathrm{d}\rho^2 + \rho^2\Big(\mathrm{d}\theta^2 + \sin^2\theta \mathrm{d}\phi^2\Big)\Big].$$

This gives the two equations

$$r'(\rho) = \frac{r(\rho)}{\rho}\sqrt{1 - \frac{2m}{r(\rho)} - \frac{\lambda}{3}r(\rho)^2}, \qquad r(\rho) = \rho\ \alpha(\rho). \tag{8.1.1}$$

Specialising to $\lambda = 0$ for the moment, we can integrate the first equation, setting the integration constant zero, and with the further transformation $\rho \to 2\rho$ we find for $r > 2m$

$$r(\rho) = \frac{1}{\rho}\Big(\rho + \frac{m}{2}\Big)^2, \qquad \alpha(\rho) = \frac{1}{\rho^2}\Big(\rho + \frac{m}{2}\Big)^2,$$

which gives the isotropic line element

$$\widetilde{g} = \Big(\frac{1 - \frac{m}{2\rho}}{1 + \frac{m}{2\rho}}\Big)^2 \mathrm{d}t^2 - \Big(1 + \frac{m}{2\rho}\Big)^4 \Big[\mathrm{d}\rho^2 + \rho^2\Big(\mathrm{d}\theta^2 + \sin^2\theta \mathrm{d}\phi^2\Big)\Big]. \tag{8.1.2}$$

It is worthwhile noting the symmetry

$$\rho \to \Big(\frac{m}{2}\Big)^2 \frac{1}{\rho},$$

which corresponds to the symmetry down the middle of its conformal diagram Figure 7.4. It is therefore enough to explore only one half of this diagram. The next stage is to choose initial data $\underline{H}, \underline{U}, \underline{Z}$ and $\underline{\Theta}$ to fix the 1-form h_a and conformal factor Θ. Friedrich makes the choice

$$\underline{\Theta} = \frac{1}{r^2} = \frac{\rho^2}{(\rho + \frac{m}{2})^4},$$

which does not compactify the initial surface in the ρ direction, i.e. it does not extend to space-like infinity. We choose $\underline{f_a} = 0$ so that $\underline{h_a} = \nabla_a \underline{\Theta}$. Finally we choose $\underline{U} = 1$ and $\underline{Z} = 0$ to fix the remaining freedom. This gives the explicit expressions for Θ as

$$\Theta = \frac{\rho^2}{(\rho + \frac{m}{2})^4} - s^2\Big(\frac{\rho - \frac{m}{2}}{\rho + \frac{m}{2}}\Big)^2, \tag{8.1.3}$$

and h_{AB} as

$$\begin{gathered} h_{00} = h_{11} = 0, \\ h_{01} = -\sqrt{2}\Big[\rho\frac{\rho - \frac{m}{2}}{(\rho + \frac{m}{2})^3} + s\Big(\frac{\rho - \frac{m}{2}}{\rho + \frac{m}{2}}\Big)^2\Big], \qquad h_{10} = -\sqrt{2}\Big[\rho\frac{\rho - \frac{m}{2}}{(\rho + \frac{m}{2})^3} - s\Big(\frac{\rho - \frac{m}{2}}{\rho + \frac{m}{2}}\Big)^2\Big]. \end{gathered} \tag{8.1.4}$$

The final step is to fix the extrinsic curvature χ_{ABCD} which is chosen to vanish initially.

Thus, the initial metric (8.1.2) with expressions (8.1.3) and (8.1.4) and $\underline{\chi}_{ABCD} = 0$ give us what we need to evolve this in our GCFE system. Once the evolution begins, the functions $r(\rho)$ and $\alpha(\rho)$ become functions of time as well, i.e. $r(s,\rho)$ and $\alpha(s,\rho)$, where $r(s,\rho)^2$ is related to the area of the 2-spheres. We know that in our GCFE system the conformal factor in front of the 2-sphere line element is R and hence we have the relationship

$$R = \rho\ \Theta\ \alpha(s,\rho) \Leftrightarrow r(s,\rho) = \frac{R}{\Theta}.$$

This allows one to compute $r(s,\rho)$ (i.e. the one from the Kottler metric (7.2.1)) over the course of the simulation. This is very useful as it will tell us where the event horizon is located and if or when we end up at the curvature singularity. We can also compute the Kretschmann scalar for the isotropic line element (8.1.2) in terms of our GCFE system variables as[1]

$$I := 48\ \Theta^6 \psi_2^2 + \frac{8}{3}\lambda,$$

which is another way to check if we are approaching the curvature singularity.

Now what happens to the above procedure if we make $\lambda \neq 0$? Unfortunately, the differential equation for $r(\rho)$ cannot be solved explicitly. But suppose for a moment that we did have $r(\rho)$ and hence also $\alpha(\rho)$ so we knew the metric at least at $t = 0 \Leftrightarrow s = 0$. Then we could again write the initial data for the conformal factor as $\underline{\Theta} = \frac{1}{r(\rho)^2}$ and again choose $\underline{f_a} = 0$. That fixes $\underline{h_a}$ and we keep the choices $\underline{U} = 1$ and $\underline{Z} = 0$. Then we get expressions for Θ and h_a overtime as functions of $r(\rho)$. We can compute the initial data for our system variables using (8.1.2) at $t = 0$ in terms of $r(\rho)$ and $\alpha(\rho)$ and set again $\underline{\chi}_{ABCD} = 0$. Then we have generalised the above procedure to $\lambda \neq 0$ given that we can somehow obtain $r(\rho)$ and $\alpha(\rho)$.

So how do we then solve for $r(\rho)$ and $\alpha(\rho)$? Given that if we compute $r(\rho)$ we also know $\alpha(\rho)$, we focus on solving for $r(\rho)$. That is, we must solve the first equation in (8.1.1). This can be done numerically using simple ODE solvers in Pythons SciPy package, although one must be careful about what values to take for the initial condition. The numerics will break down if the equation is to be solved in an interval containing a horizon, as at these points

[1] This has been simplified by setting the ψ_{ABCD} components with non-zero spin-weight to be zero.

the differential equation becomes $r'(\rho) = 0$. This means that one cannot use this method to study the cases $k \geq 1$. However this is only due to a coordinate issue, and hence one could in principle change to a coordinate system which is regular at the horizon, solve the equation there and then transform the solution back. However as this still leaves interesting cases, namely Schwarzschild-Anti-de Sitter space-time and Schwarzschild-de Sitter space-time that has distinct cosmological and event horizons, we do not do this.

A remark to make is that one can split the conformal geodesics in Schwarzschild space-time chosen with the above initial data into two distinct groups, see Figure 8.1. The first group ends up at the singularity while the second group goes through null infinity. The borderline of these groups is the conformal geodesic that goes through i^+. This can in fact be computed *a-priori* (along with the corresponding one on the left of the diagram) by looking at the conformal geodesic equations with the condition $r =$ constant. We find

$$\rho = \rho_{\pm} = \frac{3 \pm \sqrt{5}}{4} m, \tag{8.1.5}$$

one for each i^+ pictured. This is very helpful during the evolution, as we should notice different behaviours for the fields in our system on each side of ρ_+.

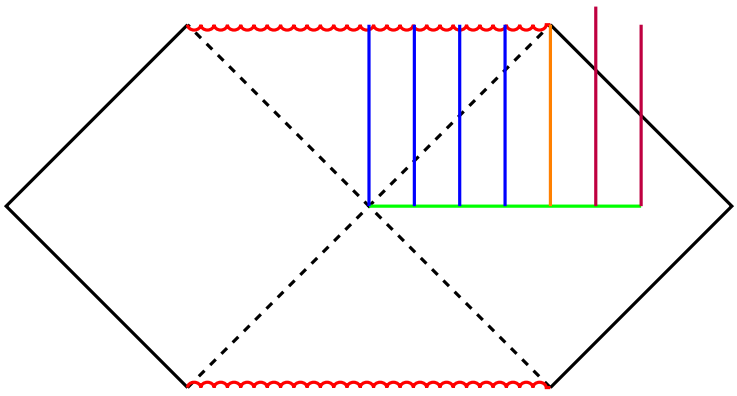

Figure 8.1: Different groups of conformal geodesics in the Schwarzschild space-time. The green line represents the initial surface, while the blue lines are the geodesics that reach the singularity, the purple lines are those that go through null infinity and the orange is the single geodesic that goes through i^+. The conformal geodesics pictured are straight lines for illustration purposes only.

From this we can also compute that

$$t \to \infty \quad \text{as} \quad s \to \frac{2}{\sqrt{5}m}. \tag{8.1.6}$$

Lastly a remark on the spin-2 zero rest-mass system. The procedure outlined in section 3 yields a PDE for ψ_2. However considering the evolution system $\Lambda_{(ABCD)} = 0$, this equation becomes an ODE by imposing that the non-zero spin-weighted functions vanish (since the three cases we are considering are spherically symmetric). We find that the evolution equation for ψ_2 simply becomes

$$\partial_t \psi_2 = -\frac{3}{2\sqrt{2}}\Big(\chi_{02} + \chi_{20} + 2\hat{\gamma}_{01} - 2\gamma_{20}\Big)\psi_2. \tag{8.1.7}$$

One can further show that in spherical symmetry, $\chi_{02} = \chi_{20}$ and $\hat{\gamma}_{01} = \gamma_{20}$ which gives the even simpler equation

$$\partial_t \psi_2 = -\frac{3}{\sqrt{2}}\chi_{02}\psi_2.$$

Using (8.1.7) as our evolution equation for ψ_2 we do not have any boundary conditions to worry about. Thus we have all we need to begin the evolution.

8.2 Schwarzschild space-time

First we look at the Schwarzschild space-time with $m = 0.5$ and use the analytic initial data at $t = 0 \Leftrightarrow s = 0$. As we are in spherical symmetry, we only need to discretise the ρ-direction. We split this into equi-distant points in the interval $[0.25, 1.25]$ so that the left boundary starts on the event horizon and is in the centre of the diagram like in Figure 8.1. We use ρ-resolutions of $\{25, 50, 100, 200, 400\}$. We confirm that the constraints which are not identically satisfied propagate and converge like we did in chapter 6 for the test cases, however we do not show these.

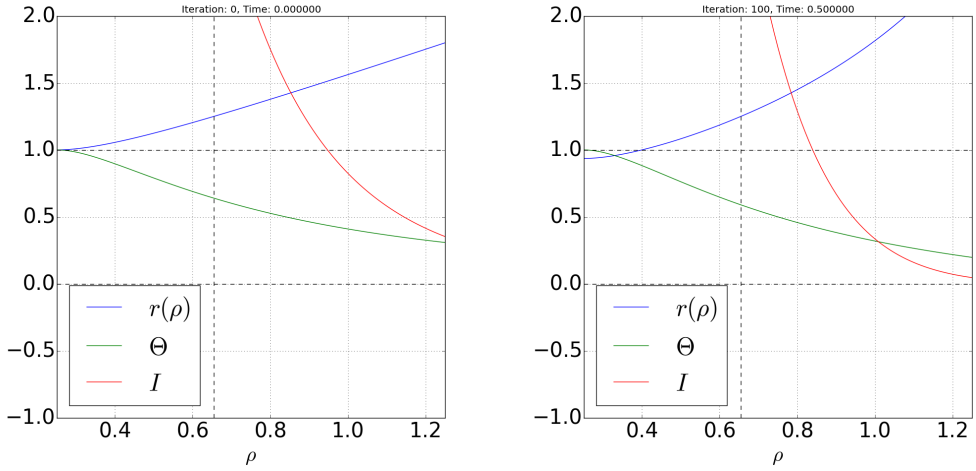

(a) $s = 0$ (b) $s = 0.5$

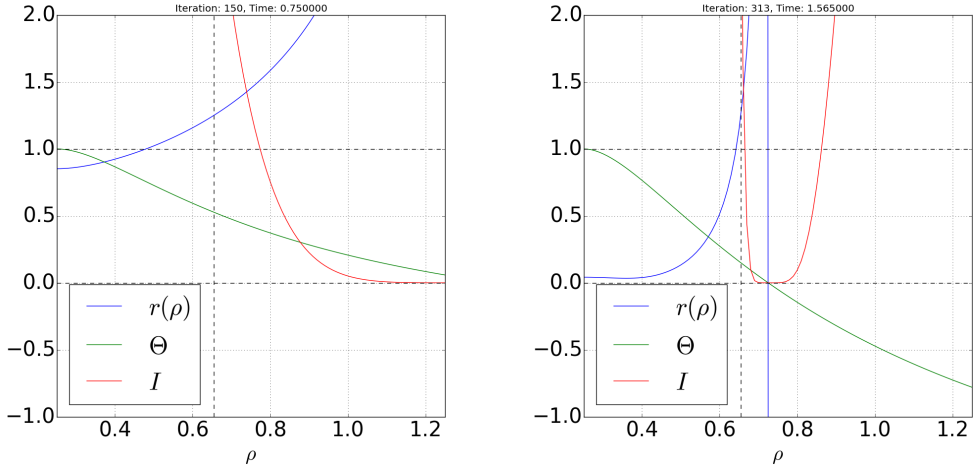

(c) $s = 0.75$ (d) $s = 1.565$

Figure 8.2: A sequence of simulation screen shots for Schwarzschild initial data. The horizontal dotted line at height 1 is there to easily differentiate fields that are within or outside the event horizon (at $r(\rho) = 1$ with our choice of $m = 0.5$). The vertical dotted line is the conformal geodesic that goes through i^+.

Some snapshots of the resulting evolution are displayed in Figure 8.2. One sees that the left boundary hits the singularity around $s \approx 1.565$ and the right boundary hits $\mathscr{I}^+$ around $s \approx 0.86$. There are some interesting observations to note: We indeed find that along the geodesic $\rho = \rho_+$ the coordinate r remains constant during the course of the evolution, as

expected from (8.1.5). Moreover, r tends to zero to the left of ρ_+, while tending to positive infinity to the right and is undefined past this. This is in exact accordance with what we would expect from our analysis of the global structure. Another property to note is that the Kretschmann scalar goes to zero as we approach null infinity (and is also undefined past $\mathscr{I}^+$), which is evident from the simulation snapshots. It also blows up in the part of the grid where r goes to zero. Hence we can conclude that we have reached an honest-to-god curvature singularity. As we have a system of ODEs, the solutions along $\rho =$ constant do not need information from neighbouring points. Hence when we reach the singularity on the left boundary, it does not end up destroying the simulation on the entire computational domain, but rather only at that point. Hence we can continue the evolution to compute more of $\mathscr{I}^+$ and approach i^+. This can be seen clearly in Figure 8.3 where we show later snapshots of the simulation. This shows that the points which hit $r = 0$ and the points for which $\Theta = 0$ come together at ρ_+ at a time $s \approx 1.78$. This is exactly what was expected from our analysis of the conformal structure, and it also verifies the time at which we hit i^+ from (8.1.6).

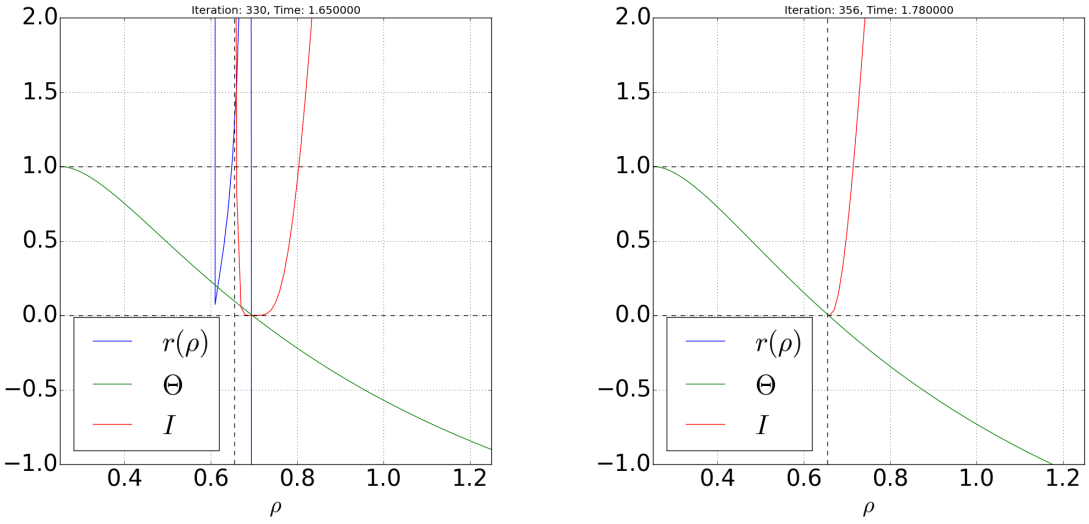

(a) $s = 1.65$ (b) $s = 1.78$

Figure 8.3: A sequence of simulation screen shots after the singularity has been reached in Figure 8.2.

A more detailed analysis of null infinity is given in section 9 where we perturb Schwarzschild with gravitational radiation and compute global properties of the system there.

8.3 Schwarzschild-Anti-de Sitter space-time

The first thing we need to do for this case is to find out where the horizon lies on the initial surface $t = 0 \Leftrightarrow s = 0$ so we can numerically solve the ODE for $r(\rho)$ (8.1.1).

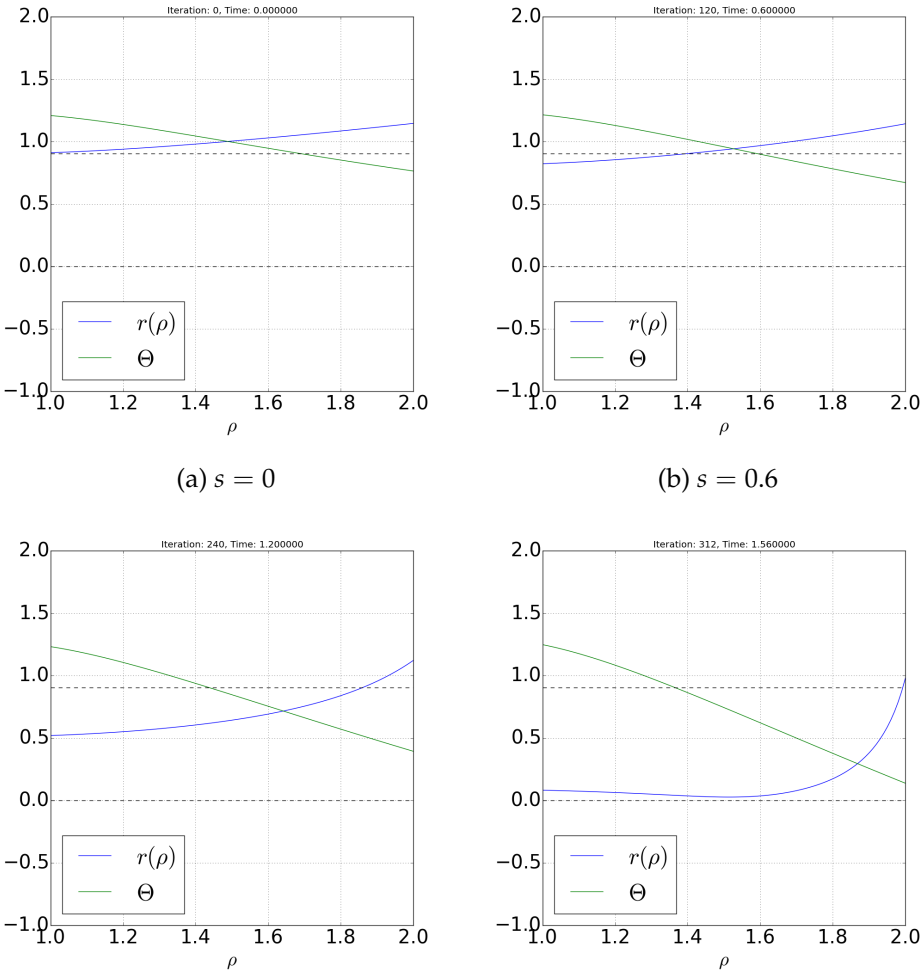

(a) $s = 0$ (b) $s = 0.6$

(c) $s = 1.2$ (d) $s = 1.56$

Figure 8.4: Sequence of simulation screen shots for Schwarzschild Anti-de Sitter initial data. The horizontal dotted line at height 0.91 is there to easily differentiate fields that are within or outside the event horizon.

We choose again $m = 0.5$ and now choose $\lambda = -0.4$ and find that the horizon is located at $r \approx 0.9$. We discretise the ρ-direction into equi-distant points in the interval $[1, 2]$ (recall we are in spherical symmetry so this is all that is needed) and choose as initial data $r(1) = 0.91$ and initial surface $s = 0$, so we start in an analogous fashion to section 8.2 having the left boundary in the centre of the diagram Figure 7.5 and the right boundary somewhere between there and the conformal boundary. We use ρ-resolutions of $\{25, 50, 100, 200, 400\}$ again and see that the constraints propagate and converge as expected.

Immediately one sees that we never get to conformal infinity in this simulation by looking at snapshots of the evolution in Figure 8.4. This is expected from the global structure portrayed in Figure 7.5 and the fact we take conformal geodesics initially orthogonal to our initial surface $s = 0$. We could potentially compute both $r = 0$ and $\mathscr{I}$ by choosing the conformal geodesics initially not to be orthogonal to $s = 0$, but at some angle so that they go toward $\mathscr{I}$ as well as $r = 0$, although we do not do this. We also see that the entire computational domain tends to the singularity from seeing that $r \to 0$. The singular nature is confirmed by computing the Kretschmann scalar and seeing it blows up everywhere. Thus we have mimicked the global structure of Schwarzschild-Anti-de Sitter space-time numerically.

8.4 Schwarzschild-de Sitter space-time

The only case we can compute for Schwarzschild-de Sitter space-time from the three possible (see (7.2.3) for the polynomial whose roots mark the locations of the horizons) is the case where there exists distinct event and cosmological horizons. By fixing $m = 0.5$ and $\lambda = 0.4$ we find that these occur at $r(\rho) \approx 1.28$ and $r(\rho) \approx 1.87$ respectively, so that we are in a region I like the leftmost one in Schwarzschild de-Sitters conformal diagram Figure 7.6, i.e. event horizon to the left and cosmological horizon to the right. We discretise the ρ-direction into equi-distant points in the interval $[1, 4.4]$ and solve the ODE for $r(\rho)$ (8.1.1) with initial data $r(1) = 1.3$ so that we start close to the event horizon. It happens, as expected, that if we moved the location of the right boundary to larger values of ρ we would approach the cosmological horizon. We find $r(4.4) \approx 1.63$ which is a reasonably compromise between distance to the cosmological horizon and resolution required. We use ρ-resolutions

of $\{25, 50, 100, 200, 400\}$ and initial surface $s = 0$. We once again see that the constraints propagate and converge as expected.

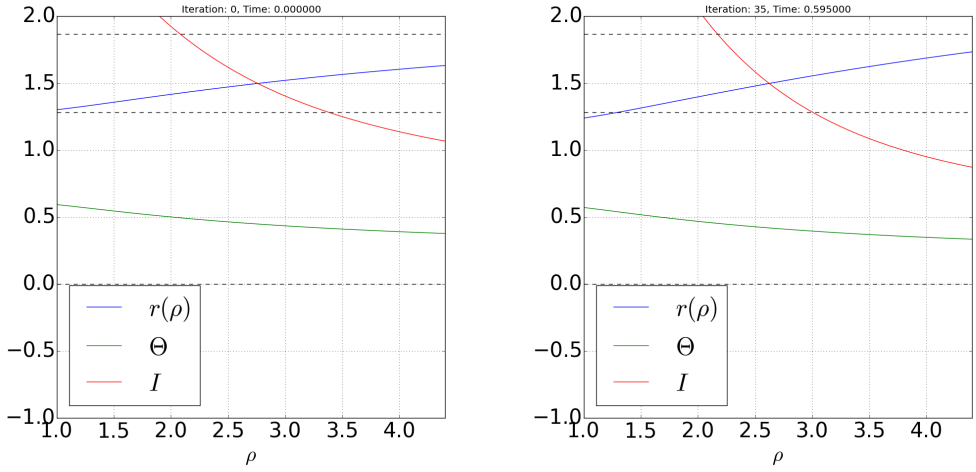

(a) $s = 0$ (b) $s = 0.595$

(c) $s = 1.19$ (d) $s = 1.67$

Figure 8.5: Sequence of simulation screen shots for Schwarzschild-de Sitter initial data with two distinct horizons. The horizontal dotted lines at heights 1.28 and 1.87 are there to easily differentiate fields that are within or outside the event and cosmological horizons respectively.

We see by looking at the snapshots of the evolution in Figure 8.5 that this case is similar to the Schwarzschild space-time case. We have a "pivot point" which has a constant $r(\rho)$ at

$\rho \approx 1.6$. To the left we see $r(\rho) \to 0$ and to the right we see $r(\rho) \to \infty$ as the conformal geodesics parameter s approaches some finite value. This is what we expected by having our initial data in the leftmost region I in Schwarzschild-de Sitter space-time's conformal diagram Figure 7.6. The difference between this case and Schwarzschild space-time is that the singularity is joined to a space-like surface instead of one which is null. That is why we reach the singularity on the left boundary before getting to $\mathscr{I}^+$ on the right, because it is further away from the initial surface with respect to the conformal metric than in the Schwarzschild case. There is no reason for the simulation to crash once one point hits the singularity (as mentioned in the Schwarzschild space-time case in section 8.2). Thus continuing the simulation (see Figure 8.6) we indeed find that we reach $\mathscr{I}^+$. We also see that on $\mathscr{I}^+$ the Kretschmann scalar remains constant. This also shows that we can get very close to time-like infinity i^+, a point which has been studied extensively recently for Schwarzschild-de Sitter space-time by Gasperin and Kroon in [60].

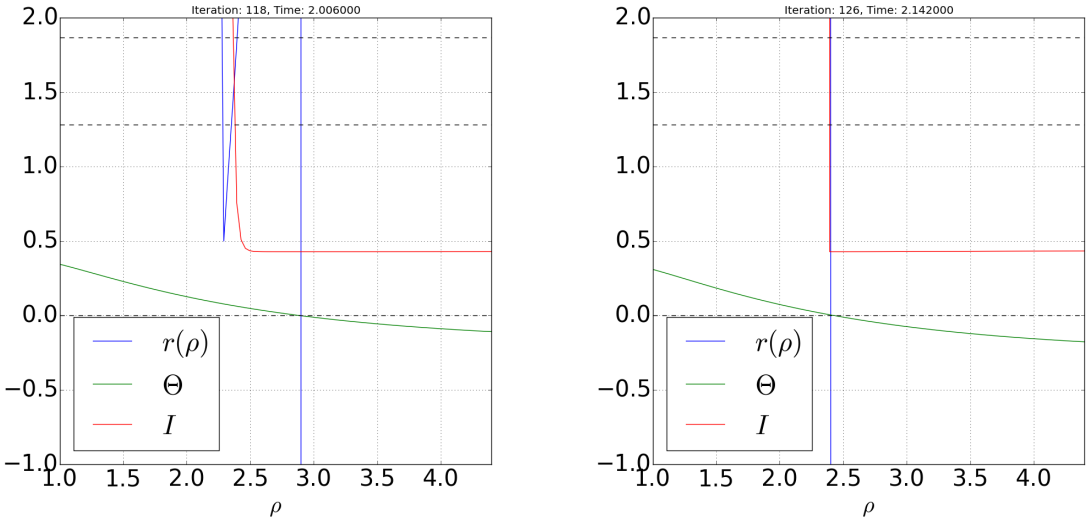

(a) $s = 2$ (b) $s = 2.14$

Figure 8.6: Sequence of simulation screen shots after the singularity has been reached in Figure 8.5.

8.5 Summary of results

We have shown in sections 8.2, 8.3 and 8.4 that our representation of the GCFE system on the computer has successfully reproduced the conformal structure of Schwarzschild, Schwarzschild-de Sitter and Schwarzschild-Anti-de Sitter space-times. The fact that we get the correct results was not surprising in itself, due to the rigorous checks performed in sections 4 and 6. What was nice to see was that the gauge did not break down before we covered the interesting parts of Schwarzschild-de Sitter and Schwarzschild-Anti-de Sitter space-times (the gauge used has only been proven analytically not to break down for Schwarzschild space-time). This allowed us to cover a large part of $\mathscr{I}^+$ in Schwarzschild and Schwarzschild-de Sitter space-times. In particular, we reproduced the fact that the surfaces $r = 0$ and $\mathscr{I}^+$ join at a point i^+. The fact that the GCFE system in spherical symmetry collapses to a system of ordinary differential equations allows us to get arbitrarily close to i^+. This could be a good start for simple gravitational perturbations of Schwarzschild-de Sitter space-time, which have been of interest recently [60].

Chapter 9

The IBVP for the Schwarzschild space-time

So far we have only looked at interesting cases in spherical symmetry, and only performed a simple test for the axially-symmetric case. In order to fully test our code in axial-symmetry we decided to look at perturbations of Schwarzschild space-time with gravitational radiation. There are multiple ways to potentially do this, so first we discuss the different approaches and decide on the approach to take. Remember that there is an obvious symmetry in the conformal diagram for Schwarzschild space-time, and so we focus only on the right half.

9.1 Different approaches

Case one: Choose as the initial surface a portion of $s = 0$. By not compactifying in the spatial direction, one has a boundary along the symmetry (down the middle of the conformal diagram) and another somewhere between there and space-like infinity. This is perfect for employing our boundary method to shoot in a gravitational wave, see Figure 9.1. Due to the nature of conformal geodesics in Schwarzschild space-time, we will be able to have the right boundary pass through $\mathscr{I}^+$ while the left boundary will go through the event horizon and eventually hit the singularity as shown for the non-perturbed case in section 8.2. This

incorporates the gravitational interaction between the wave and the event horizon, as well as the energy escaping to null infinity.

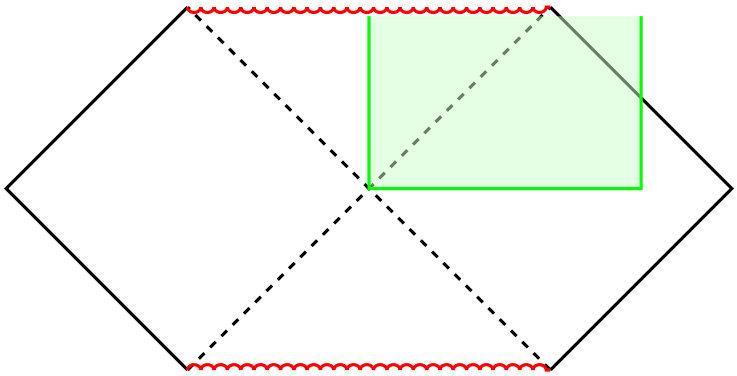

Figure 9.1: An approach to the IBVP for Schwarzschild space-time perturbed by a gravitational wave. This would involve pumping in a gravitational wave from the outer (right) boundary by employing appropriate boundary conditions.

Case two: Choose as the initial surface the entire $s = 0$ surface, i.e. fully compactify the spatial direction. This would mean that we would have to describe spatial infinity using the cylinder approach of Friedrich, as discussed for example in [53] (we do not show the cylinder explicitly and instead keep the diagram a conformal one). Due to the cylinder being a characteristic for the ψ_{ABCD} system one does not need to worry about boundary conditions there. However a consequence of the cylinder approach to space-like infinity is that the gravitational spinor becomes singular where the cylinder meets $\mathscr{I}^+$, and hence this propagates along null infinity, destroying regularity. One can however evolve arbitrarily close to null infinity. Another problem with this approach is solving the constraints on the initial space-like surface. This is a system of elliptic partial differential equations which are not so easy to solve. One would specify the initial configuration of gravitational radiation and solve for the remaining functions.

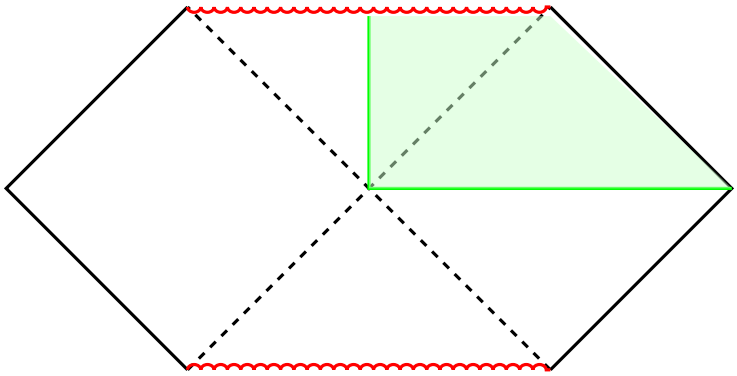

Figure 9.2: An approach to the IBVP for Schwarzschild space-time perturbed by a gravitational wave. This would involve solving the constraints on the initial compactified surface to already include a gravitational wave. Friedrich's cylinder construction of space-like infinity would have to be used.

Case three: Think of the initial surface as being the V-shaped surface as in Figure 9.3 that extends to the cylinder at i^0 (which again we do not show). One would then specify ingoing gravitational waves on $\mathscr{I}^-$ with compact support so that it is Schwarzschild space-time close to i^0 and i^-. The initial data on the event horizon is known as this will also be Schwarzschild space-time. However the problem is i^-, the joining point of these surfaces which is inherently singular. To avoid this point, one could do an "analytic time-step" to get another surface that would be arbitrarily close to these surfaces and i^-. This could then be used as the initial surface. One does not have boundary conditions on the cylinder, and they are also not needed on the leftmost boundary as the domain of dependence of the initial surface would then be as shown in Figure 9.3. Thus in this approach one has an IVP. The upshot of this way of formulating the system is that it gives us the ability to set up a full blown scattering problem. One specifies the ingoing gravitational waves on $\mathscr{I}^-$, they enter the space-time and scatter with each other and the black hole, then they travel off to $\mathscr{I}^+$ where our idealised detectors live. Another advantage is that solving the constraints on $\mathscr{I}^-$ will be simpler than on a space-like surface. This method will also avoid the problem of constraint violating modes propagating in from the boundaries (even though we have a solution for this), as we no longer "pump in" the waves but rather solve the constraints with them "already there".

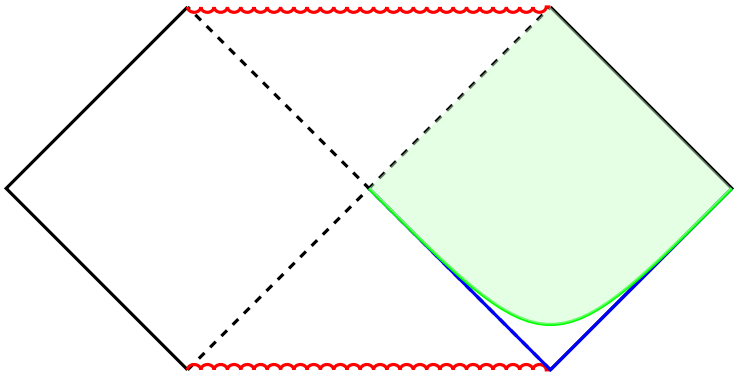

Figure 9.3: An approach to the IBVP for Schwarzschild perturbed by a gravitational wave. This would involve solving the constraints on $\mathscr{I}^-$ to already include a gravitational wave with compact support and joining it with Schwarzschild data on the event horizon (blue). Friedrichs cylinder construction of space-like infinity would have to be used. A small time-step would move the initial surface away from the problematic i^-, which would then be the initial surface used in the code (green).

9.2 The setup

We decided to choose case one in section 9.1 as our framework for gravitational perturbations of Schwarzschild space-time. This will give us an opportunity to more rigorously test our boundary treatment as well as avoiding the extra step of solving constraints.

We use the gauge choice discussed in section 8.1 that was successfully used in our numerical evolutions of unperturbed Schwarzschild space-time, and only repeat here the necessary equations. We use the representation of Schwarzschild in isotropic coordinates

$$\underset{\sim}{\widetilde{g}} = \Big(\frac{1-\frac{m}{2\rho}}{1+\frac{m}{2\rho}}\Big)^2 \mathrm{d}t^2 - \Big(1+\frac{m}{2\rho}\Big)^4 \Big[\mathrm{d}\rho^2 + \rho^2\Big(\mathrm{d}\theta^2 + \sin^2\theta \mathrm{d}\phi^2\Big)\Big], \tag{8.1.2}$$

and choose initial data so that we find the explicit expressions

$$\Theta = \frac{\rho^2}{(\rho+\frac{m}{2})^4} - s^2\Big(\frac{\rho-\frac{m}{2}}{\rho+\frac{m}{2}}\Big)^2, \tag{8.1.3}$$

and

$$h_{00} = h_{11} = 0,$$
$$h_{01} = -\sqrt{2}\Big[\rho\frac{\rho-\frac{m}{2}}{(\rho+\frac{m}{2})^3} + s\Big(\frac{\rho-\frac{m}{2}}{\rho+\frac{m}{2}}\Big)^2\Big], \qquad h_{10} = -\sqrt{2}\Big[\rho\frac{\rho-\frac{m}{2}}{(\rho+\frac{m}{2})^3} - s\Big(\frac{\rho-\frac{m}{2}}{\rho+\frac{m}{2}}\Big)^2\Big]. \tag{8.1.4}$$

We use the method described in chapter 3 to derive the spin-2 zero rest-mass system. The characteristic speeds of these equations propagating normal to the boundary must be monitored during the evolution to determine the number of ingoing modes and then impose boundary conditions accordingly. They are

$$\frac{\sqrt{2}\ c^1{}_1 - 2\ c^0{}_0 c^1{}_2 + 2\ c^0{}_1 c^1{}_1}{1 - 2(c^0{}_1)^2 + 2\ c^0{}_0 c^0{}_2}, \tag{9.2.1a}$$

$$\frac{\sqrt{2}\ c^1{}_1 + 3\ c^0{}_0 c^1{}_2 + 4\ c^0{}_1 c^1{}_1 + c^0{}_2 c^1{}_0}{2[1 - 2(c^0{}_1)^2 + 2\ c^0{}_0 c^0{}_2]}, \tag{9.2.1b}$$

$$\frac{2\ c^0{}_1 c^1{}_1 - c^0{}_0 c^1{}_2 - c^0{}_2 c^1{}_0}{1 - 2(c^0{}_1)^2 + 2\ c^0{}_0 c^0{}_2}, \tag{9.2.1c}$$

$$\frac{-\sqrt{2}\ c^1{}_1 - 3\ c^0{}_2 c^1{}_0 + 4\ c^0{}_1 c^1{}_1 + c^0{}_0 c^1{}_2}{2[1 - 2(c^0{}_1)^2 + 2\ c^0{}_0 c^0{}_2]}, \tag{9.2.1d}$$

$$\frac{-\sqrt{2}\ c^1{}_1 + 2\ c^0{}_1 c^1{}_1 - 2\ c^0{}_2 c^1{}_0}{1 - 2(c^0{}_1)^2 + 2\ c^0{}_0 c^0{}_2}, \tag{9.2.1e}$$

for $\psi_0, ..., \psi_4$ respectively. With this setup we have the initial data

$$R = \frac{\rho}{(\rho+\frac{m}{2})^2}, \qquad c^1{}_1 = \frac{(\rho+\frac{m}{2})^2}{\sqrt{2}}, \qquad \gamma_{20} = \hat{\gamma}_{01} = \frac{(\rho+\frac{m}{2})(\rho-\frac{m}{2})}{\sqrt{2}\,\rho},$$

$$P_{101} = P_{110} = \frac{m(\rho+\frac{m}{2})^2}{\rho}, \qquad \psi_2 = -\frac{m(\rho+\frac{m}{2})^6}{\rho^3},$$

with all other fields zero. We choose $m = 0.5$ and discretise the ρ and θ-directions into equidistant points in the 2-dimensional interval $[0.25, 1.25] \times [0, \pi]$. Then initially we have two ingoing, two outgoing modes and one mode propagating along each boundary, where the leftmost boundary initially lies on the event horizon. For the leftmost boundary we enforce the conditions for $\psi_3[s, \rho, \theta]$ and $\psi_4[s, \rho, \theta]$ as

$$\psi_3[s, 0.25, \theta] = -\bar{\psi}_1[s, 0.25, \theta], \qquad \psi_4[s, 0.25, \theta] = \bar{\psi}_0[s, 0.25, \theta].$$

The physical reason for choosing the left boundary conditions as we have comes from the symmetry in the conformal diagram Figure 9.1. We suppose that the situation we define on the right part of the conformal diagram is also the case on the left. Hence at the symmetry point (which is the leftmost boundary in our setup) the appropriate ψ_{ABCD} components must be related as above. Although the left boundary conditions do not seem to be of maximally dissipative form as discussed in section 3.2, they are stable. There will also be no constraint violation propagating in from this boundary as we have not violated the constraints there, it will remain as Schwarzschild space-time until the gravitational wave that will be pumped in from the right boundary reaches it.

We implement our boundary treatment discussed in detail in section 3.3 in order to kill any ingoing modes from the subsidiary system coming from the right boundary. This is done by first choosing the free data q_0 for ψ_0, which represents the ingoing gravitational radiation, on the right boundary freely. We choose the boundary condition for $\psi_0[s, \rho, \theta]$ by employing the maximally dissipative boundary conditions derived in section 3.2 and choosing the corresponding free data to be

$$q_0[s, \theta] = \begin{cases} 4a\sqrt{\frac{2\pi}{15}}\, {}_2Y_{20} \sin^8(4\pi s), & s \leq \frac{1}{4} \\ 0 & s > \frac{1}{4} \end{cases},$$

where a is a fixed constant representing the amplitude of the wave and recalling that the spin-weighted spherical harmonic ${}_2Y_{20} = \sin^2\theta$ up to a constant when written in the usual polar coordinates. Then our boundary procedure tells us to incorporate into the GCFE system the free data q_1 for ψ_1, whose evolution equation is fixed by the condition that there is no ingoing mode in the subsidiary system. The maximally dissipative boundary condition approach gives the boundary data for ψ_0 and ψ_1 as functions of the ψ_i's that are not ingoing, the frame components c^0_{AB} and c^1_{AB} and the q_i. Hence we use these as the right boundary conditions for ψ_0 and ψ_1 given the q_i defined above while there are two ingoing modes.

It is worth mentioning that the maximally dissipative boundary condition procedure is much more difficult in this case than in the case of two gravitational waves shot into Minkowski space-time as described in section 6.4. There we had chosen a particular gauge so that the

c^0_{AB} vanished for all time. This means that the spatial frame vectors remained tangential to $s =$ constant hypersurfaces and we kept the same number of ingoing modes during the evolution. It also had the additional pleasant property of simplifying the procedure to obtain the maximally dissipative boundary conditions and the evolution equations for q_1 and q_3, the free data chosen to kill the ingoing modes of the subsidiary system. The maximally dissipative boundary conditions can be computed in the general case that we have here, albeit the equations for the q_i's turn out to be rather large. A potential simplification outlined in section 3.4 may make this part simpler by taking advantage of a frame rotation that makes certain frame components vanish. However this will introduce more terms on the right-hand-sides of probably every equation in the system.

Now we have all that is needed to start evolving the system, at least until the propagation directions of the ψ_{ABCD} components change. Hence, choosing a ρ-resolution of 400, a θ-resolution of 32 and the amplitude $a = 0.5$ as a test case, we monitor the value of the characteristic speeds (9.2.1) on each boundary during the course of the evolution. Almost immediately we see that the propagation direction for ψ_2 becomes negative on the right boundary, i.e. ψ_2 becomes an ingoing mode. We know from previous discussions that this also means there is another ingoing mode in the subsidiary system, which must be dealt with. We deal with this by enforcing new boundary conditions following our boundary treatment procedure. We leave q_0 as it is but re-derive the maximally dissipative boundary conditions so that we get new conditions for ψ_0, ψ_1 and now one for ψ_2 also with all of them only containing the outgoing ψ_3 and ψ_4 (and frame components). This allows us to compute a new evolution equation for q_1 and one for q_2.

Once we have compensated for the new ingoing mode from the right boundary, we continue to monitor the characteristic speeds during the evolution. The left boundary characteristic speeds do not change much over time, in particular the ψ_2 characteristic speed remains zero, so we do not need to worry about that. However at around $s \approx 1.04$ we find that the characteristic speed for ψ_3 on the right boundary changes sign and becomes negative, hence ingoing. This tells us the rather disturbing news that all three of the subsidiary

modes of the ψ_{ABCD} system are ingoing. However we can indeed compensate for this again by reapplying our boundary treatment. Although is this really necessary? We reach $\mathscr{I}^+$ on the right boundary at $s = \frac{5}{6} \approx 0.83$ and know that all the propagating modes in our subsidiary system are time-like. Consequently, if we let constraint violating modes propagate in from the boundary by choosing arbitrary free data (i.e. the q_i) there, they should never cross into the region of the conformal space-time containing our physical space-time and its conformal boundary as $\mathscr{I}^+$ is a null hypersurface. Hence null infinity acts as a one-way membrane, letting information pass out through it but letting no information in from outside. The only catch in imposing arbitrary boundary conditions after $\mathscr{I}^+$ has been reached on the right boundary is the influence these boundary conditions have on the approximation of ρ-derivatives of our system variables. Because our finite differencing scheme uses multiple points on either side of the point the derivative is being evaluated at, the approximation at points in the physical region of the space-time close to $\mathscr{I}^+$ will be influenced by values past conformal infinity. Hence the boundary conditions will influence ρ-derivatives of fields evaluated close to $\mathscr{I}^+$ and hence the physical region of the conformal space-time. This numerical artefact will shrink as the ρ-resolution is increased. However, we decided to continue testing the validity of our boundary treatment and impose boundary conditions that will kill all three of the ingoing modes of the subsidiary system. That is, we re-derive the maximally dissipative boundary conditions on the right boundary for $\psi_0, ..., \psi_3$ in terms of ψ_4 only (and frame components) and obtain evolution equations for q_1, q_2 and q_3 while leaving q_0 as zero (since at this point the wave has already propagated in).

Now we are in a position where we need not worry about boundary conditions as we have in fact already been driven to implement the most general version of our boundary treatment. However one should be careful about the denominator appearing in the characteristic speeds, as these expressions are not regular if the denominator changes sign. The denominator is in fact the component g^{00} of the metric (see section 2.5). It turns out that g^{00} vanishing has the consequence that the determinant of the matrix A^0 for the ψ_{ABCD} system (defined in chapter 3) also vanishes. This clearly causes issues as we need to invert this in order to obtain evolution equations. We lamentably find that in fact g^{00} does change sign around

$s \approx 1.24$ on the right boundary in our simulations. This causes the ψ_{ABCD} components to blow up and our simulation inevitably crashes. So what is the geometrical consequence of this component vanishing? We describe this schematically in Figure 9.4. At the point when $g^{00} = 0$ we have that the surface $\mathrm{d}s = \nabla_a s$ i.e. the $s =$ constant surface is null. Our conformal geodesics are always time-like (as seen by $g_{00} = 1$) with their velocities initially the same, so it must be that the parameter is progressing along different conformal geodesics with different accelerations. Then as the acceleration χ_{AB} in our gauge is the same as the 1-form f_{AB} up to a constant, the initial choice of the 1-forms f_{AB}, h_{AB} and conformal factor plays an important role in the length of the covector $\mathrm{d}s$ over the course of the simulation. To amend this one needs to investigate the consequence of choosing different initial data for f_{AB}, hence changing the initial data for either h_{AB} or Θ or both, and see how the length of $\mathrm{d}s$ changes over time.

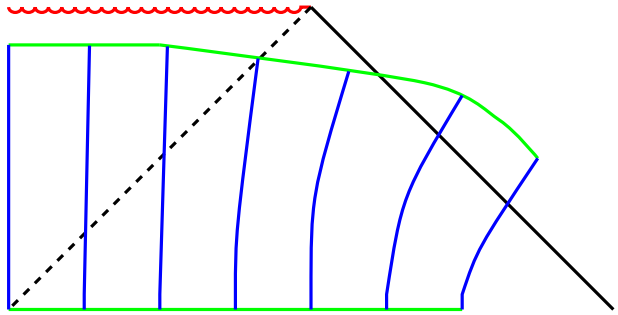

Figure 9.4: The geometrical ramifications of g^{00} going to zero. The green lines are $s =$ constant surfaces while the blue lines are conformal geodesics. The conformal geodesics remain time-like while part of the later $s =$ constant surface transitions from space-like to null.

Now that we have studied how we approach the problem of perturbing the Schwarzschild space-time with gravitational radiation and interpreted properties of the evolution, we look at the constraint propagation to see how well our boundary treatment handles this much more rigorous test.

9.3 Constraint propagation

First we note that we use a θ-resolution of 32 so that even at late times of the simulation our fields are represented up to machine precision in the spin-weighted spherical harmonic basis. We use ρ-resolutions of $\{25, 50, 100, 200, 400\}$ which gives us ample data to check the propagation of the constraints. Simulations are also performed without our boundary treatment where the appropriate q_i, $i \neq 0$ are set to zero. This will allow us to contrast the before and after of our boundary treatment to emphasise the problem that we resolve.

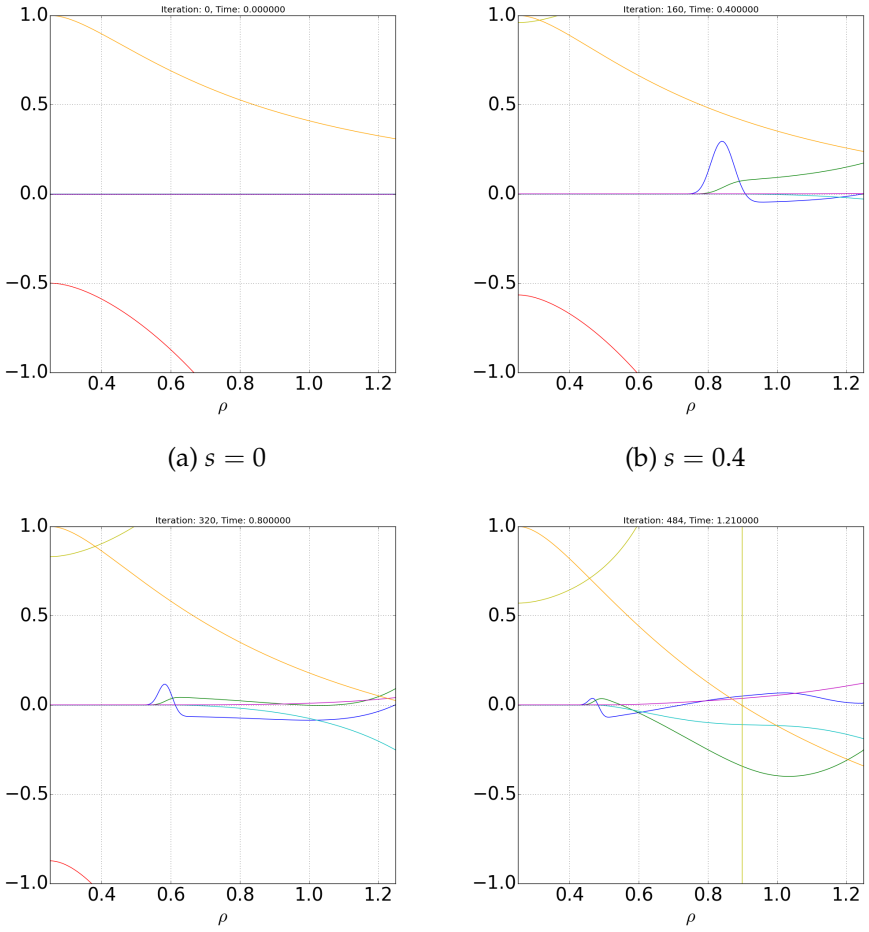

(a) $s = 0$ (b) $s = 0.4$

(c) $s = 0.8$ (d) $s = 1.21$

Figure 9.5: A sequence of simulation screen shots with ρ-resolution 200 and θ-resolution 32 of a gravitational wave being pumped into the Schwarzschild space-time. Legend: — ψ_0, — ψ_1, — ψ_2, — ψ_3, — ψ_4, — r, — Θ.

In Figure 9.5 we see snapshots of the simulation during its evolution. Everything behaves nicely close to the boundary and by the end of the simulation at $s \approx 1.21$ we have computed a large amount of $\mathscr{I}^+$. Notice that the gravitational wave appears to be shrinking as it propagates toward the left boundary. This is probably due to the stretching of the computational domain that happens due to the bending of the conformal geodesics near the right boundary.

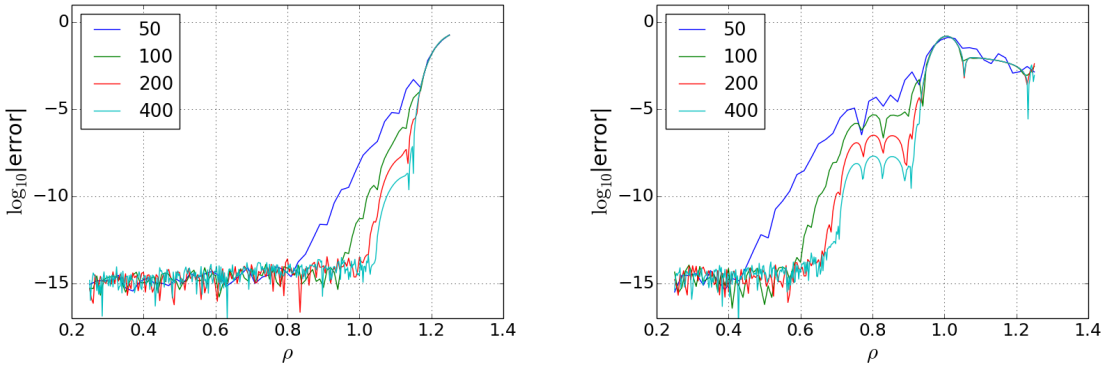

(a) $s = 0.01$ (b) $s = 0.41$

(c) $s = 0.81$ (d) $s = 1.16$

Figure 9.6: A sequence of convergence tests for a component of the constraint ψ_{ABCD} (2.4.12b) with non-constraint-preserving boundary conditions imposed computed on $s =$ constant, $\theta = \frac{\pi}{2}$ slices with increasing ρ-resolution.

Now to the constraints. We first present a convergence plot for the case of the simple, but non-constraint-preserving, choice of setting the free boundary data (but not q_0) zero. Figure

9.6 displays the convergence plots for a component of the ψ_{ABCD} constraint (2.4.12b) at $s =$ constant, $\theta = \frac{\pi}{2}$ slices. One clearly sees that there is something propagating in from the right boundary that stops the constraints from converging to machine precision. This happens not just to this constraint, but to all the constraints in our system.

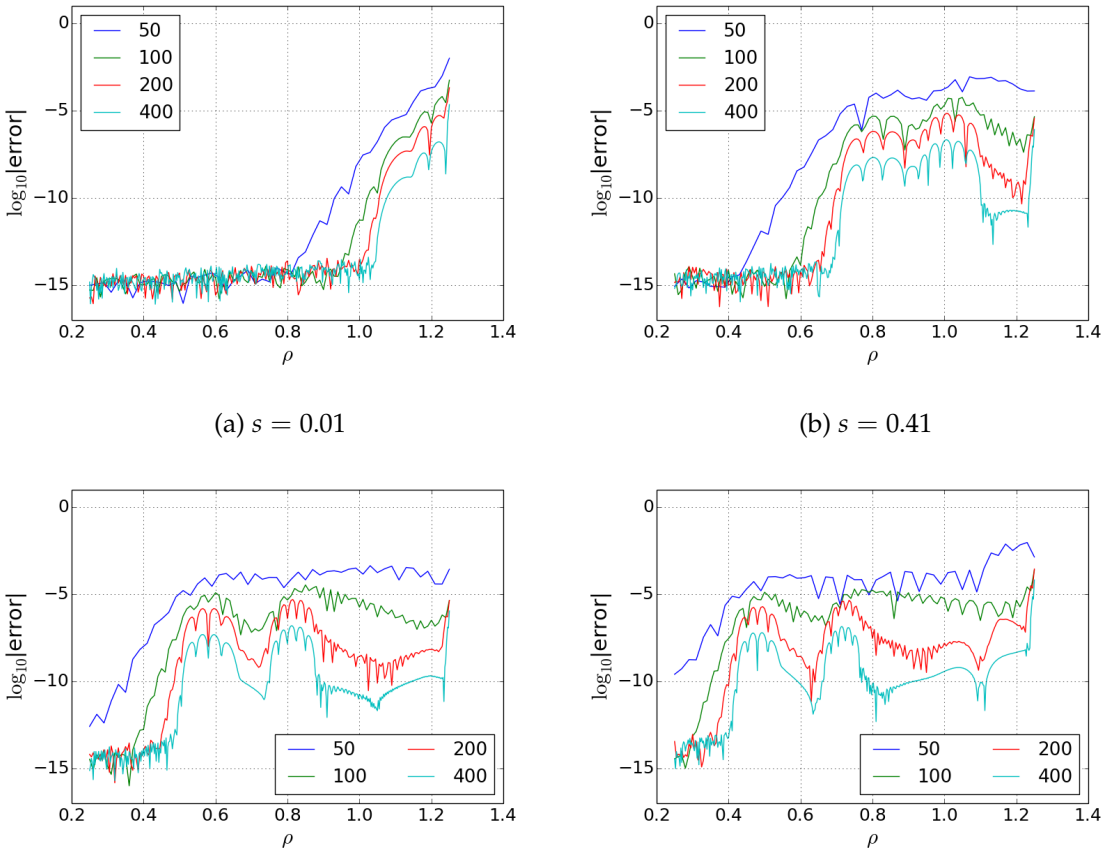

(a) $s = 0.01$

(b) $s = 0.41$

(c) $s = 0.81$

(d) $s = 1.16$

Figure 9.7: Sequence of convergence tests for a component of the constraint ψ_{ABCD} (2.4.12b) with constraint-preserving boundary conditions imposed computed on $s =$ constant, $\theta = \frac{\pi}{2}$ slices with increasing ρ-resolution.

Now we contrast these plots to the analogous ones that implement our boundary treatment, shown in Figure 9.7. Immediately one sees that these convergence plots are exceedingly better than the previous ones. We get convergence toward machine precision and in the process have moved the constraints around 1×10^8 closer to this. Looking at other constraints in the

system we see that the problem has been overcome in all of them.

One final comparison that is worth exhibiting is the case of killing only two of the three (at late times) constraint violating modes of the subsidiary system. This should allow us to see a rather slowly propagating constraint violating mode entering the system at around $s \approx 1.04$. Both simulations accurately kill the first two ingoing constraint violating modes during the simulation, as can be seen in Figure 9.7 by the constraints both correctly converging in the left and middle regions of the domain. However close to the right boundary, although not as dramatic as the previous example, one does in fact see a difference between the two. The simulation utilising our boundary treatment does not form a bump close to the right boundary as opposed to the other. This bump is analogous to what happens in Figure 9.6 (b). It is also worth mentioning that the location of Θ on the $s = 1.16$ hypersurface is at $\rho \approx 0.93$, i.e. this last constraint violating mode does not affect the accuracy of the fields on null infinity at this stage of the evolution, as discussed in section 9.2. Hence one may choose to avoid our boundary treatment for the last ingoing subsidiary mode to speed up the simulations for investigations on $\mathscr{I}^+$.

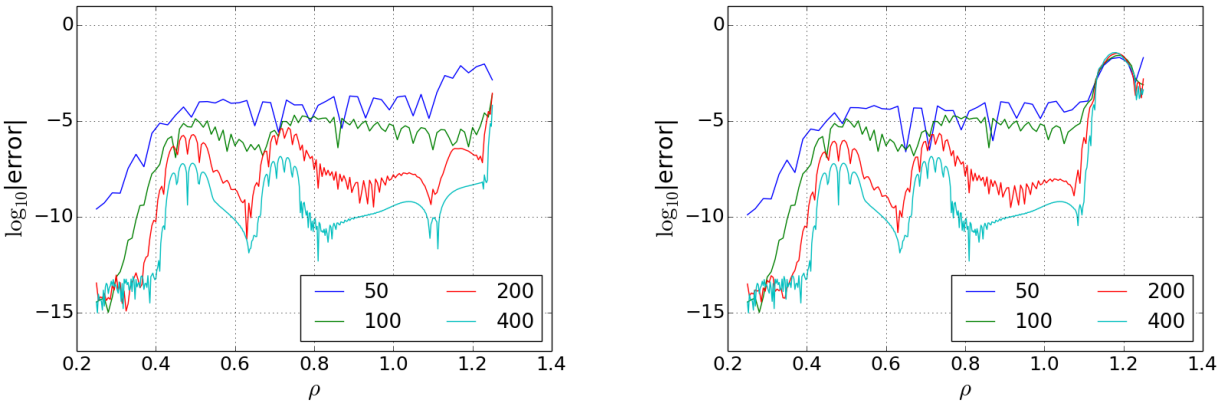

(a) (b)

Figure 9.8: Comparison of convergence tests for a component of the constraint ψ_{ABCD} (2.4.12b) computed on $s = 1.16.$, $\theta = \frac{\pi}{2}$ slices with increasing ρ-resolution.

Thus we have shown that without our boundary treatment, constraint violating modes of

the subsidiary system propagate into our computational domain and destroy constraint propagation. We have also shown in detail that killing all but one of the ingoing constraint modes still leads to destruction of convergence. Thus in general our boundary treatment is required to stop all of the three possible constraint violating modes from propagating into the computational domain.

9.4 Energy in general relativity and the BMS group

One of the most interesting global properties of asymptotically flat space-times is the notion of energy. In Newtonian physics one has a fixed background on which a field evolves, hence finding the energy of the system involves looking only at the field. However the general theory of relativity *couples* geometry and fields. Gravitational radiation must contribute to the total energy but it is not described by the energy-momentum tensor on the "fields" side of Einstein's field equation, rather it appears in the Weyl tensor on the "geometry" side. As John Wheeler famously once said, "space-time tells matter how to move; matter tells space-time how to curve". Therefore one cannot just simply read off the energy of the system at a fixed time as the relevant information is tangled with irrelevant information. However for asymptotically flat space-times, a resolution exists; at space-like and null infinity one can decouple the geometry from the fields, hence *energy is thought of only as a global property*.

At space-like infinity one can compute the so-called ADM mass, put forward by Arnowitt, Deser and Misner [3] in 1962. This is computed as the limit of a particular surface integral on an asymptotically flat slice that extends to space-like infinity. It measures the total mass on the slice and due to being calculated at space-like infinity it is independent of the slice taken. For Schwarzschild space-time, the ADM mass coincides with the Schwarzschild mass m. As we do not spatially-compactify our space-time, we do not include spatial infinity and hence we cannot compute the ADM mass exactly.

We will be more interested in the concept of mass defined on $\mathscr{I}$. A definition of the global mass of asymptotically flat space-times at null infinity was mulled over by Bondi, Metzner, Sachs, Newman and Unti among others in the early 1960's (see [18, 88, 112]). The result

became known as the Bondi-mass and is the one that is of most relevance to us, since we compute $\mathscr{I}^+$ in our simulations. Unlike the ADM mass this gives the global mass on asymptotically hyperboloidal slices. It is clear that in general this definition of mass is dependent on the cut of $\mathscr{I}^+$ one takes, i.e. the intersection of $\mathscr{I}^+$ with a space-like surface that extends there. The Bondi-mass is constant for Schwarzschild space-time due to the space-time being static and agrees with the Schwarzschild mass m.

The definitions of the ADM mass and Bondi-mass can be thought of as an application of Noether's theorem on the asymptotic symmetry groups at spatial and null infinity respectively. The theorem states that one gets conserved quantities from symmetries of the system. To further discuss the role of asymptotic symmetries in the definition of mass and to see more clearly how one can justify the decoupling of fields from geometry at null infinity we look at a mathematical quantity coined the "the asymptotic geometry" on null infinity. This is defined by Geroch in [62] as

$$\Gamma^{ab}{}_{cd} := \nabla^a\Theta\nabla^b\Theta\gamma_{cd}, \tag{9.4.1}$$

where Θ is the conformal factor and γ the induced degenerate metric on $\mathscr{I}$. The most important property of this quantity is that it is conformally invariant. Geroch shows that this mathematical quantity only contains information about the geometry on $\mathscr{I}$ and hence "does not tell one anything whatever" about the physical space-time in question. This quantity came about due to the degeneracy of the metric on null infinity. It turns out that looking only at the group of isometries on $\mathscr{I}$ gives too weak a structure. This is because distances along the null generators of $\mathscr{I}$ are of course zero and the ratios between null curves tangent to $\mathscr{I}$ are undefined. This "too weak" structure was still investigated and is called the Newman-Unti group which is infinite dimensional. However if one looks at the diffeomorphisms of $\mathscr{I}$ that leaves (9.4.1) invariant instead of just the induced metric, then one incorporates both the metric structure and the structure along the null generators. The resultant group, also infinite dimensional, is known as the Bondi-Metzner-Sachs (BMS) group. This group now incorporates the entire geometrical structure on null infinity. Penrose termed the extra structure contained in this group as incorporating the "null angles" on $\mathscr{I}$ [98], which is another way of thinking about this extra information that the Newman-Unti group lacks.

The BMS group has many interesting properties. Of particular interest is the subgroup of "supertranslations". These arise from looking at the Lie algebra of the infinitesimal generators ξ^a with

$$\mathcal{L}_{\xi}\Gamma^{ab}{}_{cd} = 0. \tag{9.4.2}$$

The special case of the vector field ξ^a being proportional to $\nabla_a\Theta$ so that $\xi^a = \alpha\nabla^a\Theta$ gives what is known as an infinitesimal supertranslation. The corresponding group of supertranslations form a normal subgroup of the BMS group and is also infinite dimensional. These supertranslations correspond to each generator of $\mathscr{I}$ being pushed along themselves by some amount $a(\theta, \phi)$ and are hence really only functions of the coordinates covering the conformal 2-spheres, i.e. cuts of $\mathscr{I}^+$. If we specialise to the case where the 2-sphere is unit, then $a(\theta, \phi)$ is made up of the spherical harmonics $l = 0$ and $l = 1$ (hence four spin-weighted spherical harmonics) and we get a 4-parameter normal subgroup called the translation group. These are in fact the transformations induced on $\mathscr{I}$ by translations in Minkowski space-time and are hence of physical relevance. Of interest is that Sachs has shown [113] that this is the only 4-dimensional subgroup of the BMS group and the group of supertranslations is the largest proper normal subgroup. Hence these groups have been singled out from their group structure alone.

The final property to discuss is the contrast between the BMS group and the Poincaré group, discussed in detail in ([82, 83, 84, 85]) among others. It just so happens that the factor group of the BMS group with the supertranslations is isomorphic to the conformal group on the 2-sphere. Using that the orthogonal group $O(p+1, q+1)$ is homomorphic to the conformal group $C(p, q)$ we find that this is in fact the orthochronous Lorentz group. However the factor group of the Poincaré group with the translations also gives the orthochronous Lorentz group. This line of thought brings the fact that the BMS group can be written as a semi-direct product of the orthochronous Lorentz group with the supertranslations and the Poincaré group can be written as the semi-direct product of the orthochronous Lorentz group with the translations. Hence the difference between the BMS and Poincaré groups boils down to the difference between supertranslations and translations. One would think

along the lines of "since the translations lie in the supertranslations, perhaps we can obtain the Poincaré group as a subgroup of the BMS group". However, Penrose answers this with the question "what would be meant by a supertranslation-free Lorentz transformation?".

The fact that the BMS group can be written as a semi-direct product of the orthochronous Lorentz group (i.e. the group of conformal transformations on the 2-sphere) and the group of supertranslations has relevance in the next section 9.6 when we define the Bondi-mass. One needs to fix an element of this group, and so one needs to fix a metric conformal to the 2-sphere and a supertranslation. With respect to our simulations, we will have already fixed the metric on $\mathscr{I}$ but it remains to fix the supertranslation. It was shown by Sachs in [112] that the 4-dimensional normal subgroup of translations is *the only* 4-dimensional normal subgroup of the BMS group. This subgroup corresponds to the four space-time translations and is therefore important in formulating energy-momentum conservation laws. Hence when fixing a group element when defining the Bondi-mass, we will always fix a translation. It can be shown that the supertranslations are identified with functions on the space of null generators that transform under a conformal rescaling of the metric with conformal weight +1, and hence define a representation of $SL(2,\mathbb{C})$. This representation has a 4-dimensional invariant subspace which corresponds to the translations. If we had a cut which is the unit 2-sphere, then a translation is a solution to the equation

$$\eth^2 W = 0,$$

the general solution of which is a combination of the first four spherical harmonics ($l = 0, 1$). However in general we will have a 2-sphere only up to a conformal rescaling, in which case the above equation is generalised to the conformally invariant version (defined in appendix A.3).

$$\eth_c^2 W = 0.$$

Hence a solution to this equation fixes a translation (i.e. a supertranslation), and most importantly, one that has physical relevance.

9.5 Spin-frame adapted to $\mathscr{I}^+$

In the previous section we proposed that the Bondi-mass is defined as an integral over cuts of $\mathscr{I}^+$ that are conformally 2-spheres. The question is how can we formulate this setup from the CGG that has already been implemented? We can easily find the locations of $\mathscr{I}^+$ in our simulations by looking at $s =$ constant surfaces and using the explicit formula for the conformal factor to obtain the sphere it resides at on each surface. This will in general be between two spheres in our simulation, however we can use interpolation methods such as barycentric interpolation [8] to accurately find the values of our fields there. However, a problem comes from our gauge choices in implementing the CGG for our evolution; the space-time frame vectors m^a and $\bar{m}^a$ are not tangent to the 2-spheres and hence are not tangent to cuts of $\mathscr{I}^+$. If left like this, it would complicate equations defined on the cuts considerably. Hence we perform a transformation of the spin-frame on $\mathscr{I}^+$ to obtain a new spin-frame $\{O, I\}$ that is adapted to the geometry there.

First we require (denoting $\approx$ to mean evaluated on $\mathscr{I}^+$)

$$-\nabla_{AA'}\Theta \approx A I_A I_{A'}, \tag{9.5.1}$$

i.e. we want the new frame vector $N^a := I^A I^{A'}$ to point along $\mathscr{I}^+$. We can obtain this property by performing a null-rotation around o^A

$$O^A \approx o^A, \qquad I^A \approx \iota^A + \alpha o^A. \tag{9.5.2}$$

Using (9.5.2) in (9.5.1) gives in the space-spinor formalism

$$\frac{1}{2}\varepsilon_{AB}\partial\Theta + \partial_{AB}\Theta \approx -A\Big(-\iota_A o_B - \alpha\, o_A o_B + \bar{\alpha}\, \iota_A \iota_B + \alpha\bar{\alpha}\, o_A \iota_B \Big).$$

Transvecting this with $o^A \iota^B$ gives (denoting $\partial_2 := \iota^A \iota^B \partial_{AB}$ etc.)

$$A \approx -\Big(\frac{1}{2}\partial\Theta + \partial_1\Theta\Big),$$

while transvecting this with $\iota^A \iota^B$ gives

$$\alpha \approx A^{-1}\partial_2\Theta \approx -\frac{2\,\partial_2\Theta}{\partial\Theta + 2\,\partial_1\Theta}.$$

The second condition is that our new frame vectors $M^A := O^A I^{A'}$ and $\bar{M}^A := I^A O^{A'}$ are tangent to the $s =$ constant cuts of $\mathscr{I}^+$. These are of course the kind of cuts we obtain from the CGG. Mathematically this is

$$t^{AA'} O_A I_{A'} = O_A \hat{I}^A = 0. \tag{9.5.3}$$

We achieve this by again performing a null rotation, this time around ι^A like

$$O^A \approx o^A + \beta\big(\iota^A - \frac{2\,\eth_2\Theta}{\eth\Theta + 2\,\eth_1\Theta} o^A\Big), \qquad I^A \approx \iota^A - \frac{2\,\eth_2\Theta}{\eth\Theta + 2\,\eth_1\Theta}, \tag{9.5.4}$$

which keeps the first condition satisfied. Combining (9.5.3) and (9.5.4) gives a single equation which yields (simplified using $\nabla_{AA'}\Theta\nabla^{AA'}\Theta = 0$)

$$\beta \approx -\frac{\eth_0\Theta}{\eth\Theta}.$$

Then after a little simplification, the spin-frame adapted to $\mathscr{I}^+$ is of the form

$$O^A \approx Q\Big(\frac{\eth\Theta + 2\,\eth_1\Theta}{2\,\eth\Theta} o^A - \frac{\eth_0\Theta}{\eth\Theta}\iota^A\Big), \qquad I^A \approx Q^{-1}\Big(\iota^A - \frac{2\,\eth_2\Theta}{\eth\Theta + 2\,\eth_1\Theta} o^A\Big), \tag{9.5.5}$$

where Q is a scale factor that can be chosen freely. It is related to A by

$$A \approx -\Big(\frac{1}{2}\eth\Theta + \eth_1\Theta\Big) Q\bar{Q}. \tag{9.5.6}$$

The choice of Q could potentially simplify equations written in this adapted gauge, however we choose $Q = 1$.

Next we look at the asymptotic Einstein condition. This is a useful equation to investigate properties of null infinity, defined to be

$$\nabla_{A'(A}\nabla_{B)B'}\Theta \approx 0,$$

which is obtained from the trace-free part of the Ricci tensor's conformal transformation law (1.4.9) evaluated on $\mathscr{I}^+$. This gives us useful information about the spin-coefficients (defined in appendix A.3) evaluated in our adapted gauge on $\mathscr{I}^+$ which in turn tell us about the geometry there. Firstly we have that $\kappa' \approx 0$ which confirms that the integral curves of N^a are null-geodesics. We also find $\sigma' \approx 0$ which tells us that $\mathscr{I}^+$ is shear-free. The last useful piece of information is that $\eth A \approx \eth' A \approx 0$, so we can regard A as being constant on

the cuts.

Now that we have our spin-frame, we can compute the spin-coefficients on $\mathscr{I}^+$ in our adapted spin-frame by using their definitions (i.e. $\rho' = -I^A O^B I^{B'} \nabla_{BB'} I_A$). These will be used in the definition of the Bondi-mass. We can also compute the conformal factor R between our space-time 2-sphere and the unit 2-sphere in our adapted frame, which we will denote $\widetilde{R}$. Denoting the unit-sphere quantities with a $\hat{}$ we can write $\hat{m}^a \nabla_a \zeta = 1$, where ζ is the unique function that satisfies $\partial_s \zeta = \partial_\rho \zeta = \delta' \zeta = 0$ and $\delta \zeta = 1$. Then as the frame vectors $\hat{m}^a$ and $M^a = O^A I^{A'}$ differ by a conformal factor, namely $M^a = \widetilde{R}^{-1} \hat{m}^a$ we find that $M^a \nabla_a \zeta = \widetilde{R}^{-1}$. Since we know the left-hand-side as we know how the coordinate derivatives act on ζ and we know M^a in terms of derivatives of the conformal factor, we can compute $\widetilde{R}$. It is found numerically in our simulations for Schwarzschild space-time perturbed by a gravitational wave that we have $R = \widetilde{R}$, so the conformal factor relating the space-time 2-spheres and the unit 2-sphere does not change under our frame transformation.

9.6 Deriving the Bondi-mass

Now we are in a position to derive the Bondi-mass. Penrose and Rindler [100] define this as the integral

$$m_B[W] := -\frac{1}{4\pi} \oint \{\psi_2 - \frac{\sigma N}{A}\} W \mathrm{d}^2\mathcal{S}, \tag{9.6.1}$$

where A is defined by (9.5.6) (during the calculation of the adapted spin-frame), W is a function with conformal weight $+1$ satisfying the conformally invariant equation

$$\eth_c^2 W = R^{-1} \eth (R^{-1} \eth + \tau) W = 0, \tag{9.6.2}$$

(see appendix A.3 for the definition of $\eth_c$), N is the so-called "News function" and the integral is defined over a cut of $\mathscr{I}$. Where did this definition and the functions N and W come from?

The reason why the function W appears in the definition of the Bondi-mass and must satisfy the above equation is so that we fix a physically relevant supertranslation (i.e. a translation), a discussion of which was given in the previous section. When the cut is a unit 2-sphere, the

solutions for W are the first four spherical harmonics ($l = 0, 1$), where the $l = 0$ mode can be thought of as giving the energy, while the $l = 1$ modes give the momentum when used in (9.6.1). These four quantities make up the so-called Bondi-energy momentum 4-vector. The Bondi-mass is then the length of this vector. In our investigations, we only look at the Bondi-energy i.e. the $l = 0$ component.

We now derive (9.6.1) in a way suggested by Penrose and Rindler in [100] and in doing so define and generalise the news function given there. The standard analytic approach found in the literature is to choose a frame on $\mathscr{I}^+$ so that it becomes divergence free, i.e. $\rho' = 0$. The situation is simplified further by choosing the conformal factor so that $\Theta =$ constant hypersurfaces in the neighbourhood of $\mathscr{I}^+$ are null. This gives also that $\tau' = 0$. Finally the conformal factor for the 2-sphere is chosen so that the cuts of $\mathscr{I}^+$ are unit spheres so that $\tau = 0$. However in our case we have already chosen the spin-frame and it cannot be specialised anymore than choosing the free function Q. We have also specified a conformal factor Θ and hence cannot change this either. Our conformal factor R for the 2-spheres is also fixed. Hence we need to generalise Penrose and Rindler's formula.

Given a cut on $\mathscr{I}^+$ there exists a null-hypersurface intersecting it. On this hypersurface we define 2-surfaces S_Θ by $\Theta =$ constant and consider the integral of the Gaussian curvature of these surfaces with W a solution of (9.6.2) as

$$I(\Theta) := \oint_{S_\Theta} \left(\Psi_2 - \sigma\sigma'\right) W \mathrm{d}^2\mathcal{S}_\Theta,$$

noting that Ψ_2 is the *physical* Weyl spinor component. This is similar to the definition of total charge in Maxwell theory. One takes a similar integral except with a component of the Faraday tensor instead of the Weyl and without the $\sigma\sigma'$ term. This is merely a generalisation to general relativity which carries the additional term $\sigma\sigma'$ that vanishes when there is no gravitational radiation. It is this non-linear term that contributes to the mass loss as will be seen later on.

One sees that this integral vanishes on $\mathscr{I}^+$ due to $\Psi_{ABCD} \approx 0$ and the fact that $\mathscr{I}^+$ is shear-free. However it is the rate at which this approaches $\mathscr{I}^+$ that defines the energy-momentum.

We thus define

$$m_B[W] := -\frac{\mathrm{d}I}{\mathrm{d}\Theta}(0) = -\frac{\text{þ}I}{\text{þ}\Theta}(0) = \frac{\text{þ}I}{A}(0).$$

To compute this we need the behaviour of Ψ_2 and σ' as they approach $\mathscr{I}^+$. The relevant spin-coefficient equation for σ' is

$$N := \text{þ}\sigma' = R^{-1}\eth'\tau' + \rho\sigma' + \bar{\sigma}\rho' - \tau'^2 - \kappa'\bar{\kappa} - \Phi_{20} \approx R^{-1}\eth'\tau' + \bar{\sigma}\rho' - \tau'^2 - \Phi_{20}, \qquad (9.6.3)$$

where $\Phi_{ABA'B'}$ is the conformal Ricci spinor. This gives us our definition of the news while the equation for Ψ_2 can be easily found as

$$\text{þ}\Psi_2 = \text{þ}(\Theta\psi_2) = \Theta\text{þ}\psi_2 + \psi_2\text{þ}\Theta \approx -A\psi_2.$$

Hence

$$\text{þ}I \approx \oint_{S_0} \Big(- A\psi_2 + \sigma N\Big) W\mathrm{d}^2\mathcal{S}_0,$$

and thus we have arrived at (9.6.1) with the definition of the news being given by (9.6.3) and as A is constant on the cuts it has been pulled inside the integral. One can see how much simpler the equations become when employing the simplifications mentioned earlier. We in fact are left with the simple expression for the news as $N = -\Phi_{20}$.

The final step is how to compute W at each cut of $\mathscr{I}^+$ in order to obtain the Bondi-energy. The equation (9.6.2) is conformally invariant which means that solutions on different conformal spheres differ by a conformal rescaling of weight $+1$. Suppose we wanted to solve the equation on a cut with intrinsic metric γ_{ab} which is related to the metric for the unit 2-sphere like $\hat{\gamma}_{ab} = \Omega^2\gamma_{ab}$. Then (recalling $\hat{}$ denotes quantities on the unit sphere) $\hat{\partial} = \Omega^{-1}\partial$ and $\hat{W} = \Omega W$. The simplest choice for $\hat{W}$ is $\hat{W} = 1$ which therefore gives $W = \Omega^{-1} = R$. Since we know R as it is a system variable, we know W on each cut of $\mathscr{I}$. Even though we need not do more, it is useful to note other ways to obtain W by means of equations for the conformal factor Ω. The equation relating the divergences $\hat{\rho}'$ and ρ' is given by

$$\hat{\rho}' = \rho' - \Omega^{-1}D'\Omega.$$

This can be used as an equation for Ω along the null generators by choosing $\hat{\rho}' = 0$ so that we maintain the same sphere along $\mathscr{I}$. We note that we can use the unphysical time s as a

parameter along the null generators which is then used to replace D'. Using an over-dot to denote $\frac{\mathrm{d}}{\mathrm{d}s}$, we find

$$D'\Omega(s) = \dot{\Omega} D's.$$

Defining

$$U := D's = O^A O^{A'} \nabla_{AA'} s,$$

which is known as we know the adapted spin-frame in terms of derivatives of the conformal factor Θ, we find the equation

$$\dot{\Omega} = U^{-1} \rho' \Omega.$$

Choosing our initial data to be $\Omega = R^{-1}$ so we start with the unit-sphere, we obtain Ω and hence W along $\mathscr{I}^+$ numerically using a simpler Euler step. This has been done and it is found that $\Omega = R^{-1}$ along $\mathscr{I}^+$ as expected.

One could also look at the conformal transformation law of τ, which appears in the equation for W. It is given by

$$\hat{\tau} = \Omega^{-1}(\tau - \Omega^{-1} R^{-1} \eth \Omega),$$

where $\hat{\tau}$ vanishes on the unit 2-sphere. Hence one finds the equation

$$\eth \Omega = \Omega R \tau,$$

on each cut of $\mathscr{I}^+$. One could solve this on each cut by "inverting" the $\eth$ operator by reversing the action of the $\eth$-operator on the spin-weighted spherical harmonics ${}_sY_{lm}$ using (2.3.4), and using that τ has spin-weight $+1$ there is just the ${}_0Y_{00}$ mode that needs to be fixed by initial data. Again using $\Omega = R^{-1}$ as initial data one could use this method also. This has also been shown to agree with R on each cut.

Thus our integral for the Bondi-energy becomes

$$m_B[R] = -\frac{1}{4\pi} \int_0^{2\pi} \int_0^{\pi} \left(\psi_2 - \frac{\sigma N}{A} \right) R^3 \mathrm{d}\theta \mathrm{d}\phi = -a_{00} Y_{00}, \tag{9.6.4}$$

where we have expanded the integrand in the (spin-weight zero) spherical harmonic basis and used that the surface area of the unit 2-sphere is 4π. All the $l \neq 0$ modes do not contribute as they are functions of θ and ϕ which vanish when integrated.

Thus we finally have a way to compute the Bondi-energy on null infinity from our simulation data. We use our explicit formula for the conformal factor and barycentric interpolation to locate $\mathscr{I}^+$. Using the explicit formula for the conformal factor we can compute the $\mathscr{I}$-adapted spin-frame so that the corresponding null-vectors M^a and $\bar{M}^a$ are tangent to $s =$ constant cuts of null infinity and we can compute A using (9.5.6). At these points we can compute the spin-coefficients in the adapted spin-frame and hence compute the news (9.6.3). We can compute the conformal Ricci spinor component Φ_{20} by using the definition of the Schouten tensor (1.4.2) to compute R_{ab} in terms of P_{ab} and then using the Schouten tensor's conformal transformation law between the conformal and Weyl connections (1.4.7) to write P_{ab} in terms of $\widehat{P}_{ab}$ and the 1-form f_a which we compute in our simulations. The fields ψ_2 and R are system variables and hence also known. We then use (9.6.4) to evaluate the integral.

9.7 Deriving the Bondi-time

Now that we know how to compute the Bondi-energy, we need to look at what kind of time coordinate it should be plotted with respect to. Currently we have the unphysical time s which is the parameter of the conformal geodesics. Is there a way to transform this into proper time so that we can get a physical interpretation of the Bondi-energy over time?

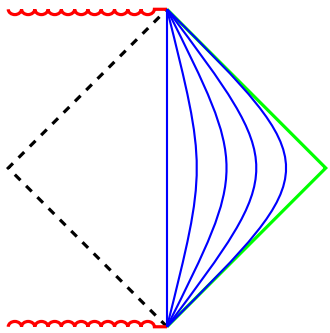

Figure 9.9: The right-hand-side of the conformal diagram for Schwarzschild space-time. The blue lines represent spatially-constant observers through different spatial points emanating from past time-like infinity and ending at future time-like infinity. The green line represents the limit of these as one goes to the conformal boundary.

Figure 9.9 shows the paths that spatially-constant physical observers follow in the Schwarzschild space-time for larger and larger r. As r increases they become closer and closer to the conformal boundary. In the limit as $r \to \infty$ one gets a notion of a proper time on null infinity described by its parameter, called Bondi-time. This is defined in Penrose and Rindler [100] as the solution to

$$\text{Þ}_c'^2 u = 0.$$

Due to being written in terms of the conformally invariant operator $\text{Þ}_c'$, this equation is manifestly conformally invariant. So the Bondi parameter is independent of the conformal factor, as well as the scale factor A. When written in terms of $\text{Þ}'$ and then D' one finds

$$\Big(\text{Þ}' - 2\rho'\Big)\text{Þ}' u = \Big(D' - \varepsilon' - \bar{\varepsilon}' - 2\rho'\Big) D' u = 0.$$

The solution u is clearly of an exponential nature, and it will inherently have the property that $u \to \infty$ as it approaches i^+. So how do we solve this equation? First we should point out that the spin-coefficient ε' *is not* spin-weighted. However the real part $\varepsilon' + \bar{\varepsilon}'$ *is*, with spin-weight 0 and so this equation makes sense from the spin-weight point of view. Then expanding $D' = U\frac{\mathrm{d}}{\mathrm{d}s}$ we get the second-order ODE

$$\ddot{u} = U^{-1}\Big(\varepsilon' + \bar{\varepsilon}' + 2\,\rho' - \dot{U}\Big)\dot{u}, \tag{9.7.1}$$

for u. This can be solved using a simple second-order leapfrog method. Interpolation could again be used to obtain more points on $\mathscr{I}^+$ for this method, or one can just use the points available depending on the resolution.

9.8 The Bondi-energy of perturbed Schwarzschild

Now that we have explained the Bondi-mass and where it comes from, what behaviour does it exhibit in our perturbations of Schwarzschild space-time? What we should expect is the following: When the gravitational wave approaches the black hole, it is influencing the system in a non-linear way. Moreover it should be influencing the system in such a way that energy leaves the system via backscattering (see Figure 9.10). That is, we should see non-zero ψ_4 modes that take energy away from the system. The backscattering effect of the gravitational wave should increase as the energy of the wave increases.

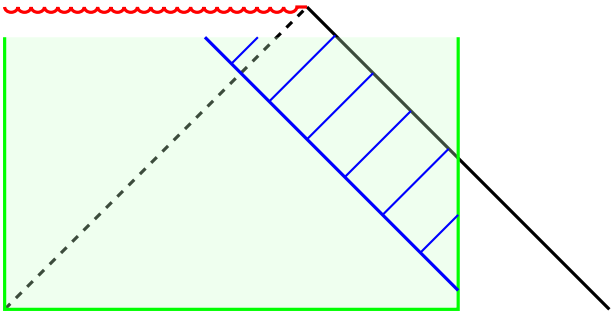

Figure 9.10: Backscattering of a gravitational wave ψ_0 (thick blue line) as seen by a non-zero ψ_4 (thin blue lines) in our computational domain bounded by the green lines.

We run simulations which pumps into Schwarzschild space-time a gravitational wave with amplitude $a = 0.5$ as described in section 9.2 but also where the amplitude is 0.1, 0.25 and 1. Together these simulations will be able to give us information about how properties of the system change when the energy being introduced varies.

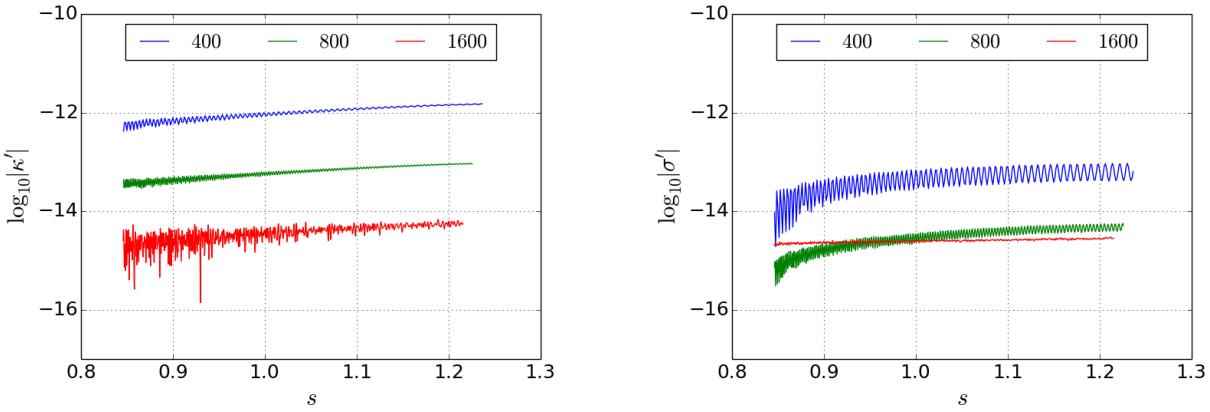

(a) κ' (b) σ'

Figure 9.11: The spin-coefficients κ' and σ' plotted for different ρ-resolutions on $\mathscr{I}^+$ with respect to the unphysical time s.

First we check that $\mathscr{I}^+$ is indeed a shear-free null hypersurface. This is verified in Figure 9.11 where we show the convergence of the spin-coefficients κ' and σ' to zero. It is good to see that we can in fact represent both of these functions as zero up to machine precision with

not too large a resolution.

Looking now at the Bondi-energy in Figure 9.12 we see that the case where no wave is pumped in agrees with the Schwarzschild mass m of 0.5. We also notice that as the amplitude increases, so does the energy at each point of $\mathscr{I}^+$. This is due to the fact that we are pumping in more and more energy into the system, and so the space-time deviates from Schwarzschild space-time and with the increased energy it is expected to have a larger Bondi-energy. However as we pump in this energy through the boundary, we never actually see the increase from the base energy of 0.5 as we would need information outside our computational domain. We also note that *the Bondi-energy decreases along $\mathscr{I}^+$ for the cases where a wave was present*. This reproduces the famous Bondi-Sachs mass loss which says that the Bondi-mass along $\mathscr{I}^+$ should decrease in the direction of future time-like infinity.

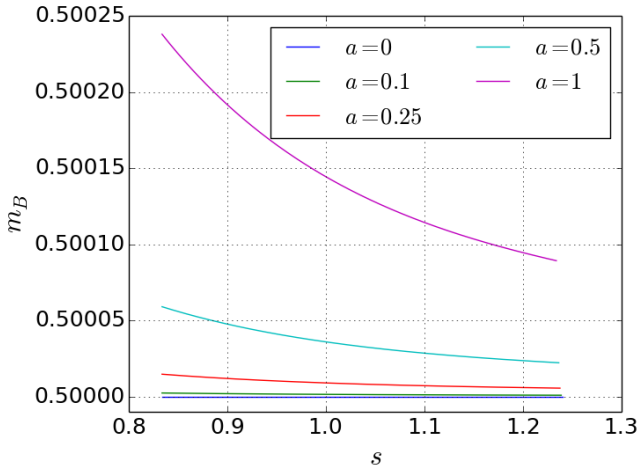

Figure 9.12: The Bondi-energy of Schwarzschild space-time perturbed with gravitational waves of amplitude a.

Another way of looking at the energy loss is given in Figure 9.13 which looks at the relative difference. It clearly shows that as the amplitude of the gravitational wave increases, so does the rate of decay of the Bondi-energy. This makes sense as when the wave is approaching the black hole it is influencing the system and in particular is influencing the component

ψ_4 which represents the back-scattered radiation that takes energy away from the system. When the wave is larger, this influence will be greater and hence it follows that more radiation will be backscattered.

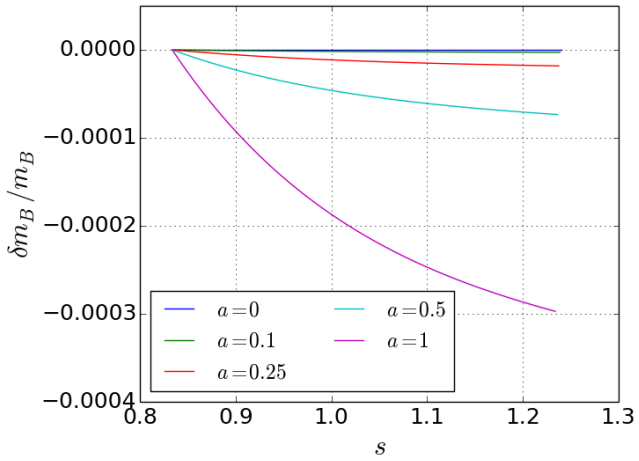

Figure 9.13: The relative difference of the Bondi-energy of Schwarzschild space-time perturbed with gravitational waves of amplitude a.

Also of interest is what the gravitational wave profile on the boundary looks like in terms of proper time. Because we introduce the gravitational wave with respect to the unphysical time s, it may appear distorted with respect to the proper time. Since we are in axial-symmetry, computing proper time could be quite hard. However, the CGG provides us the simplifications of $g_{00} = 1$ and the spatial coordinates being constant along the conformal geodesics, in particular along the boundary where we pump the wave in. Then the proper time τ is given as the solution to the equation

$$\mathrm{d}\tau^2 = \widetilde{g}_{00}\mathrm{d}s^2 = \Theta^{-2}\mathrm{d}s^2 \Rightarrow \frac{\mathrm{d}\tau}{\mathrm{d}s} = \Theta^{-1}.$$

We of course know Θ explicitly (recall (8.1.3)) which then gives the proper time as

$$\tau = \frac{(\rho + \frac{m}{2})^3}{\rho - \frac{m}{2}} \tanh^{-1}\left[\frac{s}{\rho}\left(\rho^2 - \left(\frac{m}{2}\right)^2\right)\right],$$

which on the right boundary $\rho = 1.25$ and recalling $m = 0.5$ is simply

$$\tau = \frac{27}{10}\tanh^{-1}\left(\frac{6s}{5}\right).$$

We reach $\mathscr{I}^+$ on the right boundary at $s = \frac{5}{6}$ which is exactly when $\tau = \infty$. Proper time plotted alongside the unphysical time is larger, as shown in Figure 9.14, and hence the area of the wave will be larger with respect to the proper time and the wave will look slightly sheared due to the behaviour of $\tanh^{-1}$.

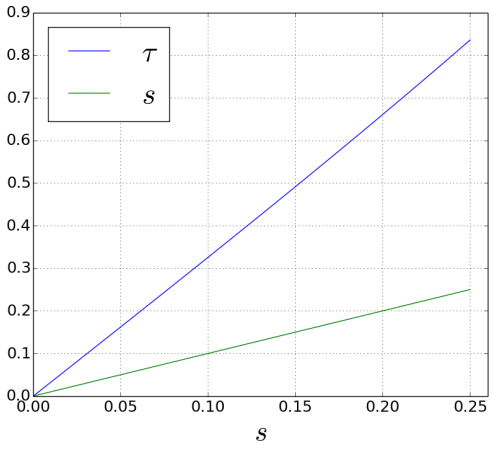

Figure 9.14: Proper time τ plotted with respect to the unphysical time s along the conformal geodesic given by $\rho = 1.25$.

9.9 The Bondi-time of perturbed Schwarzschild

The solution to the Bondi-time equation (9.7.1) is obtained in a straightforward manner using a simple staggered leap frog algorithm with initial conditions $u(0) = 0,\ \dot{u}(0) = 1$. The solution is also dependent upon the initial point on the cut of $\mathscr{I}^+$ one takes. However due to the conformal factor Θ being θ-independent, the null generators of $\mathscr{I}^+$ are also θ-independent. Thus we do not need to worry about the spherical direction in this equation. The nature of this equation is that we expect some kind of exponential-like solution, as one can easily write

$$u(s) = k_1 \int e^{\int U^{-1}\left(\varepsilon' + \bar{\varepsilon}' + 2\,\rho' - \dot{U}\right)} + k_2,$$

where the integral is along the null-generators parametrised by s and k_1, k_2 denote integration constants. The behaviour of the function

$$U^{-1}\left(\varepsilon' + \bar{\varepsilon}' + 2\,\rho' - \dot{U}\right)$$

determines what this exponential will look like. It obviously has the property that it goes to infinity as we move along $\mathscr{I}^+$ toward i^+, but this function will determine the rate at which it does so. If this function passes through zero at some stage then we would find that $u =$ constant there. However for all our simulations we find that this function is always positive and closely approximates a line.

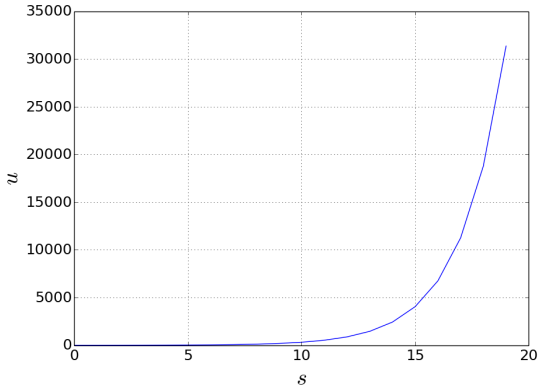

Figure 9.15: Bondi-time u for Schwarzschild space-time perturbed with a gravitational wave of amplitude 1 plotted with respect to the unphysical time s along part of $\mathscr{I}^+$.

Figure 9.15 shows the straightforward exponential-like curve that is the Bondi-time for the gravitationally perturbed Schwarzschild space-time. One notices that this becomes very large very fast. Hence the affect of plotting the Bondi-energy with respect to the Bondi-time is that it is substantially stretched out.

9.10 Characteristic ringing

Linear perturbations of the Schwarzschild space-time have been extensively studied analytically (see for example [23, 69] and references therein). For these perturbations (of the metric) one ends up with a single master wave equation for the perturbations involving a potential. This equation predicts a period of characteristic ringing of the outgoing gravitational radiation ψ_4, which is the result of the excited black hole space-time exhibiting quasi-normal modes. This ringing is found to be followed by a polynomial decay, i.e. a tail.

It is apparent that we do not see this ringing in our expression for the Bondi-energy, nor do we find this in the ψ_4 component or the news with respect to the adapted frame. The approach of perturbing the metric is completely different to how we perturb the space-time through boundary conditions, and this should be kept in mind. We list a few plausible reasons why we do not see the characteristic ringing feature:

- We do not compute a large enough portion of null infinity to see the ringing.
- We do not have a fine enough resolution to reproduce the ringing.
- Our gravitational wave is too small to excite a large enough ringing that can be seen with our current resolutions.

The first thing to mention is that we have confirmed that we really can read off signals on $\mathscr{I}^+$ in our adapted spin-frame. Without going into the details, the idea was to move the left boundary outside the event horizon and impose unphysical reflective boundary conditions. Then shoot in a wave from the right boundary (the ψ_0) as above, and let it reflect off the left boundary. The resulting reflected wave (the ψ_4) is then read off on null infinity. We see that indeed we get a wave profile for ψ_4 along $\mathscr{I}^+$ which is also reflected as a bump in the decay rate of the Bondi-energy. This confirms that our method of reading off data on $\mathscr{I}^+$ is sound.

Due to the evolution equations for the components of ψ_{ABCD} becoming unstable during the evolutions we have done in this chapter, we lose out on covering more of null infinity. It could be that we have not covered enough for the scattering of the gravitational wave on the event horizon to propagate out to null infinity.

The last two points require an increase in resolution. Firstly, a lack of resolution and the fact that we are evolving our fields with respect to an unphysical time means that a small time-step may be extremely large with respect to the physical time. This could mean that we completely miss the characteristic ringing altogether. Secondly, we may not be introducing enough energy for the ringing to be resolved at our current resolutions. The ringing comes from the back-scattered radiation ψ_4, which is very small compared to the ingoing wave packet ψ_0. We have run simulations with the larger amplitude $a = 10$, however still no

ringing. We attempted to use higher amplitudes, however the lack of resolution meant that this was not possible.

Conclusions

In this work the generalised conformal field equations were derived in the space-spinor formalism. Subsequently the manifold topology was restricted to be of the form $M_2 \times \mathbb{S}^2$ so that the $\eth$-operators could be utilised. This was accomplished by first using Cartan's structure equations to obtain equations that were then used to replace the connection coefficients γ_{01}, γ_{11} and γ_{21} appearing elsewhere in the GCFE system with other quantities, in particular with the quantity a that is a manifestation of the un-spin-weighted connection coefficients on the unit 2-sphere. The δ and δ' derivatives were replaced with $\eth$ and $\eth'$ plus a-terms dependent on the acted-on function's spin-weight using (2.3.2). Together these two replacements allowed for the cancellation of the a-terms from the entire system and gave us a system of equations that is properly spin-weighted. The resulting system was checked for correctness by an analytic comparison to an exact solution as well as a range of numerical tests.

An analysis of the field equation for the gravitational spinor ψ_{ABCD} was carried out and we confirmed our equations were symmetric hyperbolic. Moreover, we performed a change of basis that separated out the propagating modes which we then used to impose maximally dissipative boundary conditions. The change of basis was reversed and we found the corresponding boundary conditions in terms of the system variables, which later proved to be numerically stable. The issue of constraint violating modes from the subsidiary system propagating in from the boundary and destroying convergence was addressed by proposing a boundary treatment that made use of the fact that at any time there is always one more ingoing mode in the spin-2 system than in the subsidiary system. This allows one to choose the ingoing gravitational wave freely, while fixing the choice of the remaining boundary data to kill the ingoing modes of the subsidiary system. This was shown to work with only one

ingoing constraint violating mode for the case of gravitational perturbations of Minkowski space-time in $2+1$ dimensions and later it was proven to work for the extremal case of all three constraint violating modes propagating into the computational domain for the case of gravitational perturbations of Schwarzschild space-time also in $2+1$ dimensions. Thus, we have successfully developed a procedure for setting up an IBVP for the GCFE with topology $M_2 \times \mathbb{S}^2$ where the boundaries are given by conformal geodesics, which is (at least numerically) well-posed in the sense that constraints propagate.

We discussed the global structure of space-times of constant curvature and black hole space-times. The system was shown to numerically reproduce the global structure of Schwarzschild space-time in a gauge proposed by Friedrich [52] that is regular up to and for some time beyond the conformal boundary. The computational domain was chosen so that it incorporated conformal geodesics that ended up reaching the singularity and those that ended up passing through $\mathscr{I}^+$. These were separated by the single conformal geodesic that passes through i^+. This is the first numerical simulation in the world to incorporate the singularity, future time-like infinity and future null infinity in the same computational domain. This gauge was then adapted to the Schwarzschild-de Sitter and Schwarzschild-Anti-de Sitter space-times from which we could reproduce their global structure. For Schwarzschild-de Sitter space-time we were also able to include in the computational domain the singularity, future time-like infinity and future null infinity.

For a rigorous use of our $2+1$ code we investigated gravitational perturbations of the Schwarzschild space-time. The gravitational wave was introduced by imposing an appropriate boundary condition for ψ_0 while using our boundary treatment to fix the remaining degrees of freedom on the boundary and retain constraint propagation. We evolved the system up to and beyond $\mathscr{I}^+$ and covered a significant amount before the simulation crashed due to the $s =$ constant surfaces becoming null from the bending of the conformal geodesics in the neighbourhood of the right boundary. We noticed that our spin-frame chosen for stable evolution in the CGG was not suitable for reading off information on $\mathscr{I}^+$, and so we performed a frame transformation to a new frame that is adapted to the geometry there. Using

this adapted spin-frame we were able to read off the necessary spin-coefficients and fields needed to compute the Bondi-mass and Bondi-time. However the standard equations for these given in Penrose and Rindler [100] made use of additional simplifying assumptions that we could not employ. We generalised these equations to our case and subsequently solved them. We found that the Bondi-energy agrees with the Schwarzschild mass in the unperturbed case, and for the cases with a wave pumped in we found the initial Bondi-energy increased when the area of the wave was increased. Subsequently the Bondi-energy was found to decay along $\mathscr{I}^+$ in agreement with the Bondi-Sachs mass loss. The Bondi-time was found to be an exponential-like function of the unphysical time (i.e. the parameter of the conformal geodesics) which goes to infinity at i^+.

The fact that we now have a boundary procedure that gives rise to a very general IBVP for the GCFE which propagates constraints gives us the ability to investigate a huge range of problems that involve the global structure and global properties of space-times.

Future work

The problem of the $s =$ constant surfaces becoming null is something that should be investigated first. When this happens the determinant of the A^0 matrix from the spin-2 zero rest-mass system vanishes and hence the A^0 matrix becomes non-invertible, which subsequently crashes the simulation. The problem could be solved by choosing different initial conditions for f_a which is essentially the acceleration of the conformal geodesics. One would try and accelerate the conformal geodesics in the neighbourhood of the right boundary in hopes of retaining space-like timeslices for longer. The initial data for Θ, f_a and h_a are tied together via (1.6.3), and so when changing the initial value for the 1-forms one should be aware that the conformal boundary will be in a different location via the initial data $\underline{H}$ appearing in the explicit expression for the conformal factor. Also, obtaining a different initial value for f_a is a result of choosing different initial data for Θ and/or h_a, and so the resulting conformal geodesics will in general be different.

COFFEE, the Python package that is used to numerically solve the GCFE system needs to be further developed in order to perform higher resolution runs. This involves implementing parallelisation that is compatible with our boundary treatment. A computer cluster would then be utilised to dramatically decrease computation time. It was found in [42] that we could run simulations that took around two days to complete in under two hours on such a cluster. Hence this is certainly a step we need to take.

Once the accuracy of the code is increased we can attempt to reproduce the characteristic ringing behaviour of the Schwarzschild space-time under gravitational perturbations. The increased resolution would allow us to obtain a finer grid on null infinity to potentially re-

solve this ringing. It would also allow us to increase the amplitude of the gravitational wave that is pumped in without having to make the wavelength larger, so that the back-scattering would be larger and the characteristic ringing would be more obvious.

Perhaps the most obvious next step to take is to generalise to the Kerr space-time. As it is still not clear whether this space-time is stable under general perturbations, we could investigate this question from a global perspective. Investigating this problem does not require any fundamental changes to the setup for the Schwarzschild space-time, only a new initial data set is needed. To show stability we would need to investigate whether the final state of the space-time is again that of a Kerr black hole.

There is also the possibility of investigating the conditions required on an asymptotically flat time symmetric initial data set so that the resulting vacuum solution has a regular null infinity. Friedrich [55] has restricted the problem to how initial data is chosen on the blowup of the point i^0 to a 2-sphere. He has conjectured that the necessary condition for a regular null infinity is that the initial data near null infinity are those induced by asymptotically conformally stationary space-times. This still remains as just a conjecture and hence it would be intriguing to probe this question numerically by evolving sets of initial data that do and do not satisfy the necessary conditions of the conjecture.

Another open problem that would be within the scope of our methods is that of the stability of Anti-de Sitter space-time. First brought to attention by Bizoń and Rostworowski in 2012 [16], they found that the space-time is non-linearly unstable under a particular class of perturbations. Since then time-stable periodic solutions have been discovered [6, 65, 78] which hint that there are "islands of instability in the sea of perturbations". Friedrich has shown that in Anti-de Sitter space-time the evolution system for ψ_{ABCD} can be written in such a way that the subsidiary system is entirely made up of ODEs [48], so setting up a stable IBVP for probing this question should be possible. Moreover our system allows us to introduce a completely general gravitational wave, whereas currently only perturbations with symmetries have been investigated. The main issue to address will be the fact that we

only cover a finite amount of a conformal geodesic for an infinite range of its parameter. We must perform some sort of reparametrisation to "reset" the parameter and continue the evolution.

Appendices

Appendix A

Conventions, definitions and useful equations

A.1 Conventions

Following the conventions of Penrose and Rindler [99, 100], we list the geometric quantities defined by a torsion-free Weyl connection and give the transformation laws under a change of connection that respects the conformal structure.

We work with **signature** $(+,-,-,-)$.

We use **Latin letters for abstract indices** and **bold Latin letters for component indices**.

We define the curvature quantities as follows:
The **Riemann tensor**

$$(\nabla_a \nabla_b - \nabla_b \nabla_a)\alpha_c = -R_{abc}{}^{d}\alpha_d. \tag{A.1.1}$$

The **Ricci tensor**

$$R_{ab} := R_{acb}{}^{c}. \tag{A.1.2}$$

The **Ricci scalar**

$$R := R^{a}{}_{a}. \tag{A.1.3}$$

The **Schouten tensor**

$$P_{ab} := -\frac{1}{4}R_{[ab]} - \frac{1}{2}\Big(R_{(ab)} - \frac{1}{6}Rg_{ab}\Big). \tag{A.1.4}$$

The **connection coefficients**

$$\Gamma_{\mathbf{ab}}{}^{\mathbf{c}} := \delta^{\mathbf{c}}{}_{b}\delta_{\mathbf{a}}{}^{a}\nabla_{a}\delta_{\mathbf{b}}{}^{b}. \tag{A.1.5}$$

We use the definitions of Penrose and Rindler [99] for spinors. In particular, we denote the spin-frame as $\{o, \iota\}$ which is normalised so that $o_A\iota^A = 1$ (equivalently $o_{A'}\iota^{A'} = 1$). The spin-frame defines the null tetrad

$$l^a = o^A o^{A'} \qquad [= o^A \iota^B], \tag{A.1.6a}$$

$$n^a = \iota^A \iota^{A'} \qquad [= -o^A o^B], \tag{A.1.6b}$$

$$m^a = o^A \iota^{A'} \qquad [= -o^A o^B], \tag{A.1.6c}$$

$$\bar{m}^a = \iota^A o^{A'} \qquad [= \iota^A \iota^B]. \tag{A.1.6d}$$

where brackets indicate the conversion to space-spinors. The relationships between the spin-frame, null tetrad and an orthonormal frame $e^a_{\mathbf{i}}$ are given by

$$e^a_{\mathbf{0}} = \frac{1}{\sqrt{2}}(o^A o^{A'} + \iota^A \iota^{A'}) \qquad \Big[= \frac{1}{\sqrt{2}}(o^A \iota^B - \iota^A o^B)\Big], \tag{A.1.7a}$$

$$e^a_{\mathbf{1}} = \frac{1}{\sqrt{2}}(o^A o^{A'} - \iota^A \iota^{A'}) \qquad \Big[= \frac{1}{\sqrt{2}}(o^A \iota^B + \iota^A o^B)\Big], \tag{A.1.7b}$$

$$e^a_{\mathbf{2}} = \frac{1}{\sqrt{2}}(o^A \iota^{A'} + \iota^A o^{A'}) \qquad \Big[= -\frac{1}{\sqrt{2}}(o^A o^B - \iota^A \iota^B)\Big], \tag{A.1.7c}$$

$$e^a_{\mathbf{3}} = \frac{i}{\sqrt{2}}(o^A \iota^{A'} - \iota^A o^{A'}) \qquad \Big[= -\frac{i}{\sqrt{2}}(o^A o^B + \iota^A \iota^B)\Big]. \tag{A.1.7d}$$

These relationships fix the Infeld-van der Waerden symbols to be (up to a factor) the Pauli spin-matrices and the unit matrix.

Contractions of space-spinor quantities with the spin-frame are written as

$$\alpha_0 := \alpha_A o^A, \qquad \alpha_1 := \alpha_A \iota^A. \tag{A.1.8}$$

If a spinor is symmetric in a certain number of indices, then we label their components as the number of contractions with ι^A. As an example, suppose we had $\chi_{AB} = \chi_{(AB)}$ and

$P_{ABCD} = P_{(AB)CD}$. Then some components would be labelled

$$\chi_0 := \chi_{AB} o^A o^B, \qquad \chi_1 := \chi_{AB} o^A \iota^B = \chi_{AB} \iota^A o^B, \qquad P_{201} := P_{ABCD} \iota^A \iota^B o^C \iota^D. \tag{A.1.9}$$

A.2 Transformation laws

Given two torsion-free Weyl connections ∇ and $\widehat{\nabla}$ for the conformal structure defined by a metric g_{ab}, we let

$$\widehat{\nabla}_a g_{bc} - \nabla_a g_{bc} = -2 f_a g_{bc} \tag{A.2.1}$$

be the difference derivation acting on the metric. The **action of the difference derivation on vectors and covectors** is given by

$$\widehat{\nabla}_a v_b - \nabla_a v_b = -f_{ab}{}^c v_c, \tag{A.2.2}$$

$$\widehat{\nabla}_a v^b - \nabla_a v^b = f_{ac}{}^b v^c, \tag{A.2.3}$$

where

$$f_{ab}{}^c := \delta^c{}_a f_b + \delta^c{}_b f_a - g_{ab} g^{cd} f_d. \tag{A.2.4}$$

Using these definitions, the **transformation laws of the curvature quantities** are as follows:

$$\hat{R}_{abc}{}^d - R_{abc}{}^d = 2\Big(\nabla_{[a} f_{b]c}{}^d - f_{[a|c|}{}^e f_{b]e}{}^d\Big), \tag{A.2.5}$$

$$\hat{R}_{ab} - R_{ab} = 3\nabla_a f_b - \nabla_b f_a - 2 f_a f_b + g_{ab}(\nabla^c f_b + 2 f_c f^c), \tag{A.2.6}$$

$$\hat{R} - R = 6(\nabla^a f_a + f_a f^a), \tag{A.2.7}$$

$$\hat{P}_{ab} - P_{ab} = -\nabla_a f_b + f_a f_b - \frac{1}{2} g_{ab} f_c f^c, \tag{A.2.8}$$

$$\hat{C}_{abc}{}^d = C_{abc}{}^d. \tag{A.2.9}$$

It is also useful to note that the Riemann tensor can be decomposed like

$$R_{abc}{}^d = 2\Big(\delta^d{}_{[a} P_{b]c} - \delta^d{}_c P_{[ab]} - g_{c[a} P_{b]}{}^d\Big) + C_{abc}{}^d. \tag{A.2.10}$$

A.3 Spin-coefficients and the $\eth$ and þ operators

We show some definitions from the point of view of Penrose and Rindler [99]. Under a rescaling of the spin-frame $\{o, \iota\}$ like

$$o_A \mapsto \lambda o_A, \quad \iota_A \mapsto \lambda^{-1}\iota_A, \quad o^A \mapsto \lambda o^A, \quad \iota^A \mapsto \lambda^{-1}\iota^A, \tag{A.3.1}$$

a function η that transforms as

$$\eta \mapsto \lambda^p \bar{\lambda}^q \eta, \tag{A.3.2}$$

is said to have spin-weight $\frac{1}{2}(p-q)$ and boost-weight $\frac{1}{2}(p+q)$. In analogy to functions with spin-weight having the derivative operators $\eth$ and $\eth'$ that preserve this property, functions with boost-weight have the associated derivative operators þ and $\text{þ}'$ which preserve boost-weight. The definitions given in Penrose and Rindler [99] in terms of the so-called "spin-coefficients"

$$\begin{aligned}
&\kappa := o^A D o_A, \quad &&\varepsilon := \iota^A D o_A, \quad &&\gamma' := -o^A D \iota_A, \quad &&\tau' := -\iota^A D \iota_A, \\
&\rho := o^A \delta' o_A, \quad &&\alpha := \iota^A \delta' o_A, \quad &&\beta' := -o^A \delta' \iota_A, \quad &&\sigma' := -\iota^A \delta' \iota_A, \\
&\sigma := o^A \delta o_A, \quad &&\beta := \iota^A \delta o_A, \quad &&\alpha' := -o^A \delta \iota_A, \quad &&\rho' := -\iota^A \delta \iota_A, \\
&\tau := o^A D' o_A, \quad &&\gamma := \iota^A D' o_A, \quad &&\varepsilon' := -o^A D' \iota_A, \quad &&\kappa' := -\iota^A D' \iota_A,
\end{aligned} \tag{A.3.3}$$

are

$$\begin{aligned}
&\text{þ}\eta := (D + p\gamma' + q\bar{\gamma}')\eta, \quad &&\text{þ}'\eta := (D' - p\gamma - q\bar{\gamma})\eta, \\
&\eth\eta := (\delta - p\beta + q\bar{\beta}')\eta, \quad &&\eth'\eta := (\delta' + p\beta' - q\bar{\beta})\eta,
\end{aligned} \tag{A.3.4}$$

where

$$D := l^a \nabla_a, \qquad D' := n^a \nabla_a, \qquad \delta := m^a \nabla_a, \qquad \delta' := \bar{m}^a \nabla_a.$$

Now suppose we had a rescaling of the spin-frame like

$$o_A \mapsto \Theta^{w_0+1} o_A, \quad \iota_A \mapsto \Theta^{w_1+1} \iota_A, \quad o^A \mapsto \Theta^{w_0} o^A, \quad \iota^A \mapsto \Theta^{w_1} \iota^A, \tag{A.3.5}$$

and we have a function η that transforms like (A.3.2) under the transformation (A.3.1) and transforms like

$$\eta \mapsto \Theta^{w}\eta,$$

under the transformation(A.3.5). Then the conformally invariant ð and þ are defined in Penrose Rindler [99] as

$$\text{þ}_c := \text{þ} + [w + (p+q)w_1]\rho, \qquad \text{þ}'_c := \text{þ}' + [w - (p+q)w_0]\rho',$$

$$\text{ð}_c := \text{ð} + [w + pw_1 - qw_0]\tau, \qquad \text{ð}'_c := \text{ð}' + [w - pw_0 + qw_1]\tau'. \tag{A.3.6}$$

Appendix B

Derivation of the GCFE in the space-spinor formalism

B.1 Derivation of the remaining equations

Out of the four equations that make up the tensorial GCFE we have derived the equation for the Schouten tensor 1.6.21c as an example in section 2.2. Here we present the remaining derivations.

We start by converting the equations for the frame components (1.6.21a) and connection coefficients (1.6.21b), but first we need to connect the commutators of the ∂ and ∂_{AB} operators with those for the D and D_{AB} operators. For action on a spinor we find

$$\begin{aligned}[D_{AB}, D_{CD}]\,\alpha_E = {}& [\partial_{AB}, \partial_{CD}]\,\alpha_E + \left(\chi_{AB(C}{}^{(F}\delta_{D)}^{H)} - \chi_{CD(A}{}^{(F}\delta_{B)}^{H)}\right)\,\partial_{FH}\,\alpha_E \\ & + \frac{1}{2}\left(\partial_{AB}\chi_{CDE}{}^{F} - \partial_{CD}\chi_{ABE}{}^{F}\right)\,\alpha_F + \frac{1}{2}\left(\chi_{AB(C}{}^{H}\chi_{D)HE}{}^{F} - \chi_{CD(A}{}^{H}\chi_{B)HE}{}^{F}\right)\alpha_F \\ & + \frac{1}{2}\chi_{ABH(E}\chi_{|CD|F)}{}^{H}\alpha^{F},\end{aligned}$$

$$\begin{aligned}\left[D, D_{AB}\right]\alpha_C = {}& \left[\partial, \partial_{AB}\right]\alpha_C + \chi_{(A}{}^{E}\,\partial_{B)E}\,\alpha_C + \frac{1}{2}\chi_{(A}{}^{E}\chi_{B)EC}{}^{D}\,\alpha_D + \frac{1}{2}\left(\partial\chi_{ABC}{}^{D} - \partial_{AB}\chi_{C}{}^{D}\right)\alpha_D \\ & + \frac{1}{2}\chi_{AB(C}{}^{E}\chi_{D)E}\,\alpha^{D}.\end{aligned}$$

Note that all the information contained in the first commutator is contained in the expression

$$\begin{aligned}2D_{E(A}D^{E}{}_{B)}\alpha_C = 2\partial_{E(A}\partial^{E}{}_{B)}\alpha_C &+ \chi_{E(A}{}^{EF}\left(\partial_{B)F}\alpha_C + \frac{1}{2}\chi_{B)FC}{}^{D}\alpha_D\right)\\ &- \chi^{E}{}_{(AB)}{}^{F}\left(\partial_{EF}\alpha_C + \frac{1}{2}\chi_{EFC}{}^{D}\alpha_D\right)\\ &+ \left(\partial_{E(A}\chi^{E}{}_{B)C}{}^{D} + \frac{1}{2}\chi_{E(A|C|}{}^{F}\chi^{E}{}_{B)F}{}^{D}\right)\alpha_D.\end{aligned}$$

The next step is to express the D and D_{AB} commutators in terms of the curvature of the conformal Weyl connection. We write out the commutator

$$\left[\widehat{\nabla}_{AA'}, \widehat{\nabla}_{BB'}\right]\alpha_C = \left[\nabla_{AA'}, \nabla_{BB'}\right]\alpha_C - \nabla_a f_{CB'}\alpha_B + \nabla_b f_{CA'}\alpha_A + f_{AB'}f_{CA'}\alpha_B - f_{BA'}f_{CB'}\alpha_A,$$

and contract with the appropriate t^a's. Then the commutator on the right hand side gives

$$\begin{aligned}t^{EE'}t_{(A}{}^{B'}\left[\nabla_{EE'}, \nabla_{B)B'}\right]\alpha_C &= \left[D, D_{AB}\right]\alpha_C + \frac{1}{2}\chi_{AB}D\alpha_C - \chi_{(A}{}^{E}D_{B)E}\alpha_C + \chi_{AB}{}^{ED}D_{ED}\alpha_C\\ &= \left[\partial, \partial_{AB}\right]\alpha_C + \chi_{(A}{}^{E}\partial_{B)E}\alpha_C + \frac{1}{2}\chi_{(A}{}^{E}\chi_{B)EC}{}^{F}\alpha_F + \frac{1}{2}\partial\chi_{ABC}{}^{E}\alpha_E\\ &\quad - \frac{1}{2}\partial_{AB}\chi_C{}^{E}\alpha_E + \frac{1}{2}\chi_{AB(C}{}^{E}\chi_{D)E}\alpha^D + \frac{1}{2}\chi_{AB}D\alpha_C - \chi_{(A}{}^{E}D_{B)E}\alpha_C\\ &\quad + \chi_{AB}{}^{ED}D_{ED}\alpha_C\\ &= \left[\partial, \partial_{AB}\right]\alpha_C + \chi_{(A}{}^{E}\partial_{B)E}\alpha_C + \frac{1}{2}\chi_{(A}{}^{E}\chi_{B)EC}{}^{F}\alpha_F + \frac{1}{2}\partial\chi_{ABC}{}^{E}\alpha_E\\ &\quad - \frac{1}{2}\partial_{AB}\chi_C{}^{E}\alpha_E + \frac{1}{2}\chi_{AB(C}{}^{E}\chi_{D)E}\alpha^D + \frac{1}{2}\chi_{AB}\partial\alpha_C\\ &\quad + \frac{1}{4}\chi_{AB}\chi_C{}^{D}\alpha_D - \chi_{(A}{}^{E}\partial_{B)E}\alpha_C - \frac{1}{2}\chi_{(A}{}^{E}\chi_{B)EC}{}^{F}\alpha_F\\ &\quad + \chi_{AB}{}^{ED}\partial_{ED}\alpha_C + \frac{1}{2}\chi_{AB}{}^{ED}\chi_{EDC}{}^{F}\alpha_F\\ &= \left[\partial, \partial_{AB}\right]\alpha_C + \frac{1}{2}\chi_{AB}\partial\alpha_C + \chi_{AB}{}^{ED}\partial_{ED}\alpha_C\\ &\quad + \frac{1}{2}\left(\partial\chi_{ABC}{}^{E} - \partial_{AB}\chi_C{}^{E}\right)\alpha_E + \frac{1}{4}\chi_{AB}\chi_C{}^{D}\alpha_D\\ &\quad + \frac{1}{2}\chi_{AB}{}^{ED}\chi_{EDC}{}^{F}\alpha_F + \frac{1}{2}\chi_{AB(C}{}^{E}\chi_{D)E}\alpha^D.\end{aligned}$$

The terms involving derivatives of $f_{AA'}$ become

$$\begin{aligned}&- t^e t_{(A}{}^{B'}\nabla_e f_{CB'}\alpha_{B)} + t^e t_{(A}{}^{B'}\nabla_{B)B'}f_{CE'}\alpha_E\\ &= -Df_{CB'}t_{(A}{}^{B'}\alpha_{B)} + t^{EE'}D_{AB}f_{CE'}\alpha_E\\ &= -\partial f_{C(A}\alpha_{B)} - \frac{1}{2}\chi_C{}^{E}f_{E(A}\alpha_{B)} + \frac{1}{2}f_{CE}\chi_{(A}{}^{E}\alpha_{B)} - \partial_{AB}f_{CE}\alpha^E - \frac{1}{2}\chi_{ABC}{}^{F}f_{FE}\alpha^E + \frac{1}{2}\chi_{ABE}{}^{F}f_{CF}\alpha^E.\end{aligned}$$

Note that $f_{AB} := f_{AA'}t_B{}^{A'}$ is not symmetric *a-priori*. Finally, the terms quadratic in $f_{AA'}$ become

$$t^{EE'}f_{EB'}f_{CE'}t_{(A}{}^{B'}\alpha_{B)} - t^{EE'}f_{E'(B}t_{A)}{}^{B'}f_{CB'}\alpha_E = f_C{}^E f_{E(A}\alpha_{B)} - f_{C(A}f_{B)}{}^E\alpha_E.$$

Taking everything together we obtain the equation

$$\begin{aligned}\widehat{\boxtimes}_{AB}\alpha_C - \boxtimes_{AB}\alpha_C = {} & [\partial, \partial_{AB}]\,\alpha_C + \frac{1}{2}\chi_{AB}\partial\alpha_C + \chi_{AB}{}^{ED}\partial_{ED}\alpha_C + \frac{1}{2}\left(\partial\chi_{ABC}{}^E - \partial_{AB}\chi_C{}^E\right)\alpha_E \\ & + \frac{1}{4}\chi_{AB}\chi_C{}^D\alpha_D + \frac{1}{2}\chi_{AB}{}^{ED}\chi_{EDC}{}^F\alpha_F + \frac{1}{2}\chi_{AB(C}{}^E\chi_{D)E}\alpha^D \\ & - \partial f_{C(A}\alpha_{B)} - \frac{1}{2}\chi_C{}^E f_{E(A}\alpha_{B)} + \frac{1}{2}f_{CE}\chi_{(A}{}^E\alpha_{B)} - \partial_{AB}f_{CE}\alpha^E \\ & - \frac{1}{2}\chi_{ABC}{}^F f_{FE}\alpha^E + \frac{1}{2}\chi_{ABE}{}^F f_{CF}\alpha^E + f_C{}^E f_{E(A}\alpha_{B)} - f_{C(A}f_{B)}{}^E\alpha_E,\end{aligned} \tag{B.1.1}$$

where we have defined

$$\boxtimes_{AB} := \nabla_{X'(A}\nabla_{B)}{}^{X'}. \tag{B.1.2}$$

We need to isolate the terms containing the derivatives of χ_{ABCD} and χ_{AB}. To do this we note that

$$\widehat{[\partial, \partial_{AB}]}\,\alpha_C = -\,[\partial, \partial_{AB}]\,\hat{\alpha}_C.$$

To eliminate the commutator from (B.1.1) above, we replace α_C by $\hat{\alpha}_C$ and add to this equation the complex conjugate of the above equation. We need to remember the reality conditions of the spinors involved, such as

$$\hat{\chi}_{AB} = -\chi_{AB}, \qquad \hat{\chi}_{ABCD} = \chi_{ABCD}, \qquad \hat{f}_{AB} = -f_{BA}.$$

In order to disentangle the various terms containing $f_{AA'}$ we write

$$f_{AA'}t_B{}^{A'} = \frac{1}{2}\varepsilon_{AB}f + f_{AB}.$$

Note, that this implies the substitution $f_{AB} \mapsto \frac{1}{2}\varepsilon_{AB}f + f_{AB}$ in (B.1.1) above. Then $\bar{f} = f$ and $\hat{f}_{AB} = -f_{AB}$. We also write the left-hand-side as a tensorial expression $Q_{ABC}{}^E\alpha_E$.

In the following table we list on the left all the terms in (B.1.1) with α_A replaced by $\hat{\alpha}_A$ and

on the right the complex conjugate of the original terms.

$Q_{ABC}{}^{E}\hat{\alpha}_{E}$	$\widehat{Q}_{ABC}{}^{E}\hat{\alpha}_{E}$
$+\left[\partial,\partial_{AB}\right]\hat{\alpha}_{C}$	$-\left[\partial,\partial_{AB}\right]\hat{\alpha}_{C}$
$+\frac{1}{2}\chi_{AB}\partial\hat{\alpha}_{C}$	$-\frac{1}{2}\chi_{AB}\partial\hat{\alpha}_{C}$
$+\chi_{AB}{}^{ED}\partial_{ED}\hat{\alpha}_{C}$	$-\chi_{AB}{}^{ED}\partial_{ED}\hat{\alpha}_{C}$
$+\frac{1}{2}\left(\partial\chi_{ABC}{}^{E}-\partial_{AB}\chi_{C}{}^{E}\right)\hat{\alpha}_{E}$	$+\frac{1}{2}\left(\partial\chi_{ABC}{}^{E}-\partial_{AB}\chi_{C}{}^{E}\right)\hat{\alpha}_{E}$
$+\frac{1}{4}\chi_{AB}\chi_{C}{}^{D}\hat{\alpha}_{D}$	$+\frac{1}{4}\chi_{AB}\chi_{C}{}^{D}\hat{\alpha}_{D}$
$+\frac{1}{2}\chi_{AB}{}^{ED}\chi_{EDC}{}^{F}\hat{\alpha}_{F}$	$+\frac{1}{2}\chi_{AB}{}^{ED}\chi_{EDC}{}^{F}\hat{\alpha}_{F}$
$+\frac{1}{2}\chi_{AB(C}{}^{E}\chi_{D)E}\hat{\alpha}^{D}$	$-\frac{1}{2}\chi_{AB(C}{}^{E}\chi_{D)E}\hat{\alpha}^{D}$
$-\frac{1}{2}f\chi_{C(A}\alpha_{B)}$	$+\frac{1}{2}f\chi_{C(A}\alpha_{B)}$
$-\frac{1}{2}\partial f\varepsilon_{C(A}\hat{\alpha}_{B)}-\partial f_{C(A}\hat{\alpha}_{B)}$	$-\frac{1}{2}\partial f\varepsilon_{C(A}\hat{\alpha}_{B)}+\partial f_{C(A}\hat{\alpha}_{B)}$
$+\frac{1}{2}\partial_{AB}f\hat{\alpha}_{C}-\partial_{AB}f_{CE}\hat{\alpha}^{E}$	$-\frac{1}{2}\partial_{AB}f\hat{\alpha}_{C}-\partial_{AB}f_{CE}\hat{\alpha}^{E}$
$-\frac{1}{2}\left(\chi_{C}{}^{D}f_{D(A}\hat{\alpha}_{B)}-f_{CD}\chi_{(A}{}^{D}\hat{\alpha}_{B)}\right)$	$-\frac{1}{2}\left(\chi_{C}{}^{D}f_{D(A}\hat{\alpha}_{B)}-f_{CD}\chi_{(A}{}^{D}\hat{\alpha}_{B)}\right)$
$-\frac{1}{2}\left(\chi_{ABCD}f\hat{\alpha}^{D}+\chi_{ABDE}f^{DE}\hat{\alpha}_{C}\right)$	$-\frac{1}{2}\left(\chi_{ABCD}f\hat{\alpha}^{D}-\chi_{ABDE}f^{DE}\hat{\alpha}_{C}\right)$
$+\frac{1}{2}ff_{C(A}\varepsilon_{B)}{}^{D}\hat{\alpha}_{D}+\frac{1}{2}ff^{D}{}_{(A}\varepsilon_{B)C}\hat{\alpha}_{D}$	$-\frac{1}{2}ff_{C(A}\varepsilon_{B)}{}^{D}\hat{\alpha}_{D}-\frac{1}{2}ff^{D}{}_{(A}\varepsilon_{B)C}\hat{\alpha}_{D}$
$-f_{AB}f_{C}{}^{D}\hat{\alpha}_{D}-\varepsilon_{C(A}\varepsilon_{B)}{}^{D}f_{EF}f^{EF}\hat{\alpha}_{D}$	$-f_{AB}f_{C}{}^{D}\hat{\alpha}_{D}-\varepsilon_{C(A}\varepsilon_{B)}{}^{D}f_{EF}f^{EF}\hat{\alpha}_{D}$

The terms below the second line have already been rewritten compared to (B.1.1). Adding and subtracting the two columns will now give us two equations, one being the evolution equation for χ_{ABCD} and the other containing the commutator of the derivatives. The equation for χ_{ABCD} is

$$\begin{aligned}\partial\chi_{ABCD}-\partial_{AB}\chi_{CD}=&-\frac{1}{2}\chi_{AB}\chi_{CD}-\chi_{AB}{}^{EF}\chi_{EFCD}+\partial f\varepsilon_{C(A}\varepsilon_{B)D}-2\partial_{AB}f_{CD}+\chi_{C}{}^{E}f_{E(A}\varepsilon_{B)D}\\&-f_{CE}\chi_{(A}{}^{E}\varepsilon_{B)D}-f\chi_{ABCD}+2f_{AB}f_{CD}+2\varepsilon_{C(A}\varepsilon_{B)D}f_{EF}f^{EF}+Q_{ABCD}+\widehat{Q}_{ABCD}.\end{aligned}\tag{B.1.3}$$

Here, we have eliminated the arbitrary spinor $\hat{\alpha}_D$, which we cannot do for the equation with the commutator. However, we can drop the hat and we obtain for this equation

$$\begin{aligned} 2\left[\partial, \partial_{AB}\right]\alpha_C = &-\chi_{AB}\partial\alpha_C - 2\chi_{AB}{}^{ED}\partial_{ED}\alpha_C - \chi_{AB(C}{}^{E}\chi_{D)E}\alpha^D + f\chi_{C(A}\alpha_{B)} + 2\partial f_{C(A}\alpha_{B)} \\ &- \partial_{AB}f\alpha_C + \chi_{ABDE}f^{DE}\alpha_C - ff_{C(A}\varepsilon_{B)}{}^{D}\alpha_D - ff^{D}{}_{(A}\varepsilon_{B)C}\alpha_D + Q_{ABC}{}^{E}\alpha_E - \widehat{Q}_{ABC}{}^{E}\alpha_E. \end{aligned} \tag{B.1.4}$$

Action of the commutator on ε yields an evolution equation for f_{AB}

$$\partial f_{AB} = \partial_{AB}f - \frac{1}{2}f\chi_{AB} - \chi_{ABEF}f^{EF} - \frac{1}{2}\left(Q_{ABE}{}^{E} - \hat{Q}_{ABE}{}^{E}\right). \tag{B.1.5}$$

Note that we do not need to find an evolution equation (nor a constraint equation) for the scalar f[1].

Finally, we need to determine the spinor Q_{ABCD}. It was defined in terms of the conformal curvature derivations $\boxtimes_{AB}$ and $\boxtimes_{A'B'}$. Those, in turn, are defined in terms of the conformal Riemann tensor $\hat{R}_{abc}{}^{d}$. Let us define

$$\boxtimes_{AB}\alpha_C = -R_{ABC}{}^{D}\alpha_D, \qquad \boxtimes_{A'B'}\alpha_C = -R_{A'B'C}{}^{D}\alpha_D.$$

Then comparing with the decomposition of $\hat{R}_{abc}{}^{d}$ in terms of the Weyl tensor and the Schouten tensor, we can derive the following spinorial expressions (see appendix B.2)

$$R_{AB}{}^{CD} = \Psi_{AB}{}^{CD} - \varepsilon_{(A}{}^{(C}\hat{P}_{B)E'}{}^{D)E'} + \frac{1}{2}\varepsilon^{CD}\hat{P}_{(A}{}^{E'}{}_{B)E'}, \qquad R_{A'B'}{}^{CD} = \hat{P}^{(C}{}_{(A'}{}^{D)}{}_{B')} - \frac{1}{2}\varepsilon^{CD}\hat{P}_{E(A'}{}^{E}{}_{B')}.$$

Keeping in mind that the general Schouten tensor is not symmetric the last terms in these equations do not in general vanish.

The spinor $Q_{AB}{}^{CD}$ can now be obtained by writing the commutator relation $\left[\widehat{\nabla}_a, \widehat{\nabla}_b\right]$ acting on a spinor and contracting with the appropriate combination of t^a's. Then one obtains

$$Q_{AB}{}^{CD} = R_{AB}{}^{CD} - t_A{}^{A'}t_B{}^{B'}R_{A'B'}{}^{CD}.$$

We then find the expressions

$$Q_{AB}{}^{CD} = \Psi_{AB}{}^{CD} - P^{(C}{}_{(A}{}^{D)}{}_{B)} - \varepsilon_{(A}{}^{(C}P_{B)E}{}^{D)E} + \frac{1}{2}\varepsilon^{CD}\left(P_E{}^{E}{}_{(AB)} - P_{(AB)E}{}^{E}\right),$$

[1] One can see why by expanding $\widehat{\Gamma}$ in Cartan's second structure equation (1.6.21b), and then contracting to find $e_a(f_b) - e_b(f_a) = ...$

and

$$\widehat{Q}_{AB}{}^{CD} = \widehat{\Psi}_{AB}{}^{CD} - P_{(A}{}^{(C}{}_{B)}{}^{D)} - \varepsilon_{(A}{}^{(C}P_{|E|B)}{}^{|E|D)} - \frac{1}{2}\varepsilon^{CD}\left(P_E{}^E{}_{(AB)} - P_{(AB)E}{}^E\right).$$

By replacing the $Q's$ in the evolution equation for f_{AB}, we find

$$\partial f_{AB} = \partial_{AB} f - \chi_{ABEF} f^{EF} + P_{(AB)C}{}^C - P_C{}^C{}_{(AB)}. \tag{B.1.6}$$

The final equation to consider is the Bianchi equation, which when written in spinors is

$$\nabla_{A'}{}^E \psi_{ABCE} = 0.$$

This is the exact equation that describes a spin-2 zero rest-mass field, the so-called graviton. Hence we will sometimes call this equation the spin-2 equation. Converting the primed index, splitting into D and D_{AB} derivatives and expressing in terms of ∂ and ∂_{AB} yields the equation

$$-\frac{1}{2}\partial\psi_{ABCD} - \chi_{(A}{}^E\psi_{BCD)E} + \partial_D{}^E\psi_{ABCE} + \frac{3}{2}\chi_D{}^E{}_{(A}{}^F\psi_{BC)EF} + \frac{1}{2}\chi_D{}^E{}_E{}^F\psi_{ABCF} = 0. \tag{B.1.7}$$

Clearly this equation is symmetric in ABC. Taking the totally symmetric part gives an evolution equation for ψ_{ABCD}

$$\partial\psi_{ABCD} - 2\partial_{(A}{}^E\psi_{BCD)E} = -2\chi_{(A}{}^E\psi_{BCD)E} + 3\chi_{(A}{}^E{}_B{}^F\psi_{CD)EF} - \chi_{E(A}{}^{EF}\psi_{BCD)F}, \tag{B.1.8}$$

while the anti-symmetric part gives us a constraint

$$\partial^{CD}\psi_{ABCD} = -\chi^{CE}{}_E{}^D\psi_{ABCD} - \chi^{CDE}{}_{(A}\psi_{B)CDE}. \tag{B.1.9}$$

B.2 Derivation of the curvature spinors

The decomposition of the Riemann tensor with respect to a Weyl connection can be written in the spinor formalism as

$$\begin{aligned}\hat{R}_{abcd} &= \varepsilon_{AB}\varepsilon_{A'D'}\hat{P}_{DB'CC'} + \varepsilon_{A'B'}\varepsilon_{AD}\hat{P}_{BD'CC'} - \varepsilon_{CD}\varepsilon_{C'D'}\left(\varepsilon_{AB}\hat{P}_{EA'}{}^E{}_{B'} + \varepsilon_{A'B'}\hat{P}_{AE'B}{}^{E'}\right)\\ &\quad - \varepsilon_{AB}\varepsilon_{A'C'}\hat{P}_{CB'DD'} - \varepsilon_{A'B'}\varepsilon_{AC}\hat{P}_{BC'DD'} + \varepsilon_{A'B'}\varepsilon_{C'D'}\psi_{ABCD} + \varepsilon_{AB}\varepsilon_{CD}\overline{\psi}_{A'B'C'D'}\\ &= \hat{X}_{ABCD}\varepsilon_{A'B'}\varepsilon_{C'D'} + \hat{Y}_{A'B'CD}\varepsilon_{AB}\varepsilon_{C'D'} + \overline{\hat{Y}}_{ABC'D'}\varepsilon_{A'B'}\varepsilon_{CD} + \overline{\hat{X}}_{A'B'C'D'}\varepsilon_{AB}\varepsilon_{CD},\end{aligned}$$

for some spinors $\hat{X}, \hat{Y}$ symmetric in their first two indices. To solve for them in terms of the Schouten spinor, we note the particular decompositions

$$\hat{X}_{ABCD} = \hat{X}_{AB(CD)} + \frac{1}{2}\varepsilon_{CD}\hat{X}_{ABE}{}^{E}, \qquad \hat{Y}_{A'B'CD} = \hat{Y}_{A'B'(CD)} + \frac{1}{2}\varepsilon_{CD}\hat{Y}_{A'B'E}{}^{E}.$$

Transvecting $\hat{R}_{abcd}$ with $\varepsilon^{A'B'}\varepsilon^{C'D'}$ we obtain

$$\begin{aligned} 4\hat{X}_{ABCD} + 2\overline{\hat{Y}}_{ABC'}{}^{C'}\varepsilon_{CD} = &-2\varepsilon_{AB}\hat{P}_{(CC'D)}{}^{C'} - 4\varepsilon_{A(C}\hat{P}_{|B|C'D)}{}^{C'} - 2\varepsilon_{CD}\left(\varepsilon_{AB}\hat{P}_{EE'}{}^{EE'} + 2\hat{P}_{AE'B}{}^{E'}\right) \\ &+ 4\psi_{ABCD}. \end{aligned}$$

Symmetrising over CD and noting that $\hat{X}$ is symmetric in the first pair of indices gives

$$\hat{X}_{AB}{}^{(CD)} = \psi_{AB}{}^{CD} - \varepsilon_{(A}{}^{(C}\hat{P}_{B)E'}{}^{D)E'}.$$

If we transvect with ε^{CD} instead of symmetrising, we find

$$\hat{X}_{ABC}{}^{C} + \overline{\hat{Y}}_{ABC'}{}^{C'} = -2\hat{P}_{E'(AB)}{}^{E'}.$$

Now we use the identity $\hat{X}_{ABC}{}^{C} = \overline{\hat{Y}}_{ABC'}{}^{C'}$, which can be derived by expressing the action of $[\hat{\nabla}_a, \hat{\nabla}_b]$ on the associated metric in two ways: in terms of the action of $\hat{\nabla}$ on the metric; and in terms of the curvature spinors. Using this, we immediately see that

$$\hat{X}_{ABC}{}^{C} = -\hat{P}_{E'(AB)}{}^{E'}, \qquad \hat{Y}_{A'B'E}{}^{E} = -\hat{P}_{E(A'}{}^{E}{}_{B')}.$$

Next we transvect $\hat{R}_{abcd}$ with $\varepsilon^{AB}\varepsilon^{C'D'}$, giving

$$4\hat{Y}_{A'B'CD} + 2\overline{\hat{X}}_{A'B'C'}{}^{C'}\varepsilon_{CD} = 4\hat{P}_{(CB'D)A'} - 2\varepsilon_{A'B'}\hat{P}_{(CC'D)}{}^{C'} - 2\varepsilon_{CD}\left(2\hat{P}_{EA'}{}^{E}{}_{B'} + \varepsilon_{A'B'}\hat{P}_{EE'}{}^{EE'}\right).$$

Symmetrising over CD and noting that $\hat{Y}$ is symmetric in the first pair of indices gives

$$\hat{Y}_{A'B'}{}^{(CD)} = \hat{P}^{(C}{}_{(A'}{}^{D)}{}_{B')}.$$

Now we can write the curvature spinors as

$$\hat{X}_{AB}{}^{CD} = \psi_{AB}{}^{CD} - \varepsilon_{(A}{}^{(C}\hat{P}_{B)E'}{}^{D)E'} - \frac{1}{2}\varepsilon^{CD}\hat{P}_{E'(AB)}{}^{E'}, \qquad \hat{Y}_{A'B'}{}^{CD} = \hat{P}^{(C}{}_{(A'}{}^{D)}{}_{B')} - \frac{1}{2}\varepsilon^{CD}\hat{P}_{E(A'}{}^{E}{}_{B')}. \tag{B.2.1}$$

B.3 Equation roadmap

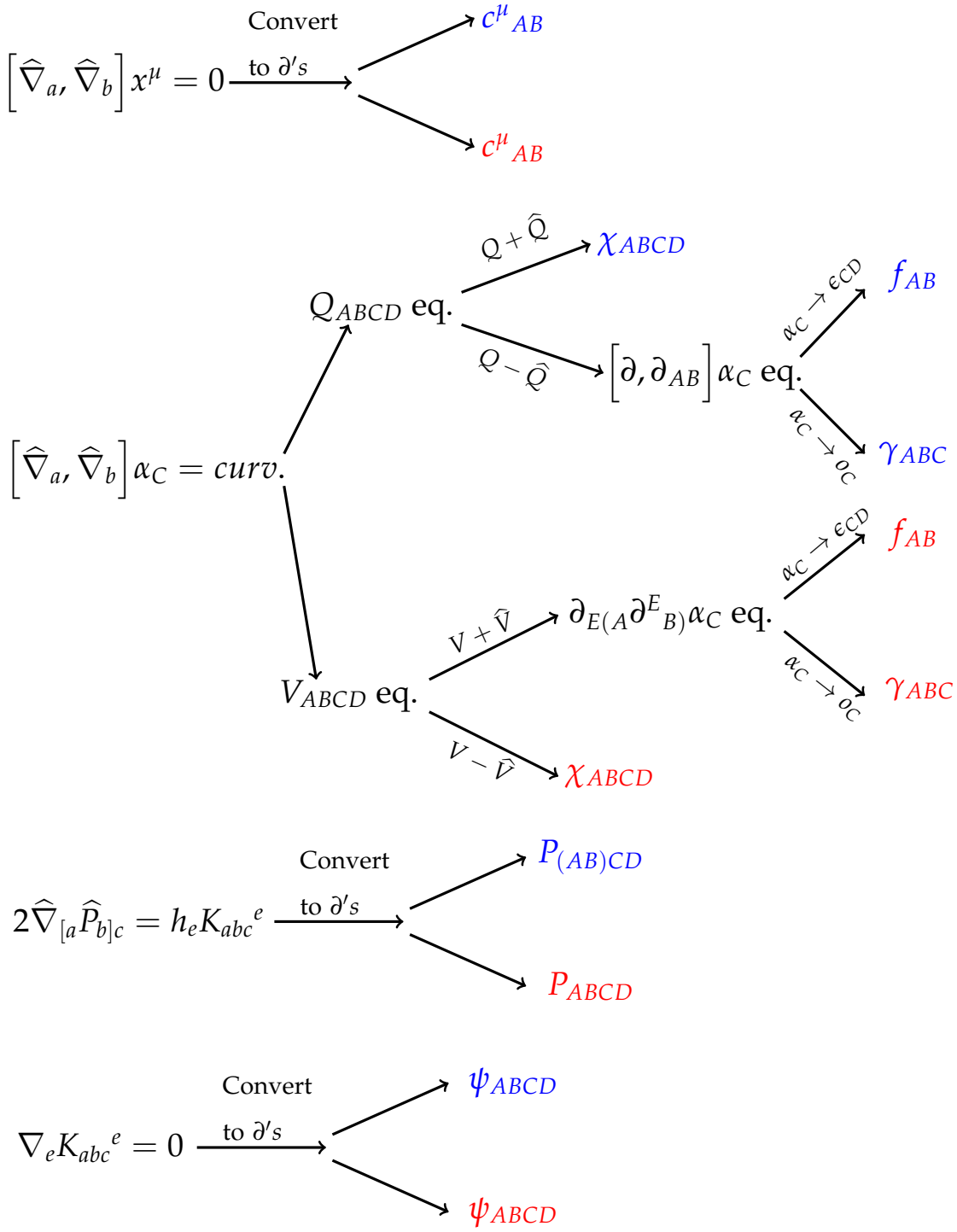

Figure B.1: The "roadmap" that we follow to rewrite the tensorial GCFE in the space-spinor formalism. The colour blue indicates an evolution equation for the corresponding quantity while the colour red indicates a constraint.

Bibliography

[1] B. Abbott, R. Abbott, T. Abbott, M. Abernathy, F. Acernese, K. Ackley, C. Adams, T. Adams, P. Addesso, R. Adhikari, et al. Gw151226: Observation of gravitational waves from a 22-solar-mass binary black hole coalescence. *Physical Review Letters*, 116(24):241103, 2016.

[2] B. Abbott, R. Abbott, T. Abbott, M. Abernathy, F. Acernese, K. Ackley, C. Adams, T. Adams, P. Addesso, R. Adhikari, et al. Observation of gravitational waves from a binary black hole merger. *Physical Review Letters*, 116(6):061102, 2016.

[3] R. Arnowitt, S. Deser, and C. W. Misner. Republication of: The dynamics of general relativity. *General Relativity and Gravitation*, 40(9):1997–2027, 2008.

[4] A. Ashtekar and R. O. Hansen. A unified treatment of null and spatial infinity in general relativity. I. Universal structure, asymptotic symmetries, and conserved quantities at spatial infinity. *Journal of Mathematical Physics*, 19(7):1542–1566, 1978.

[5] A. Ashtekar and J. D. Romano. Spatial infinity as a boundary of spacetime. *Classical and Quantum Gravity*, 9(4):1069, 1992.

[6] V. Balasubramanian, A. Buchel, S. R. Green, L. Lehner, and S. L. Liebling. Holographic thermalization, stability of Anti-de Sitter space, and the Fermi-Pasta-Ulam paradox. *Physical Review Letters*, 113(7):071601, 2014.

[7] T. W. Baumgarte and S. L. Shapiro. Numerical integration of Einstein's field equations. *Physical Review D*, 59(2):024007, 1998.

[8] J.-P. Berrut and L. N. Trefethen. Barycentric Lagrange interpolation. *Siam Review*, 46(3):501–517, 2004.

[9] F. Beyer. Asymptotics and singularities in cosmological models with positive cosmological constant. *arXiv preprint arXiv:0710.4297*, 2007.

[10] F. Beyer, G. Doulis, J. Frauendiener, and B. Whale. Numerical space-times near space-like and null infinity. the spin-2 system on Minkowski space. *Classical and Quantum Gravity*, 29(24):245013, 2012.

[11] F. Beyer, G. Doulis, J. Frauendiener, and B. Whale. Linearized gravitational waves near space-like and null infinity. In *Progress in Mathematical Relativity, Gravitation and Cosmology*, pages 3–17. Springer, 2014.

[12] F. Beyer, G. Doulis, J. Frauendiener, and B. Whale. The spin-2 equation on Minkowski background. In *Progress in Mathematical Relativity, Gravitation and Cosmology*, pages 465–468. Springer, 2014.

[13] F. Beyer, L. Escobar, and J. Frauendiener. Numerical solutions of Einstein's equations for cosmological spacetimes with spatial topology $\mathbb{S}^3$ and symmetry group U(1). *arXiv preprint arXiv:1505.05920*, 2015.

[14] P. Bizoń. Is AdS stable? *General Relativity and Gravitation*, 46(5):1–14, 2014.

[15] P. Bizoń, M. Maliborski, and A. Rostworowski. Resonant dynamics and the instability of Anti-de Sitter spacetime. *Physical Review Letters*, 115(8):081103, 2015.

[16] P. Bizoń and A. Rostworowski. Weakly turbulent instability of Anti-de Sitter spacetime. *Physical Review Letters*, 107(3):031102, 2011.

[17] H. Bondi, F. A. Pirani, and I. Robinson. Gravitational waves in general relativity. III. Exact plane waves. In *Proceedings of the Royal Society of London A: Mathematical, Physical and Engineering Sciences*, volume 251, pages 519–533. The Royal Society, 1959.

[18] H. Bondi, M. Van der Burg, and A. Metzner. Gravitational waves in general relativity. VII. Waves from axi-symmetric isolated systems. In *Proceedings of the Royal Society*

of London A: Mathematical, Physical and Engineering Sciences, volume 269, pages 21–52. The Royal Society, 1962.

[19] J. P. Boyd. *Chebyshev and Fourier Spectral Methods*. Courier Corporation, 2001.

[20] A. Buchel, L. Lehner, and S. L. Liebling. Scalar collapse in AdS spacetimes. *Physical Review D*, 86(12):123011, 2012.

[21] M. H. Carpenter, D. Gottlieb, and S. Abarbanel. Time-stable boundary conditions for finite-difference schemes solving hyperbolic systems: methodology and application to high-order compact schemes. *Journal of Computational Physics*, 111(2):220–236, 1994.

[22] M. H. Carpenter, J. Nordström, and D. Gottlieb. A stable and conservative interface treatment of arbitrary spatial accuracy. *Journal of Computational Physics*, 148(2):341–365, 1999.

[23] S. Chandrasekhar. *The Mathematical Theory of Black Holes*, volume 69. Oxford University Press, 1998.

[24] R. Courant, K. Friedrichs, and H. Lewy. Über die partiellen Differenzengleichungen der mathematischen Physik. *Mathematische Annalen*, 100(1):32–74, 1928.

[25] W. De Sitter. On the relativity of inertia. Remarks concerning Einstein's latest hypothesis. *Proc. Kkl. Akad. Amsterdam*, 19:1217–1225, 1917.

[26] O. J. Dias, G. T. Horowitz, D. Marolf, and J. E. Santos. On the nonlinear stability of asymptotically Anti-de Sitter solutions. *Classical and Quantum Gravity*, 29(23):235019, 2012.

[27] O. J. Dias, G. T. Horowitz, and J. E. Santos. Gravitational turbulent instability of Anti-de Sitter space. *Classical and Quantum Gravity*, 29(19):194002, 2012.

[28] P. Diener, E. N. Dorband, E. Schnetter, and M. Tiglio. Optimized high-order derivative and dissipation operators satisfying summation by parts, and applications in three-dimensional multi-block evolutions. *Journal of Scientific Computing*, 32(1):109–145, 2007.

[29] G. Doulis and J. Frauendiener. The second order spin-2 system in flat space near space-like and null-infinity. *General Relativity and Gravitation*, 45(7):1365–1385, 2013.

[30] A. Einstein. Ist die Trägheit eines Körpers von seinem Energieinhalt abhängig? *Annalen der Physik*, 323(13):639–641, 1905.

[31] A. Einstein. Über die von der molekularkinetischen Theorie der Wärme geforderte Bewegung von in ruhenden Flüssigkeiten suspendierten Teilchen. *Annalen der Physik*, 322(8):549–560, 1905.

[32] A. Einstein. Zur Elektrodynamik bewegter Körper. *Annalen der Physik*, 322(10):891–921, 1905.

[33] A. Einstein. Über gravitationswellen. *Sitzungsberichte der Königlich Preußischen Akademie der Wissenschaften (Berlin), Seite 154-167.*, 1918.

[34] A. Einstein. *A Heuristic Viewpoint Concerning the Production and Transformation of Light*. 1929.

[35] A. Einstein. *On gravitational waves*. Springer, 1990.

[36] J. Frauendiener. Calculating initial data for the conformal field equations by pseudo-spectral methods. *Comp. Appl. Math*, 1998.

[37] J. Frauendiener. Numerical treatment of the hyperboloidal initial value problem for the vacuum Einstein equations. I. The conformal field equations. *Physical Review D*, 58(6):064002, 1998.

[38] J. Frauendiener. Numerical treatment of the hyperboloidal initial value problem for the vacuum Einstein equations. II. The evolution equations. *Physical Review D*, 58(6):064003, 1998.

[39] J. Frauendiener. *Conformal methods in numerical relativity*. PhD thesis, Habilitationsschrift,(Universität Tübingen, Tübingen, 1999). 4, 4.3, 1999.

[40] J. Frauendiener. Numerical treatment of the hyperboloidal initial value problem for the vacuum Einstein equations: III. On the determination of radiation. *Classical and Quantum Gravity*, 17(2):373, 2000.

[41] J. Frauendiener. Conformal infinity. *Living Rev. Relativity*, 7, 2004.

[42] J. Frauendiener, C. Stevens, and B. Whale. Numerical evolution of plane gravitational waves in the Friedrich-Nagy gauge. *Physical Review D*, 89(10):104026, 2014.

[43] A. Friedmann. Über die Krümmung des Raumes. *Zeitschrift für Physik A Hadrons and Nuclei*, 10(1):377–386, 1922.

[44] A. Friedmann. Über die Möglichkeit einer Welt mit konstanter negativer Krümmung des Raumes. *Zeitschrift für Physik A Hadrons and Nuclei*, 21(1):326–332, 1924.

[45] H. Friedrich. The asymptotic characteristic initial value problem for Einstein's vacuum field equations as an initial value problem for a first-order quasilinear symmetric hyperbolic system. In *Proceedings of the Royal Society of London A: Mathematical, Physical and Engineering Sciences*, volume 378, pages 401–421. The Royal Society, 1981.

[46] H. Friedrich. On the regular and the asymptotic characteristic initial value problem for Einstein's vacuum field equations. In *Proceedings of the Royal Society of London A: Mathematical, Physical and Engineering Sciences*, volume 375, pages 169–184. The Royal Society, 1981.

[47] H. Friedrich. On the hyperbolicity of Einstein's and other gauge field equations. *Communications in Mathematical Physics*, 100(4):525–543, 1985.

[48] H. Friedrich. Einstein equations and conformal structure: existence of Anti-de Sitter-type space-times. *Journal of Geometry and Physics*, 17(2):125–184, 1995.

[49] H. Friedrich. Hyperbolic reductions for Einstein's equations. *Classical and Quantum Gravity*, 13(6):1451, 1996.

[50] H. Friedrich. Gravitational fields near space-like and null infinity. *Journal of Geometry and Physics*, 24(2):83–163, 1998.

[51] H. Friedrich. Conformal Einstein evolution. In *The conformal structure of space-time*, pages 1–50. Springer, 2002.

[52] H. Friedrich. Conformal geodesics on vacuum space-times. *Communications in mathematical physics*, 235(3):513–543, 2003.

[53] H. Friedrich. Smoothness at null infinity and the structure of initial data. In *The Einstein equations and the large scale behavior of gravitational fields*, pages 121–203. Springer, 2004.

[54] H. Friedrich. Is general relativity essentially understood? *arXiv preprint gr-qc/0508016*, 2005.

[55] H. Friedrich. Static vacuum solutions from convergent null data expansions at spacelike infinity. In *Annales Henri Poincaré*, volume 8, pages 817–884. Springer, 2007.

[56] H. Friedrich. Geometric asymptotics and beyond. *arXiv preprint arXiv:1411.3854*, 2014.

[57] H. Friedrich. On the AdS stability problem. *Classical and Quantum Gravity*, 31(10):105001, 2014.

[58] H. Friedrich and G. Nagy. The initial boundary value problem for Einstein's vacuum field equation. *Communications in Mathematical Physics*, 201(3):619–655, 1999.

[59] D. Garfinkle. Harmonic coordinate method for simulating generic singularities. *Physical Review D*, 65(4):044029, 2002.

[60] E. Gasperin and J. A. V. Kroon. Conformal properties of the extremal Schwarzschild-de Sitter spacetime. *arXiv preprint arXiv:1506.00030*, 2015.

[61] R. Geroch. Structure of the gravitational field at spatial infinity. *Journal of Mathematical Physics*, 13(7):956–968, 1972.

[62] R. Geroch. Asymptotic structure of space-time. In *Asymptotic structure of space-time*, pages 1–105. Springer, 1977.

[63] J. Goldberg, A. Macfarlane, E. T. Newman, F. Rohrlich, and E. Sudarshan. Spin-s spherical harmonics and ð. *Journal of Mathematical Physics*, 8(11):2155–2161, 1967.

[64] J. Gong and J. Nordström. Interface procedures for finite difference approximations of the advection–diffusion equation. *Journal of Computational and Applied Mathematics*, 236(5):602–620, 2011.

[65] S. R. Green, A. Maillard, L. Lehner, and S. L. Liebling. Islands of stability and recurrence times in AdS. *Physical Review D*, 92(8):084001, 2015.

[66] K. M. Huffenberger and B. D. Wandelt. Fast and exact spin-s spherical harmonic transforms. *The Astrophysical Journal Supplement Series*, 189(2):255, 2010.

[67] M. Ko, E. Newman, and K. Tod. H-space and null infinity. In *Asymptotic Structure of Space-Time*, pages 227–271. Springer, 1977.

[68] S. Kobayashi and K. Nomizu. *Foundations of Differential Geometry*, volume 1. New York, 1963.

[69] K. D. Kokkotas and B. G. Schmidt. Quasi-normal modes of stars and black holes. *Living Rev. Rel*, 2(2):262, 1999.

[70] O. Korobkin, B. Aksoylu, M. Holst, E. Pazos, and M. Tiglio. Solving the Einstein constraint equations on multi-block triangulations using finite element methods. *Classical and Quantum Gravity*, 26(14):145007, 2009.

[71] F. Kottler. Über die physikalischen grundlagen der einsteinschen gravitationstheorie. *Annalen der Physik*, 361(14):401–462, 1918.

[72] H.-O. Kreiss and O. E. Ortiz. Some mathematical and numerical questions connected with first and second order time-dependent systems of partial differential equations. In *The Conformal Structure of Space-Time*, pages 359–370. Springer, 2002.

[73] H.-O. Kreiss and G. Scherer. On the existence of energy estimates for difference approximations for hyperbolic systems. Technical report, Technical report, Dept. of Scientific Computing, Uppsala University, 1977.

[74] L. Lehner, D. Neilsen, O. Reula, and M. Tiglio. The discrete energy method in numerical relativity: towards long-term stability. *Classical and Quantum Gravity*, 21(24):5819, 2004.

[75] L. Lehner, O. Reula, and M. Tiglio. Multi-block simulations in general relativity: high-order discretizations, numerical stability and applications. *Classical and Quantum Gravity*, 22(24):5283, 2005.

[76] A. Lichnerowicz. Sur les ondes et radiations gravitationnelles. *COMPTES RENDUS HEBDOMADAIRES DES SEANCES DE L ACADEMIE DES SCIENCES*, 246(6):893–896, 1958.

[77] J. Maldacena. The large-n limit of superconformal field theories and supergravity. *International journal of theoretical physics*, 38(4):1113–1133, 1999.

[78] M. Maliborski and A. Rostworowski. Time-periodic solutions in an Einstein AdS–massless-scalar-field system. *Physical Review Letters*, 111(5):051102, 2013.

[79] L. Marder. Gravitational waves in general relativity. I. Cylindrical waves. In *Proceedings of the Royal Society of London A: Mathematical, Physical and Engineering Sciences*, volume 244, pages 524–537. The Royal Society, 1958.

[80] L. Marder. Gravitational waves in general relativity V. An exact spherical wave. In *Proceedings of the Royal Society of London A: Mathematical, Physical and Engineering Sciences*, volume 261, pages 91–96. The Royal Society, 1961.

[81] J. M. Martin-Garcia et al. xAct: Efficient tensor computer algebra for Mathematica. *URl: http://xact. es/(c it. on pp. 12, 13)*, 2002.

[82] P. McCarthy. Representations of the Bondi-Metzner-Sachs group. I. Determination of the representations. In *Proceedings of the Royal Society of London A: Mathematical, Physical and Engineering Sciences*, volume 330, pages 517–535. The Royal Society, 1972.

[83] P. McCarthy. Structure of the Bondi-Metzner-Sachs group. *Journal of Mathematical Physics*, 13(11):1837–1842, 1972.

[84] P. McCarthy. Representations of the Bondi-Metzner-Sachs group. II. Properties and classification of the representations. In *Proceedings of the Royal Society of London A: Mathematical, Physical and Engineering Sciences*, volume 333, pages 317–336. The Royal Society, 1973.

[85] P. McCarthy. The Bondi-Metzner-Sachs group in the nuclear topology. In *Proceedings of the Royal Society of London A: Mathematical, Physical and Engineering Sciences*, volume 343, pages 489–523. The Royal Society, 1975.

[86] E. T. Newman and R. Penrose. An approach to gravitational radiation by a method of spin coefficients. *Journal of Mathematical Physics*, 3(3):566–578, 1962.

[87] E. T. Newman and R. Penrose. Note on the Bondi-Metzner-Sachs group. *Journal of Mathematical Physics*, 7(5):863–870, 1966.

[88] E. T. Newman and T. W. Unti. Behavior of asymptotically flat empty spaces. *Journal of Mathematical Physics*, 3(5):891–901, 1962.

[89] I. Newton. *Philosophiae Naturalis Principia Mathematica*, volume 1. excudit G. Brookman; impensis TT et J. Tegg, Londini, 1833.

[90] G. Patterson Jr and S. A. Orszag. Spectral calculations of isotropic turbulence: Efficient removal of aliasing interactions. *Physics of Fluids (1958-1988)*, 14(11):2538–2541, 1971.

[91] E. Pazos, M. Tiglio, M. D. Duez, L. E. Kidder, and S. A. Teukolsky. Orbiting binary black hole evolutions with a multipatch high order finite-difference approach. *Physical Review D*, 80(2):024027, 2009.

[92] R. Penrose. A spinor approach to general relativity. *Annals of Physics*, 10(2):171–201, 1960.

[93] R. Penrose. The light-cone at infinity. Technical report, DTIC Document, 1962.

[94] R. Penrose. Asymptotic properties of fields and space-times. *Physical Review Letters*, 10(2):66, 1963.

[95] R. Penrose. Zero rest-mass fields including gravitation: asymptotic behaviour. In *Proceedings of the Royal Society of London A: Mathematical, Physical and Engineering Sciences*, volume 284, pages 159–203. The Royal Society, 1965.

[96] R. Penrose. Structure of space–time. Technical report, Cornell Univ., Ithaca, NY, 1968.

[97] R. Penrose. Gravitational collapse: The role of general relativity. Technical report, Birkbeck Coll., London, 1969.

[98] R. Penrose. Relativistic symmetry groups. In *Group Theory in non-linear Problems*, pages 1–58. Springer, 1974.

[99] R. Penrose and W. Rindler. *Spinors and Space-time: Volume 1, Two-spinor Calculus and Relativistic Fields*, volume 1. Cambridge University Press, 1986.

[100] R. Penrose and W. Rindler. *Spinors and Space-time: Volume 2, Spinor and Twistor Methods in Space-time Geometry*, volume 2. Cambridge University Press, 1988.

[101] S. Persides. A definition of asymptotically Minkowskian space–times. *Journal of Mathematical Physics*, 20(8):1731–1740, 1979.

[102] S. Persides. Structure of the gravitational field at spatial infinity. I. Asymptotically Euclidean spaces. *Journal of Mathematical Physics*, 21(1):135–141, 1980.

[103] F. Pirani. Invariant formulation of gravitational radiation theory. *Physical Review*, 105(3):1089, 1957.

[104] F. Pirani. Gravitational waves in general relativity. IV. The gravitational field of a fast-moving particle. In *Proceedings of the Royal Society of London A: Mathematical, Physical and Engineering Sciences*, volume 252, pages 96–101. The Royal Society, 1959.

[105] F. Pretorius. Evolution of binary black-hole spacetimes. *Physical Review Letters*, 95(12):121101, 2005.

[106] F. Pretorius. Numerical relativity using a generalized harmonic decomposition. *Classical and Quantum Gravity*, 22(2):425, 2005.

[107] F. Pretorius. Simulation of binary black hole spacetimes with a harmonic evolution scheme. *Classical and Quantum Gravity*, 23(16):S529, 2006.

[108] F. Pretorius. Binary black hole coalescence. In *Physics of relativistic objects in compact binaries: From birth to coalescence*, pages 305–369. Springer, 2009.

[109] H. Reissner. Über die Eigengravitation des elektrischen Feldes nach der Einsteinschen Theorie. *Annalen der Physik*, 355(9):106–120, 1916.

[110] N. Rosen. Plane polarised waves in the general theory of relativity. *Phys. Z. Sowjetunion*, 12:366–372, 1937.

[111] R. K. Sachs. Gravitational waves in general relativity. VI. The outgoing radiation condition. In *Proceedings of the Royal Society of London A: Mathematical, Physical and Engineering Sciences*, volume 264, pages 309–338. The Royal Society, 1961.

[112] R. K. Sachs. Asymptotic symmetries in gravitational theory. *Physical Review*, 128(6):2851, 1962.

[113] R. K. Sachs. Gravitational waves in general relativity. VIII. Waves in asymptotically flat space-time. In *Proceedings of the Royal Society of London A: Mathematical, Physical and Engineering Sciences*, volume 270, pages 103–126. The Royal Society, 1962.

[114] B. Schmidt. A new definition of singular points in general relativity. *General relativity and gravitation*, 1(3):269–280, 1971.

[115] B. Schmidt. Asymptotic structure of isolated systems. In *Isolated Gravitating Systems in General Relativity*. 1979.

[116] E. Schnetter, P. Diener, E. N. Dorband, and M. Tiglio. A multi-block infrastructure for three-dimensional time-dependent numerical relativity. *Classical and Quantum Gravity*, 23(16):S553, 2006.

[117] K. Schwarzschild. Über das Gravitationsfeld eines Massenpunktes nach der Einsteinschen Theorie. *Sitzungsberichte der Königlich Preußischen Akademie der Wissenschaften (Berlin), 1916, Seite 189-196*, 1:189–196, 1916.

[118] M. Shibata and T. Nakamura. Evolution of three-dimensional gravitational waves: Harmonic slicing case. *Physical Review D*, 52(10):5428, 1995.

[119] P. Sommers. The geometry of the gravitational field at spacelike infinity. *Journal of Mathematical Physics*, 19(3):549–554, 1978.

[120] P. Sommers. Space spinors. *Journal of mathematical physics*, 21(10):2567–2571, 1980.

[121] B. Strand. Summation by parts for finite difference approximations for d/dx. *Journal of Computational Physics*, 110(1):47–67, 1994.

[122] S. Trapani and J. Navaza. Calculation of spherical harmonics and Wigner d functions by FFT. Applications to fast rotational matching in molecular replacement and implementation into amore. *Acta Crystallographica Section A: Foundations of Crystallography*, 62(4):262–269, 2006.

[123] E. Trefftz. Das statische Gravitationsfeld zweier Massenpunkte in der Einsteinschen Theorie. *Mathematische Annalen*, 86(3):317–326, 1922.

[124] H. Weyl. Uber die statischen kugelsymmetrischen Lösungen von Einsteins kosmologischen Gravitationsgleichungen. *Phys. Z*, 20:31–34, 1919.